Technical University of Denmark

DTU

Analysis of trait-based models in marine ecosystems.

Heilmann, Irene Louise Torpe; Sørensen, Mads Peter; Starke , Jens; Thygesen, Uffe Høgsbro; Andersen, Ken Haste

Publication date:
2017

Document Version
Publisher's PDF, also known as Version of record

DTU Library
Technical Information Center of Denmark

Analysis of trait-based models in marine ecosystems

Irene Louise Torpe Heilmann
Kongens Lyngby 2017
PHD-2017-453

DTU Compute
Department of Applied Mathematics and Computer Science

Summary (English)

The overarching theme for this thesis is spatial and temporal variations in ecosystems. The focus is on describing mechanisms that are responsible for generating the spatial and temporal patterns. The thesis contains two separate projects, each exploring a possible mechanism for pattern formation. In both projects, the model formulations result in partial integro-differential equations.

The first project in the thesis considers temporal patterns in a size structured population. Size structure is relevant for species that goes through significant changes through their lifetime. The population's response to regular temporal variations in the environment is investigated by introducing a periodic forcing in the system. This can for instance represent seasonal changes. The effect of an imposed forcing is explored both when the underlying unforced system has a stable equilibrium and when it has stable oscillatory dynamics. The numerical solutions show regular cycles where the period is equal to, or an integer multiple of, the forcing period and where the population can have one or more pulses of reproduction in each cycle. Additionally, the numerical results indicate quasi-periodic or chaotic solutions, period doubling bifurcations and coexisting attractors. The bifurcation structure is similar to results for comparable unstructured population models in the literature. This indicates that size structure does not affect the response to periodic forcing.

The next project in the thesis considers spatio-temporal pattern formation in a predator–prey system where animals move towards higher fitness. Reaction–diffusion systems have been used extensively to describe spatio-temporal patterns in a variety of systems. However, animals rarely move completely at random, as expressed by diffusion. This has lead to models with taxis terms, describing individuals moving in the direction of an attractant. An example is chemotaxis models, where bacteria are attracted to a chemical substance. From an evolutionary perspective, it is expected that animals act as to optimize their fitness. Based on this principle, a predator–prey system with fitness taxis and diffusion is proposed. Here, fitness taxis refer to animals moving towards higher values of fitness, and the specific growth rates of the populations are used as a measure of the fitness values.

To determine the conditions for pattern formation, a linear stability analysis is conducted. The analysis reveals that the fitness taxis leads to mechanisms for pattern formation, which are based on the prey gathering together. It turns out,

that in some cases the problem is not well-posed and an ultraviolet catastrophe occurs, i.e., perturbations with infinitely short wavelength grow infinitely fast. To prevent this, the population dynamics are revised with a spatial feeding kernel, that defines a spatial range wherein a predator consumes prey. A linear stability analysis for the revised system reveals the ultraviolet catastrophe is avoided and the basic mechanisms for pattern formation are unchanged. Numerical solutions to the revised system are computed to visualize the patterns. The solutions encompass stationary spatial patterns in addition to traveling waves, standing waves and irregular solutions that might be spatio-temporal chaos. The modeling approach of fitness taxis presents a general way to express movement and it is concluded that the model provides a useful framework for describing generic mechanisms for pattern formation.

Resumé (Danish)

Det overordnede tema for denne afhandling er spatielle og temporale variationer i økosystemer med fokus på at beskrive de bagvedliggende mekanismer. Afhandlingen omfatter to separate projekter der undersøger mønsterdannelse for hvert deres system. I begge projekter er modellerne formuleret som partielle differentialligninger med integralled.

Det første projekt i afhandlingen omhandler temporale mønstre i en størrelsesstruktureret population. Størrelsesstrukturerede populationsmodeller er relevante når dyr ændrer sig markant i løbet af deres levetid. Systemet påtrykkes periodiske svingninger for at undersøge hvordan populationsdynamikken påvirkes af regelmæssige variationer i omgivelserne, som fx sæsonvariationer. Effekten af de påtrykte svingninger undersøges både når det bagvedliggende system har en stabil ligevægtsløsning og når det har stabile svingninger. Blandt de numeriske løsninger forekommer der periodiske løsninger med et eller flere udsving i fødselraten for hver periode og hvor længden af perioden er én eller flere gange den påtrykte periode. Desuden viser de numeriske resultater kvasi-periodiske eller kaotiske løsninger, periodedoblinger og sameksisterende attraktorer. Bifurkationsdiagrammerne har samme opbygning som sammenlignelige ustrukturede populationsmodeller i literaturen. Dette tyder på at effekten af de påtrykte svingninger ikke ændres ved at gøre populationen størrelsesstruktureret.

Det andet projekt i afhandlingen omhandler spatio-temporal mønsterdannelse i en rovdyr-byttedyrsmodel hvor dyrene bevæger sig i retning af højere fitnessværdi. Reaktions-diffusionsligninger bliver hyppigt brugt til at modellere spatio-temporale mønstre i diverse typer af systemer. Diffusion modellerer tilfædige bevægelser, men dyr bevæger sig sjældent fuldstændigt tilfældigt. Taxisled derimod beskriver hvordan individer bevæger sig i retning af en bestemt substans; som for eksempel i modeller af kemotaxi hvor bakterier bliver tiltrukket af et kemisk stof. Med udgangspunkt i evolutionsteorien, må det forventes at dyrs opførsel er et udtryk for en strategi der optimerer deres fitnessværdi. Dette leder natuligt til idéen om fitness-taxi der, som navnet antyder, er en bevægelse mod højere værdier af fitness. Der opstilles en rovdyr-byttedyrsmodel med fitness-taxi og diffusion, hvor den specifikke vækstrate bliver brugt som et mål for fitnessværdien.

Der gennemføres en lineær stabilitetsanalyse for at afgøre hvornår systemet udviser mønsterdannelse. Denne analyse viser at fitness-taxi kan føre til mønster-

dannelse gennem mekanismer der er baseret på at byttedyrene samler sig i grupper. Det viser sig også at problemet ikke altid er velstillet, men i nogle tilfælde kan føre til en ultraviolet katastrofe, hvilket indebærer at perturbationer med en uendelig kort bølgelængde vokser uendeligt hurtigt. For at undgå dette, indføres en integrationskerne der tillader at rovdyr kan spise byttedyr indenfor en vis afstand. Der gennemføres en lineær stabilitetsanalyse for det ændrede system som viser at der ikke længere opstår en ultraviolet katastrofe og at mekanismerne for møsnterdannelse grundlæggende er de samme som før. De numeriske løsninger til det ændrede system omfatter stationære rumlige mønstre, stående bølger, vandrende bølger og løsninger der ligner spatio-temporalt kaos. Fitness-taxi er en generisk tilgang til at beskrive dyrs bevægelse og konklusionen er at modellen kan bruges til at beskrive mulige mekanismer for mønsterdannelse i populationer.

Preface

This thesis was prepared at the Technical University of Denmark (DTU) at the Department of Applied Mathematics and Computer Science as part of fulfilling the requirements for acquiring a PhD degree. The main supervisor on the project was Professor Mads Peter Sørensen from DTU Compute and the co-supervisors were Professor Jens Starke from University of Rostock, Institute of Mathematics (previously from DTU Compute), Associate Professor Uffe Høgsbro Thygesen from DTU Compute (previously from DTU Aqua) and Professor Ken Haste Andersen from DTU Aqua.

The project was a part of the Centre for Ocean Life, a Villum Kann Rasmussen Centre of Excellence for the study of life in a changing ocean. The Centre is a collaboration between researchers from DTU Aqua, DTU Physics and DTU Compute as well as Roskilde University and University of Copenhagen. The aim of the Centre is to develop a novel paradigm for describing and modeling marine ecosystems, namely the trait-based approach. As a contrast to traditional models with large complex food webs, trait-based modeling focuses on traits rather than species. Individual organisms are characterized by traits that are essential for their role in the ecosystem; e.g. their size and feeding mode. The foundation for trait-based modeling is a mechanistic description of processes on the level of individual organisms and an evolutionary principle expressing that the traits of organisms are the result of an optimal fitness strategy.

The thesis considers the spatial and temporal patterns exhibited by ecosystems. The mechanisms behind such variations are explored through two separate projects. The first project studies regular temporal variations in the environment in a size structured population and the second project investigates spatio-temporal pattern formation in a predator–prey system where animals move in the direction of higher individual fitness. The thesis introduces to the overall subject, presents the relevant background for each project, summarizes and discusses the main results and ends with a conclusion. The appendix contains two scientific papers written during the PhD project.

Kgs. Lyngby, June 2017
Irene L. T. Heilmann

Acknowledgments

First, I would like to thank my supervisors for their support and guidance. I would like to thank Mads Peter Sørensen for being encouraging and helping me structure the project. Mads would always provide an interesting perspective on the nonlinear phenomena in the projects, we have worked on. I would like to thank Uffe Høgsbro Thygesen for his valuable input about the different aspects of the models, both with regards to the mathematics and the ecology. Jens Starke's knowledge and understanding of dynamical systems have been a great help for me. Ken Haste Andersen's guidance was very helpful to structure the process of writing a paper.

I am also thankful for all my colleagues at the section for Dynamical Systems and at the Centre for Ocean Life. I would like to thank Sofia Piltz, with whom I shared an office both at the Centre for Ocean Life and at the section for Dynamical Systems. I enjoyed our conversations about different aspects of science and life in general. I also had a great time sharing an office with Christian Marschler and Michael Elmegård. The conversations with Christian and Michael were always interesting, whether we discussed dynamical systems or we talked about more mundane things.

Finally, I would like to thank my family for their support and understanding throughout the project. I would like to thank my parents Merete Torpe and Ole Heilmann. My mother has been a great support and has helped to remind me that there are other things in life than mathematics. My father has always encouraged me in my work and our countless discussions about scientific topics have been very valuable to me. I am also very grateful to my partner Kasper Hornbak Steenstrup. Kasper has always been there for me, both when times were hard and when things were going well.

Contents

Introduction

Ecosystems are rarely in a complete uniform equilibrium. Instead the abundance of animals and plants vary in time and across space. Researchers have devoted a lot of attention to explore the mechanisms behind the variability in ecosystems.

Ecosystems can show many fascinating spatial patterns, see figure 1.1. Vegetation can form spatial patterns where shrubs, bushes or trees gathers on an otherwise sparsely vegetated ground to create patterns in the form of stripes, labyrinths, gaps and holes [RvdK08]. Some spatial patterns show great variability in length scale; for example have spatial patterns of coral reefs been documented on scales ranging from 0.1 m to 1-10 km [RvdK08]. Observations of mussels beds show they are structured in large bands that are 2-20 m apart and within these bands mussels are organized in smaller labyrinth patterns with a scale of < 20 cm [LHM$^+$14].

Many populations exhibit regular variations in abundance over time, i.e., a temporal pattern. Changes over the course of a year is a natural example, but inter-annual variations are also not unusual. Populations of insects, fish, rodents, birds and lynx have been shown to display regular multi-year cycles with periods that lie in the range 2-11 years [FGBS00, SS08]. The distribution of populations can also change on much shorter time scales. Observations of the seabird murre and its prey capelin revealed nested spatial structures of both populations at three different length scales: > 300 km, ~ 50 km and ~ 3 km [FES00]. The study showed an overlap between the two populations at the two largest spatial scales which changed at time scales of weeks and days, respectively. Combined observations of spatial and temporal abundances may often appear to be irregular, but sometimes a regular pattern, such as traveling waves, can be discerned. Traveling waves have been documented for populations of larch budmoth, red grouse and Kielder Forest field voles [SS08]. Another example of regular spatio-temporal patterns is the daily

(a) Tiger bush (striped pattern) near Niamey, Niger.
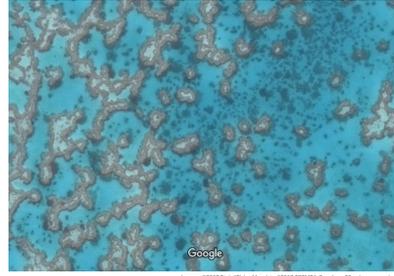
(b) Pattern formation at Wistari reef of the coast of Australia.

(c) Labyrinth pattern in Niger.

(d) Gap pattern in Mali.

Figure 1.1: Naturally occurring spatial patterns in ecosystems. The photos are from Google Maps and the locations are found via `https://johanvandekoppel.nl/research/patterns-across-the-world`.

vertical migration by tuna [TSEP16].

There are many mechanisms that can cause spatial and temporal variations of ecosystems. Naturally, variations in a system can be imposed externally by variations in the environment. The environment can have spatial variations, such as hills and rivers, and it can have temporal variations, such as seasonal changes. Daily variations, seasonal changes, sunspots cycles and effects of the North Atlantic Oscillation have all been proposed as playing a part in population cycles [Sel06, SKH+02, SER+04, TSEP16] . When external variations are combined with the internal dynamics of the system, it can lead to less obvious effects where the systems does not just follow the imposed variations. For instance are seasonal variations thought to be behind multi-year cycles in vole populations [SKH+02, TWS13], and multiple plankton blooms in a year has also been attributed to seasonal variations [SRKvN97]. Phenomena as these can be explained by applying bifurcation theory for forced systems to the ecological models.

A system can also exhibit variations without being subjected to external variations. This is demonstrated by the Lotka–Volterra equations where the interactions between a prey population and a predator population can drive the system to have periodic variations in time. These oscillations are referred to as predator–

prey cycles and does not involve a spatial dimension. When a spatial dimension is included and animals move around, the internal processes in a system can lead to spatio-temporal patterns. The combination of predator–prey cycles and random movement can lead to traveling waves or irregular spatio-temporal patterns [Mur03, SS08]. Turing patterns are a classic example of how a system can self-organize into stationary spatial patterns. The mechanisms behind Turing patterns can be described as a combination of two effects, namely local activation and long range inhibition [Mur03, RvdK08]. Extensive theory have been developed to analyze spatio-temporal pattern formation [CG09, CH93].

Spatial and temporal variations in ecosystems does not always have an obvious explanation since they are often a combination of different effects. Dynamical systems theory provides a valuable framework for understanding the underlying mechanisms in such systems.

The overall aim of this thesis is to investigate mechanisms for spatial and temporal variations in population densities. The work comprises two specific projects: The first project investigates the effect of imposing periodic temporal variations on a population with size structure (chapter 3). The second project investigates the spatio-temporal pattern formations that occur when populations move to optimize their fitness (chapter 4).

We consider models that represent a single link in a food web, that is, models with two populations where one population forage on the other. This is the simplest version of an ecosystem that still encompasses interaction between populations and thus allows for feedback loops. Basic predator–prey models are described in section 1.2. We use theory from dynamical systems to analyze the models and interpret numerical results. Both projects involve partial integro-differential equations, which are introduced in section 1.1.

1.1 Partial integro-differential equations

This section provides a short presentation of the type of systems that occurs in the projects. The systems, we consider, are partial integro-differential equations and the approach is based on dynamical systems. An introduction to dynamical systems can be found in [Mei07] and a classic approach to partial differential equations (PDEs) is given in [Eva10].

Viewing the equations as dynamical systems, we write a general system as

$$\frac{\partial u}{\partial t} = \mathcal{F}(u), \qquad u(\cdot, t) \in M, \quad \mathcal{F} : M \to M, \quad t \in \mathbb{R}_+ \tag{1.1}$$

where $u(\cdot, t)$ is the state of the system at time t. The state space M consists of functions from a space $\Omega \subseteq \mathbb{R}^d$ into $\mathbb{R}^n$. For example can $x \in \Omega$ represent the coordinates in a d-dimensional physical space. The operator $\mathcal{F}$ acts on the state space M and, typically, it contains spatial operators such as gradients. Since the system is an integro-differential equation, it can also contain integrals of the form

$\int_\Omega \mathrm{d}x$. Usually, the system (1.1) is augmented with boundary conditions, i.e., equations for $u(x,t)$ on the boundary $x \in \partial\Omega$.

Two important types of solutions to dynamical systems are fixed points and periodic solutions. A fixed point (or equilibrium state) $\tilde{u} \in M$ is a solution of system (1.1) where

$$u(x,t) = \tilde{u}(x) \quad \forall t \geq 0\,.$$

A periodic solution (or cycle) of system (1.1) fulfills

$$u(x,t) = u(x,t+T) \quad \forall t \geq 0$$

for some fixed time $T > 0$. The smallest possible value for T is called the period of the solution. Whether the solutions are stable or unstable is also important. Loosely speaking, a fixed point or periodic solution is stable if solutions that start nearby continue to stay close. There are different notions of stability, see for example [Mei07] for a precise definition of Lyapunov stability in a dynamical system.

We will typically be concerned with the long-term behavior of the system. The system may approach a stable fixed point or periodic solution, or alternatively it can have an irregular solution; the system can never approach an unstable solution. Irregular solutions of a dynamical system can be classified as, for example, quasi-periodic or chaotic. The precise definition of chaos vary in the literature, but it consistently involves sensitive dependence on initial condition and usually it also include a requirement of aperiodicity [Mei07]. A quasi-periodic solution is aperiodic, but does not have sensitive dependence on initial conditions. Different initial conditions may lead to different long-term behavior of the system, in which case we say the system has coexisting attractors.

1.2 Predator–prey models

The interactions between predators and prey constitutes a fundamental link between populations in an ecosystem. In this section, we consider a basic model for a predator population and a prey population and their interactions. The first model of this kind was the Lotka–Volterra equations. There have been numerous variations of the Lotka–Volterra equations and these are typically referred to as predator–prey models or consumer–resource models. Descriptions of predator–prey interactions can, for example, be found in [Mur03].

A predator–prey model, with the amount of prey $N(t)$ and the amount of predator $P(t)$ at time t, has the general form

$$\frac{\mathrm{d}N}{\mathrm{d}t} = \rho(N) - f(N,P) \tag{1.2a}$$

$$\frac{\mathrm{d}P}{\mathrm{d}t} = \varepsilon f(N,P) - \mu(P) \tag{1.2b}$$

In this model, $\rho(N)$ is the growth rate of the prey population in the absence of predators, $\mu(P)$ is the mortality of the predators and $f(N,P)$ represent the feeding

rate of the predators on the prey population. The predators convert prey into new predators with efficiency $\varepsilon \in [0, 1]$. There is no spatial dimension in the model and the variables N and P can be viewed either as the total number of animals in a region or as population densities for a uniform distribution of animals.

In the original Lotka–Volterra model, the grow rate of prey is a linear function $\rho(N) = rN$. This gives an unbounded exponential increase of prey in the absence of predator. By adding a quadratic term the growth rate is decreased at high amounts of prey:

$$\rho(N) = rN\left(1 - \frac{N}{K}\right).$$

This is called logistic growth and is often used in population models. It prevents the amount of prey N to increase beyond the carrying capacity K. A frequent assumption is that the predators have a constant background mortality, which is modeled by

$$\mu(P) = \mu_1 P.$$

Sometimes a quadratic term is added to reflect increased mortality at high densities due to crowding effects

$$\mu(P) = \mu_1 P + \mu_2 P^2.$$
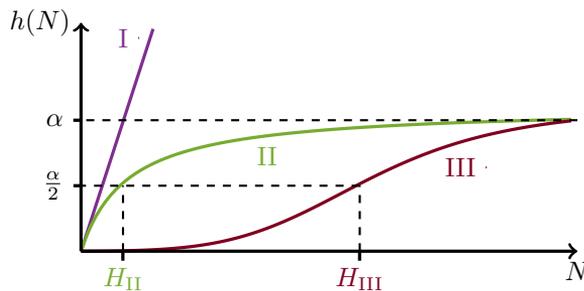
Figure 1.2: Functional response of Holling type I, II and III.

The feeding rate is often described through a functional response $h(N)$ of the predator, leading to

$$f(N, P) = h(N)P.$$

The functional response $h(N)$ describes the food intake of a predator for different amounts of prey N. Traditionally, three types of functional responses are considered, namely Holling type I, II and III, see figure 1.2. Holling type I is a simple linear relation

$$h(N) = aN.$$

where the attack rate a represent how effectively a predator can search for and capture prey. Holling type II includes a saturation of the predator's food intake for high levels of prey

$$h(N) = \alpha \frac{N}{H + N} \, .$$

This expression can be derived by assuming that a predator divides its time between searching for prey and handling captured prey. The maximum ingestion rate of a predator is α and the half-saturation constant H is the level of prey at which a predator ingests $\alpha/2$. Holling type III is a sigmoid function of N, reflecting that, at low levels of prey, it is not worth the effort for the predators to search for the prey. This can be modeled with an expression of the form

$$h(N) = \alpha \frac{N^p}{H^p + N^p}$$

where α and H still represent the maximum ingestion rate and the half-saturation constant, respectively. The parameter p controls how pronounced the S-shape of the function is.

Predator–prey systems such as (1.2) will usually show one of the following three types of solutions:

- The predator goes extinct and the prey stabilizes at its carrying capacity.

- The system stabilizes at an equilibrium with positive values of both prey and predator.

- The system stabilizes at periodic solution, often referred to as predator–prey cycles.

Which solution type is exhibited, typically depends on parameter values.

1.3   Thesis outline

The structure of the thesis is as follows. The numerical methods used in simulations are described in chapter 2. The thesis consists of two projects and a chapter has been devoted to each: Chapter 3 considers the effect of periodic forcing of a size structured population and chapter 4 investigates the spatio-temporal pattern formations in a predator–prey system with fitness taxis. Each of these chapters contains the relevant background for the project and summarizes the results. Chapter 5 presents the conclusion for the thesis. Finally, the papers for the thesis are listed in appendix A.

Paper I   Dynamics of a physiologically structured population in a time-varying environment

Paper II   Spatio-temporal pattern formation in predator–prey systems with fitness taxis

Numerical methods

The models in this thesis are partial differential equations and, in this section, we present the methods that are used to obtain numerical solutions to the models. Such methods are for example described in [HV13, LeV02, MM05]. The overall approach to solving the partial differential equations is the method of lines. The method of lines consists of two steps: the first step is to discretize the model in space, thereby transforming each partial differential equation to a system of ordinary differential equations, and the second step is to solve the ordinary differential equations in time. There exist many numerical solvers for finding solutions to ordinary differential equations; we use the built-in ode-solvers in Matlab. For the discretization in space, we use the finite volume method. In the following, we present the principles of the finite volume method and apply the method to some general examples.

The finite volume method is based on Gauss' theorem (also known as the divergence theorem). The theorem connects a vector field $\boldsymbol{F}$ in a volume V to the vector field on the boundary ∂V of the volume, see figure 2.1. The theorem states that

$$\int_V \nabla \cdot \boldsymbol{F} \, dV = \int_{\partial V} \boldsymbol{F} \cdot \boldsymbol{n} \, dS \tag{2.1}$$

where $\boldsymbol{n}$ denotes the outward normal of the surface ∂V. The theorem holds if the volume $V \subset \mathbb{R}^3$, (or more generally $V \subset \mathbb{R}^n$) is compact and its boundary ∂V is piecewise smooth. Further, the vector field $\boldsymbol{F}$ is required to be continuously differentiable in a neighborhood of V.

An intuition of the theorem comes from considering a concentration $u(\boldsymbol{x})$ of particles in a fluid that moves with velocity $\boldsymbol{c}(\boldsymbol{x})$. The concentration and velocity may vary across space $\boldsymbol{x}$ and in time. Then the flux of particles is $\boldsymbol{F}(\boldsymbol{x}) = u(\boldsymbol{x})\boldsymbol{c}(\boldsymbol{x})$ and the change in concentration per time is $\nabla \cdot \boldsymbol{F}$. Hence, the theorem states that

the total change of particles per time in the volume V is equal to the flow of particles across the boundary ∂V of the volume.
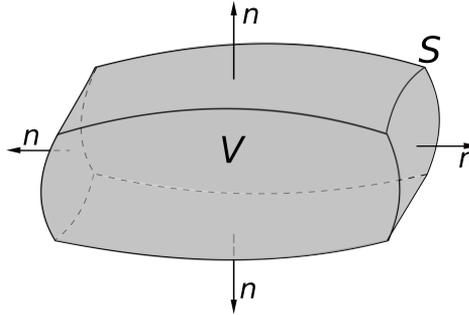
Figure 2.1: The volume V and its boundary $\partial V = S$ with outward normal $\boldsymbol{n}$ for Gauss' theorem.[1]

2.1　The finite volume method

We illustrate the finite volume method by considering a partial differential equation in a general form that covers both the systems studied in this thesis. The general equation is for the dependent variable $u = u(\boldsymbol{x}, t)$ in space $\boldsymbol{x} \in \Omega$ and for time $t > 0$ and it reads

$$\frac{\partial u}{\partial t} = r - \nabla \cdot \boldsymbol{F} \,. \tag{2.2}$$

Source/sink contributions are represented by r and transport is covered by the flux $\boldsymbol{F}$. To employ Gauss' theorem, the equation is integrated over the volume $V \subseteq \Omega$,

$$\int_V \frac{\partial u}{\partial t} \, \mathrm{d}V = \int_V r \, \mathrm{d}V - \int_V \nabla \cdot \boldsymbol{F} \, \mathrm{d}V \,.$$

Assuming the volume V is constant, the differentiation with respect to time is moved out of the integral and Gauss' theorem is applied to the last term on the right hand side,

$$\frac{\mathrm{d}}{\mathrm{d}t} \int_V u \, \mathrm{d}V = \int_V r \, \mathrm{d}V - \int_{\partial V} \boldsymbol{F} \cdot \boldsymbol{n} \, \mathrm{d}S \tag{2.3}$$

This is called the integral formulation of the system.

The finite volume method employs a division of space Ω into small control volumes V_i ($i = 1, \ldots, N$), see figure 2.2a. The boundary ∂V_i of a control volume

---

[1]Image by user: Cronholm144 (Own work), published under CC-BY-SA-3.0 http://creativecommons.org/licenses/by-sa/3.0/, via Wikimedia Commons

consist of surfaces S_k between the control volume and each of its neighbors. Hence, the integral form (2.3) for a control volume V_i can be written as

$$\frac{\mathrm{d}}{\mathrm{d}t} \int_{V_i} u \, \mathrm{d}V = \int_{V_i} r \, \mathrm{d}V - \sum_{k \in B(i)} \int_{S_k} \boldsymbol{F} \cdot \boldsymbol{n} \, \mathrm{d}S \tag{2.4}$$

where the notation $k \in B(i)$ represents that the surface S_k is a part of the boundary ∂V_i. In one and two dimensional space the control volumes are really intervals and areas, respectively, and the boundaries between control volumes are points and lines, respectively. In general, we refer to control volumes as cells and to boundaries between control volumes as interfaces.

(a) 1D   *(b) 2D*
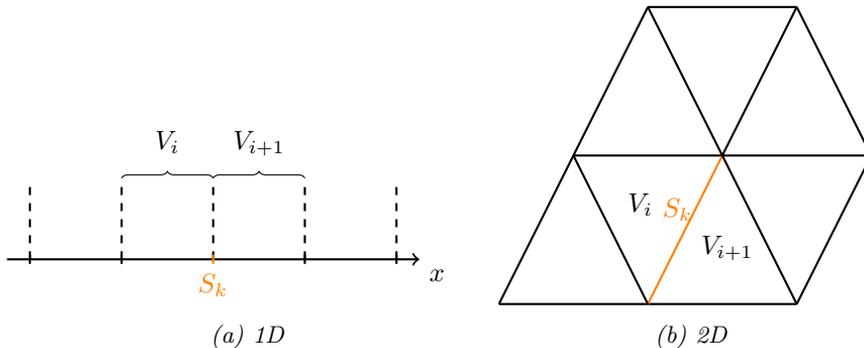
Figure 2.2: Examples of spatial grids for the finite volume method. The two cells V_i and V_{i+1} share the interface S_k (orange).

The finite volume method gives a numerical scheme for approximating the cell averages of the system variable u,

$$U_i(t) \approx \frac{1}{|V_i|} \int_{V_i} u(\boldsymbol{x}, t) \, \mathrm{d}V \tag{2.5}$$

where $|V_i| := \int_{V_i} \mathrm{d}V$ denotes the size (volume, area or length) of cell V_i. Sometimes we may also view it as a point-wise approximation $U_i(t) \approx u(\boldsymbol{x}_i, t)$. Let R_i be an approximation for the cell averages of the source term,

$$R_i \approx \frac{1}{|V_i|} \int_{V_i} r \, \mathrm{d}V \tag{2.6}$$

and let J_k approximate the flux over an interface,

$$J_k \approx \int_{S_k} \boldsymbol{F} \cdot \boldsymbol{n} \, \mathrm{d}S \,. \tag{2.7}$$

Then equation (2.4) for each cell is approximated with the scheme

$$\frac{\mathrm{d}}{\mathrm{d}t} U_i = R_i - \frac{1}{|V_i|} \sum_{k \in B(i)} J_k \,. \tag{2.8}$$

The estimation of the source terms R_i and the fluxes J_k depends on the specific problem at hand. Notice that, in this notation, the sign of a flux J_k depends on which of the interface's two cells are considered. Equation (2.8) is a finite volume scheme for the system (2.2) that approximates the partial differential equation with N ordinary differential equations.

Now let us consider the case of one spatial dimension and divide the domain $\Omega = [0, L]$ into cells V_i, for $i = 1, \ldots, N$. Each cell V_i is an interval centered at a point x_i and the cells are numbered from left to right on the x-axis, see figure 2.3. The interface between cell V_i and V_{i+1} is the point $x_{i+1/2}$ and the approximate flux across the interface is labeled $J_{i+1/2} \approx \boldsymbol{F}|_{x=x_{i+1/2}}$. By convention, a flux is positive if it goes to the right and negative if it goes to the left. In one dimension, the finite volume scheme (2.8) becomes

$$\frac{\mathrm{d}}{\mathrm{d}t}U_i = R_i - \frac{J_{i+\frac{1}{2}} - J_{i-\frac{1}{2}}}{x_{i+\frac{1}{2}} - x_{i-\frac{1}{2}}} \tag{2.9}$$

We have used that the size of the intervals are $|V_i| = \Delta x_i = x_{i+1/2} - x_{i-1/2}$. Next we look at how to approximate the fluxes for different equations.
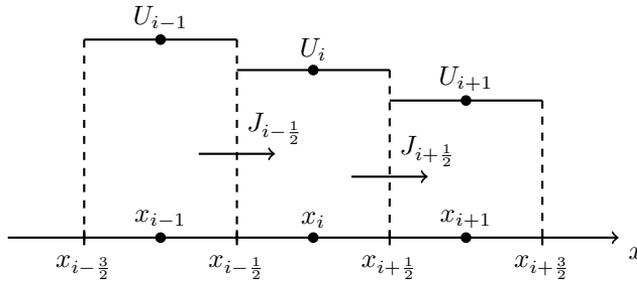
Figure 2.3: Finite volume grid for one-dimensional space, $x \in \mathbb{R}$. Here, U_i is the average value of u in cell i and $J_{i+1/2}$ is the flux across interface $x_{i+1/2}$.

2.1.1 The advection equation

First, we consider the advection equation in one dimension,

$$\frac{\partial u}{\partial t} = -\frac{\partial}{\partial x}(cu). \tag{2.10}$$

The equation can, for example, represent particles in a fluid moving with velocity c. In this case, $u(x,t)$ is the concentration of particles in space x at time t. If the velocity is constant, the initial particle concentration $u_0(x) = u(x,0)$ propagates with velocity c without changing shape, and the solution to the system is a traveling wave $u(x,t) = u_0(x - ct)$ for $t > 0$. In general, however, we consider a non-constant velocity and it is not so easy to find a solution, analytically or numerically. The solution $u(x,t)$ to equation (2.10) will never become negative for $t > 0$ if the

initial profile is non-negative, $u(x,0) \geq 0$. This is in accordance with the physical interpretation of u as a concentration. However, non-negativity of the solution is not necessarily preserved by a numerical scheme.

Equation (2.10) is equivalent to the general form (2.2) with no source term, $r = 0$, and the flux $\boldsymbol{F} = cu$. A basic finite volume scheme for the advection equation on a uniform grid with spacing $\Delta x = x_{i+1} - x_i$ reads

$$\frac{\mathrm{d}}{\mathrm{d}t} U_i = \frac{J_{i-\frac{1}{2}} - J_{i+\frac{1}{2}}}{\Delta x} \, . \tag{2.11}$$

There are several approaches to approximating an advective flux. When we have the velocities $c_{i+1/2} = c|_{x=x_{i+1/2}}$ at the interfaces, the flux approximations take the form

$$J_{i+\frac{1}{2}} = c_{i+\frac{1}{2}} U_{i+\frac{1}{2}} \approx \boldsymbol{F}|_{x=x_{i+\frac{1}{2}}}$$

Here, $U_{i+1/2}$ denotes an approximation of the density at the interface and we will consider two ways to choose it. One possibility is to use the average of the density to the left and to the right of the interface, and this gives

$$J_{i+\frac{1}{2}} = c_{i+\frac{1}{2}} \frac{U_i + U_{i+1}}{2} \tag{2.12}$$

This flux results in a second order central scheme. Another possibility is to use an upwind method. If the velocity is positive, the flux of particles goes from cell i to cell $i+1$ and therefore U_i is used to approximate the flux. Conversely, if the velocity is negative, the density U_{i+1} is used. This gives the approximation

$$J_{i+\frac{1}{2}} = \begin{cases} c_{i+\frac{1}{2}} U_i \, , & c_{i+\frac{1}{2}} > 0 \\ c_{i+\frac{1}{2}} U_{i+1} \, , & c_{i+\frac{1}{2}} < 0 \end{cases} \tag{2.13}$$

This flux gives a first order upwind scheme.

Though the central scheme is second order accurate and the upwind scheme is only first order, the central scheme is not necessarily the best choice. The central scheme may create oscillations that do not exist in the exact solution. This can lead to unphysical solutions where the concentrations $U_i(t)$ become negative, even though the initial concentrations $U_i(0)$ are all non-negative. The upwind scheme, on the other hand, always preserves the non-negativity of the solution. The downside is the upwind scheme introduces artificial diffusion in the system and, therefore, the numerical solution tends to be leveled out compared to the exact solution. For a standard linear scheme that preserve non-negativity of the solution, the highest possible order is one and, in this sense, the upwind method is optimal. For higher order accuracy, we would need another type of method.

2.1.2 The diffusion equation

Next, we consider the diffusion equation in one dimension,

$$\frac{\partial u}{\partial t} = D \frac{\partial^2 u}{\partial x^2} \tag{2.14}$$

with a constant diffusion coefficient $D > 0$. If $u(x, t)$ represents a concentration of particles in space x at time t, then this equation describes random movement of the particles.

Comparing the diffusion equation (2.14) with the general form (2.2), this corresponds to no sources, $r = 0$, and the flux $\boldsymbol{F} = -D\frac{\partial u}{\partial x}$. The flux at the interfaces can be approximated with a first order central difference for the derivative,

$$J_{i+\frac{1}{2}} = -D\frac{U_{i+1} - U_i}{x_{i+1} - x_i} \approx -D\frac{\partial u}{\partial x}\bigg|_{x=x_{i+\frac{1}{2}}} .$$

On a uniform grid with spacing $\Delta x = x_{i+1} - x_i$, the finite volume scheme (2.9) becomes

$$\frac{\mathrm{d}}{\mathrm{d}t}U_i = D\frac{U_{i-1} - 2U_i + U_{i+1}}{\Delta x^2} . \tag{2.15}$$

This gives a second order central scheme for the diffusion equation. The scheme preserves non-negativity of the solution and works well in many applications.

2.1.3   The advection–diffusion equation

A system can have both advective and diffusive movement, leading to the advection–diffusion equation,

$$\frac{\partial u}{\partial t} = -\frac{\partial}{\partial x}(cu) + D\frac{\partial^2 u}{\partial x^2} . \tag{2.16}$$

To obtain a discretization in space, we can combine the above schemes for advection (2.11) and diffusion (2.15); for the advection term we can choose either the central flux (2.12) or the upwind flux (2.13). The behavior of the system depends on the relative magnitude between advection and diffusion, which is measured with the dimensionless Péclet number. The Péclet number for grid cell of length Δx is

$$Pe = \frac{c\Delta x}{D} . \tag{2.17}$$

With the central flux for advection, the overall scheme becomes second order accurate. If $Pe \leq 2$, non-negativity of the solution is preserved, but otherwise the scheme may give rise to artificial oscillations and negative solution values. With the upwind flux for advection, the overall scheme is first order accurate and non-negativity of the solution is preserved, regardless of grid size. We can conclude that for diffusion dominated problems, the central scheme works well and is more accurate than the upwind scheme. For advection dominated problems, the central scheme requires very small grid size to preserve positivity and it may be better to use the upwind scheme.

Periodic forcing of a size structured population

Size structured population models have received a substantial interest in the last two decades. Many traditional models use a single variable, such as the number of individuals or the total biomass, to represent an entire population. In contrast, physiologically structured models also characterize the physiological state (e.g. size) of the individuals, which is relevant for many species. These models can capture dynamics that cannot be seen in traditional unstructured models. In this chapter, we aim to investigates the effect of imposing periodic temporal variations on size structured populations. Periodic variations of the environment have mainly been studied for unstructured populations, and we seek to extend the situation to size structured populations.

Imposed temporal variations of ecosystems occur on a variety of time scales: daily changes, e.g., in light level; weather phenomena on weekly time scales; seasonal variations; and decadal fluctuations, such as the North Atlantic Oscillation. Especially seasonal variations have been studied in the literature and they can have a great impact on ecosystems [MMH⁺15]. During the year, animals experience variations in the environment, such as light, temperature and available food, and these changes influence processes such as growth and mortality. To adapt to seasonal variations, animals have developed different strategies; for example, many animals have a distinct breeding season and some animals migrate or hibernate to survive winter [MH08]. To understand how ecosystems function, we need to understand the effect of periodic temporal variations in the environment.

External variations can be applied to a population model in different ways. A straight forward and common approach is to vary one or more parameters over time. For example, a varying amount of available food can be modeled with a

forcing of the growth rate, and the changing activity level of a predator can be reflected by forcing of parameters in a functional response. The authors of [RMK93] consider no less than six different ways to force the parameters of a predator–prey model, each representing different effects of seasonality. Often the parameters are varied with a sinusoidal function where the amplitude represents the strength of the variations. For variations in temperature, the changes in biological rates (such as growth rate) can be modeled using a Q10 law [FMS+06]. If all rates are forced with the same scaling factor, the forcing essentially becomes a rescaling of time [vdWdRP08]. Another way to impose periodic variations on a system is to employ seasonal reproduction, where a population only reproduces at fixed time intervals, typically once a year.

We will focus on forcing of parameters and the mathematical framework for this is introduced in section 3.1. Size structured populations are introduced in section 3.2. In section 3.3 we summarize the main results and in section 3.4 the implications of the results are discussed.

3.1   Periodically forced systems

In this section, periodically forced systems are described mathematically and in section 3.1.1 we review some applications to predator–prey systems. To present the concepts more clearly, the systems are represented as ordinary differential equations. See also [Kuz98, Wig03, PRK03]. We consider the periodically forced system

$$\frac{\mathrm{d}u}{\mathrm{d}t} = f(u,t), \qquad u \in \mathbb{R}^n, \quad f : \mathbb{R}^n \times \mathbb{R} \to \mathbb{R}^n, \quad t \in \mathbb{R}. \tag{3.1}$$

where the function f is periodic in time t with the period T. The state of the system at time t is represented by the vector $u(t)$. Since f depends explicitly on time, equation (3.1) is a non-autonomous system, but it can rewritten as an autonomous system. By including an extra dependent variable $\theta \in S$ that lies on the circle, the system is transformed into

$$\frac{\mathrm{d}}{\mathrm{d}t} \begin{pmatrix} u \\ \theta \end{pmatrix} = \tilde{f}(u,\theta) := \begin{pmatrix} f(u, \frac{\theta}{\omega}) \\ \omega \end{pmatrix} \tag{3.2}$$

where the parameter $\omega = \frac{2\pi}{T}$ is the frequency of the forcing. The added variable θ has the solution

$$\theta(t) = \theta_0 + \omega t \mod 2\pi \tag{3.3}$$

for initial condition $\theta(0) = \theta_0$. For each time interval of length T, the variable θ makes one tour around the circle.

To examine a periodically forced system, it is often useful to apply a Poincaré map [Kuz98, Wig03]. Poincaré maps allows us to analyze continuous systems through a discrete map. For periodically forced systems, the Poincaré map shifts the solution forward in time with one forcing period T. Let $u(t; (u_0, \theta_0))$ denote

the solution for u in the autonomous system (3.2) with initial condition $u(0) = u_0$, $\theta(0) = \theta_0$. We define the Poincaré map P as

$$u_0 \mapsto P(u_0) = u(T; (u_0, \theta_0)). \tag{3.4}$$

The map belongs to a Poincaré section defined by

$$\Sigma = \left\{ (x, \theta) \in \mathbb{R}^n \times S \mid \theta = \theta_0 \right\} \tag{3.5}$$

This is a cross-section of the state space for system (3.2) that intersect the circle at $\theta_0 \in [0, 2\pi)$. The Poincaré map takes the solution from an intersection with Σ to its next intersection, see figure 3.1. The specific value of θ_0 is not important for the properties of the map, since maps corresponding to different cross-sections are equivalent [Kuz98, Wig03].
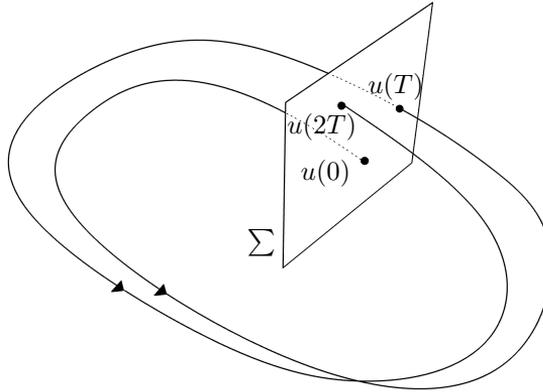
Figure 3.1: Poincaré map for cross-section Σ with $\theta_0 = 0$.

The trajectories of the discrete Poincaré map (3.4) can be used to derive information about the continuous system (3.2) as follows [Kuz98, Wig03]:

- An equilibrium point of the Poincaré map, $u_0 = P(u_0)$, corresponds to a cycle in the continuous system with period T.

- Period-k points of the Poincaré map, $u_0 = P^k(u_0)$, correspond to a cycle in the continuous system with period kT. There are k points for one cycle.

- A closed invariant curve in the Poincaré map corresponds to a quasi-periodic solution to the continuous system.

- An irregular invariant set for the Poincaré map corresponds to a chaotic solution in the continuous system.

Forced oscillator

If the unforced system has a periodic solution, then the introduction of forcing results in a system that is influenced by two frequencies. Interaction of these two oscillations can lead to variety of dynamics, including phase-locking and chaos.

We introduce the phase equation for generic forced oscillator [PRK03]. We start by considering an unforced system that has a periodic solution with period T_0. The phase $\phi \in S$ is introduced as a coordinate that runs along the cycle, such that

$$\phi(t) = \phi_0 + \omega_0 t \mod 2\pi. \tag{3.6}$$

on the cycle. The value $\omega_0 = \frac{2\pi}{T_0}$ is referred to as the natural frequency of the system. The definition of the coordinate ϕ can be extended to a neighborhood around the cycle. If we add a forcing with period T and amplitude ϵ, we can approximate the system of the forced oscillator with the phase equation

$$\frac{\mathrm{d}\phi}{\mathrm{d}t} = \omega_0 + \epsilon Q(\phi, t). \tag{3.7}$$

The function Q is 2π-periodic in ϕ and T-periodic in t. It turns out, the phase equation is not only valid for small values of ϵ, but also describes a forced oscillator for larger amplitudes, where the system is no longer close to the cycle used to define ϕ [PRK03]. The system of a forced oscillator can be viewed as motions on a torus where one angle $\phi \in S$ is the phase of the system and the other angle $\theta \in S$ represents the forcing, see equation (3.3).

The circle map represents a Poincaré map for the phase equation (3.7). Shifting the phase ϕ forward in time with T gives the map [PRK03]

$$\phi_i \mapsto \phi_{i+1} = \phi_i + 2\pi\alpha + \epsilon F(\phi_i) \mod 2\pi \tag{3.8}$$

where $\alpha = \frac{\omega_0}{\omega}$. The function F expresses the effect exerted by the forcing on the phase. The effect only depends on the phase since the forcing is always at the same point in its rotation for the evaluation of the map. Often the function $F(\phi_i) = \sin(\phi_i)$ is used, in which case equation (3.8) is called the standard circle map.

If the forcing does not affect the phase of the system, i.e., $F = 0$, the variables ϕ and θ are decoupled and obey equations (3.3), (3.6). The solution to the circle map is determined by $\alpha = \frac{\omega_0}{\omega}$, the (partial) number of rotations on the circle during one forcing period. If $\alpha = \frac{m}{k}$ is an irreducible fraction for positive integers m, k, the phase ϕ makes exactly m tours around the circle for every k forcing periods and the solution is kT-periodic. If α is irrational, the trajectory of the circle map covers every point on the circle. This corresponds to a quasi-periodic solution of the phase equation where the trajectory covers every point on the surface of the torus.

For $\epsilon < 1$, the solutions of the circle map represent either periodic or quasi-periodic motions of the forced oscillator. For $\epsilon = 0$, the periodic solutions only occur for rational values of α, but as the amplitude increases the periodic solutions

occur for a larger range of α, see figure 3.2. These windows of periodic solutions are called Arnold tongues [Arn92, PRK03]. The tongues exist for every rational number $\frac{m}{k}$, but rapidly becomes smaller with increasing k. For $\epsilon > 1$, the tongues start to overlap and stable solutions with different periods can co-exist. In this part of parameter space, we also encounter period doubling bifurcations and chaotic behavior. In general, a forced oscillator behaves qualitatively similar to the circle map. This means, the system has quasi-periodic solution interrupted by windows of periodic solutions for small forcing amplitudes, and, for larger forcing amplitudes, we can expect more complicated behavior.
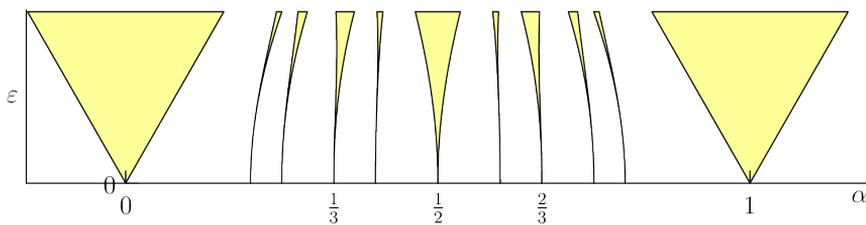

Figure 3.2: Arnold tongues for the standard circle map. Periodic solutions (color) and quasi-periodic solutions (white) for ϵ, the forcing amplitude, and α, the ratio between the natural frequency and the forcing frequency. Only the largest tongues are shown.[1]

3.1.1 Forcing in predator–prey models

The dynamics of predator–prey models with periodic variation of parameters have been explored for a variety of systems, see for example [KMR92, RMK93, SS93, SMM97, TSW13, VSB01]. The systems are analyzed with direct numerical simulations and/or numerical continuation methods [KMR92, TSW13]. They display a variety of dynamics, showing cycles with different periods, quasi-periodic solutions and chaotic solutions. The authors of [TSW13] consider the Rosenzweig–MacArthur model for predator–prey interactions and investigate the effect of forcing a parameter that does not affect the solution type of the unforced system. When the unforced system has a stable equilibrium, the forced system can have stable one- and two-year cycles. When the unforced system has a stable cycle, the dynamics of the forced system resemble the dynamics described by the circle map. The Rosenzweig–MacArthur model is also considered in [KMR92], but with forcing of a parameter that affects the solution type of the unforced system. This leads to a different bifurcation structure than for the circle map. In [RMK93], the study is extended to different scenarios of forcing. The scenarios has forcing of different parameters, but in all cases the parameters affect the same Hopf bifurcation. The bifurcation diagrams constructed for the different scenarios all have a similar structure. These results emphasize the significance of the dynamics of the underlying predator–prey system.

---

[1] Image by Ilya Voyager, published under Creative Commons Universal Public Domain Dedication (CC0 1.0) https://commons.wikimedia.org/w/index.php?curid=20867424 .

Predator–prey models with forcing have also been used to describe the dynamics of specific populations; in the following we mention some examples. A model of Fennoscandian voles and a specialist predator with forcing of the growth rates is considered in [TWS13]. The forcing is used to represent the breeding season and a forcing function with a wider peak corresponds to a longer breeding season. The model shows a variety of different dynamics including cycles with different periods, quasi-periodic solutions and coexistence of stable states. The results concurs with observations of different multi-year cycles in vole populations in different geographical regions. In [SRKvN97] is investigated a model of algae and zooplankton where several parameters are forced with a sinusoidal function to reflect seasonal variations. The system shows solutions with different number of blooms or a turbid solution with very few zooplankton throughout the year, depending on parameter values. Their results suggest variations in fish predation as an explanation for different bloom scenarios observed in lakes. Another model for blooms of phytoplankton and zooplankton is considered in [FMS+06] where seasonality is represented as variations in temperature. The system has two coexisting stable cycles with period of one year, corresponding to either a bloom or a non-bloom solution. Based on the perturbations needed to make the system switch from one solution to the other, rapid increase in temperature is proposed as a trigger mechanism for bloom events. These examples show that relatively simple models can capture phenomena displayed by real ecosystems.

3.2   Size structured population models

In many species, individuals go through significant changes during their life time from offspring to mature individual. To describe this diversity within a population, physiologically structured models were introduced. In such models, the individuals in population are characterized by their physiological state. Since many traits of an individual is related to its size [ABG+16], this is often used to characterize the individuals of a population. In this section, we give a short description of size structured populations; for a more comprehensive description, see for example [MD86, dRP13].

In a size structured model, a population is represented with a density distribution $n(\cdot, t)$ at each time t. An individual is described by its size x and $n(x, t)$ describes how individuals in the population are distributed over sizes x. More generally, x can describe the physiological state of an individual and is a vector with variables, such as size, age and storage. Here, we only consider the case where $x \in \mathbb{R}_+$ is the size of the individual.

The individuals in the population are characterized by their birth rate $b(F, x)$, mortality rate $\mu(F, x)$ and somatic growth rate $g(F, x)$. These functions may depend on other variables F in the system; often F will include a food resource. The functions can be constructed from assumptions on how an individual allocates

energy to different processes. The size x of an individual follows the equation

$$\frac{\mathrm{d}x}{\mathrm{d}t} = g(F, x)\,.$$

In terms of the whole population, the dynamics become

$$\frac{\partial n(x,t)}{\partial t} + \frac{\partial g(F,x)n(x,t)}{\partial x} = -\mu(F,x)n(x,t)\,. \tag{3.9}$$

This equation describes how the density distribution $n(\cdot, t)$ changes over time.

All individuals in the population are assumed to have the same size x_0 at birth. This leads to a boundary condition at x_0 for the flow of newborns into the system

$$g(F,x_0)n(x_0,t) = \int_{x_0}^{\infty} b(F,x)n(x,t)\,\mathrm{d}x\,. \tag{3.10}$$

Typically, only individuals above a certain size x_j reproduce and the population can be divided into juveniles and adults.

A size structured population model can show different types of solutions. Equation (3.9) always has the equilibrium solution $n(x,t) = 0$, which corresponds to extinction of the population. Depending on the growth and mortality functions, it can also have an equilibrium with a constant non-zero density distribution $n(x,t) = n^*(x)$. These equilibria may be stable or unstable.

If the system includes another dependent variable, such as a variable F representing a food resource, stable periodic solutions can occur. The periodic solutions may be classified as either predator–prey cycles or cohort cycles. Cohort cycles, have a single cohort of individuals that all have (approximately) the same size. The individuals in the cohort grows larger and, when they reach maturity, they give birth to a new cohort that takes over. Mathematically, cohort cycles can take the form of shock waves. Predator–prey cycles are similar to the cycles found in predator–prey models without size structure. Individuals of all sizes increases and decrease more in less together over the course of a cycle. There is no formal distinction between the two types of cycles, but sometimes an approximate criteria can be defined, see [dRMEL90].

3.2.1   Seasonality in size structured populations

There are examples of size structured models with imposed temporal variations in the form of seasonal reproduction [CdRP00, PLdR$^+$98, vdWdRP08]. With seasonal reproduction, the size distribution becomes a set of cohorts; one cohort for each year's offspring. This reduces the size structured model from a partial differential equation to a set of ordinary differential equations [PLdR$^+$98]. The effect of size dependent attack rates in a size structured population with seasonal reproduction is investigated in [PLdR$^+$98]. The solutions to the system includes one- and multi-year cycles, quasi-periodic solutions and chaotic solutions. In [vdWdRP08], a size structured population model with seasonal reproduction is used to derive conditions

for juveniles to survive winter. The model is similar to the one in [PLdR$^+$98], but the system is also forced with a step function to represent summer and winter periods, and this changes some of the dynamics. In [SdR17], a size structured population model with seasonal reproduction is compared to a simplified model with only two size classes, representing juveniles and adults. It is concluded that the two models give similar results except for cohort cycles.

3.3   Summary of results

Periodic variations, such as seasonal variations, can have a great impact on an ecosystem. The study of these systems have mainly concentrated on unstructured populations. However, size structure is relevant for many species and can change the dynamics of a system. The aim of Paper I is to investigate the response of a size structured population to periodic variations of the resource growth rate.

We use a size structured population model presented in [dR97]. It is based on the Kooijman–Metz model and describes a size structured daphnia population and an unstructured algae resource. The system shows different types of solutions depending on the parameter values of daphnia mortality and carrying capacity of algae. We extend the model with a periodic forcing of the algae growth rate, representing variations of conditions such as light and nutrients. The periodic variations are characterized by two parameters: the period and amplitude of the forcing.

To explore the effect of adding forcing, we concentrate on two cases: In the first case (A), the unforced system has a stable equilibrium where both algae and daphnia are present, and in the second case (B), the unforced system has stable predator–prey cycles. In both cases, the unforced systems has oscillations with a period of approximately 27 days (case A has oscillatory decay toward the equilibrium). The forcing period is varied in the range [5, 100] days, and the forcing amplitude relative to the mean amplitude is varied in the range [0, 1].

Solutions to the system are obtained by numerically integrating the equations until transients have settled. For each point in time, the daphnia population is represented by a size distribution. To characterize the entire population with a single measure, we use the combined birth rate of the population. For each solution, the period of the solution is estimated, and if a period cannot be found, the solution is labeled as irregular. Additionally, we compute a value representing the number of birth pulses per forcing period. Pulses are counted proportional to their amplitude, so this value varies continually as the solution changes smoothly.

The forcing amplitude and period are varied for the two cases. For case A, the typical behavior of the system are solutions that oscillates around the equilibrium with same period as the forcing. Increasing the forcing amplitude can lead to period doubling bifurcations, especially when the forcing period is close to the natural period of the system. When the period and forcing are varied in case B, the system has periodic solutions in a pattern that looks like Arnold tongues.

3.4   Discussion

The results show the daphnia and algae populations are more inclined to exhibit regular oscillations when the forcing period is close to the natural period of the system of roughly one month. When the forcing period is much larger or shorter, it depends to a large degree on values of the unforced parameters, whether the system has regular oscillations (case A) or irregular oscillations (case B). The results correspond with results for a similar, but unstructured, predator–prey model in [TSW13]. The ratio of natural frequency to forcing frequency appears to have a similar effect as in the standard forced oscillator model. I seems likely that the influence of this dimensionless ratio can be generalized to other population systems with similar dynamics, even though the value of the natural period might be very different.

The results were obtained for a forcing of the algae growth rate, a parameter that does not affect the solution type of the underlying model. Other studies of unstructured populations [RMK93] have indicated that forcing of parameters that affect the solution type of the underlying model can lead to dynamics with a different bifurcation structure than the standard forced oscillator model. An interesting extension of our work would be to study the effect of forcing other parameters in the model. Another possible extension could be to look at a case where the unforced system shows cohort cycles. These cycles are interesting because they only occur in structured populations, but they could not be computed accurately with the numerical methods we have used.

Predator–prey systems with fitness taxis

From an evolutionary perspective, we expect that animals behave in a way that optimizes their fitness. In a biological context, an animals fitness is its success in passing on its genes. In this chapter, we investigate the spatio-temporal pattern formations that can emerge when populations move to optimize their fitness. Linear stability analysis, a method to determine spatio-temporal pattern formations in models, is described in section 4.1. In section 4.2, we review some models used for studying pattern formation in ecology. The results from Paper II are presented in section 4.3, and some additional numerical results are presented in section 4.4. Finally, the results are discussed in section 4.5.

4.1 Linear stability analysis

Linear stability analysis is used to determine the onset of pattern formation in a model. It may also provide a description of the patterns close to the threshold, but as the system move away from the threshold, nonlinear terms of the system have an increasing effect and such a description is no longer applicable. In the following, we present the key points of a linear stability analysis and look at the information it relates. The presentation is based on [CH93, CG09].

We consider a system of partial differential equations

$$\frac{\partial u}{\partial t} = \mathcal{F}(u) \tag{4.1}$$

where the dependent variable $u(\boldsymbol{x}, t) \in \mathbb{R}^n$ is function of space $\boldsymbol{x}$ and time t. The right hand side of the system is a function of u and the spatial derivatives of u.

It is convenient to assume an infinite spatial domain $\boldsymbol{x} \in \mathbb{R}^d$ since this gives a translational invariant system and eliminates any boundary effects. The boundary effects can be considered separately afterwards; however we will not discuss how to do this here.

The starting point for a linear stability analysis is a uniform equilibrium solution $u(\boldsymbol{x},t) = u^*$ for the system (4.1). Such a solution represent a state with no pattern formation and a transition to pattern formation occurs when the solution changes from stable to unstable. The system is linearized around the uniform equilibrium by considering the addition of a small perturbation $\tilde{u}(\boldsymbol{x},t)$

$$u(\boldsymbol{x},t) = u^* + \tilde{u}(\boldsymbol{x},t) \, .$$

This solution is inserted into the system equations (4.1). Since the perturbation is assumed to be small, only terms that are first order in the perturbation are kept while higher order terms are discarded. This leads to a set of linear equations for the perturbation of the form

$$\frac{\partial \tilde{u}}{\partial t} = \mathcal{L}(\tilde{u}) \tag{4.2}$$

where $\mathcal{L}$ is a linear operator. This is the linearization of system (4.1) around the uniform equilibrium.

The next step is to use a general solution ansatz for the perturbation; in one spatial dimension, it reads

$$\tilde{u}(x,t) = u_0 e^{\lambda t} e^{ikx} \, . \tag{4.3}$$

This represent disturbances with wavenumber k that increase or decrease in time according to the growth rate λ. In more than one spatial dimension, the product kx is generalized to the inner product $\boldsymbol{k} \cdot \boldsymbol{x}$ and the wavenumber is the magnitude of the wave vector $\boldsymbol{k}$. When the system is translational invariant, the ansatz (4.3) is a solution to the linearized equations (4.2) for the perturbation. Inserting the ansatz into the linearized system gives a set equations that can be solved to obtain expressions of the form $\lambda_j(k)$, $j = 1, \ldots, n$. When the real part of all growth rates $\lambda_j(k)$ are negative for all wavenumbers k, the uniform state is stable, otherwise it is unstable. Real growth rates correspond to stationary perturbations and complex growth rates correspond to perturbations that oscillates in time.

The results from a linear stability analysis can be visualized by plotting the dispersion relation, that is, the largest real part of the growth rates $\max_j \operatorname{Re}(\lambda_j(k))$ as function of wavenumber k, see figure 4.1. When this function is negative for all wavenumbers k, the uniform equilibrium is stable, otherwise it is unstable. To see how pattern formation depends on a parameter p of the system, we can study how the dispersion relation varies with the value of p. We assume there is a critical value p_c, such that for $p < p_c$ the uniform equilibrium in stable and for $p > p_c$ the uniform equilibrium is unstable. This implies, that for $p = p_c$, there is a critical wavenumber k_c where $\max_j \operatorname{Re}(\lambda_j(k_c)) = 0$. If the parameter p is increased above its critical value, we might expect the initial pattern formation to have the wavelength $2\pi/k_c$.
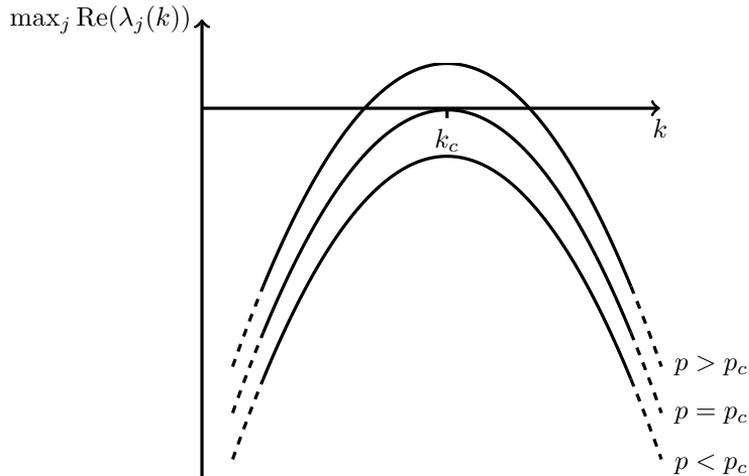
Figure 4.1: Schematic example of the dispersion relation for different parameter values p. The horizontal axis represents the wavenumber k and the vertical axis represent the growth rate $\mathrm{Re}(\lambda)$ *of perturbations to the system.*

For $p > p_c$, but still close to the threshold, the dispersion relation suggest that the possible wavelengths of the patterns correspond to the wavenumbers k where the function is positive, $\max_j \mathrm{Re}(\lambda_j(k)) > 0$.

Whether the solutions of the system indeed resemble the patterns predicted by the linear stability analysis depends on the nonlinear terms. If the transition at $p = p_c$ is a supercritical bifurcation such that the solution varies continuously with p in a neighborhood of $p = p_c$, we can expect the linearization gives an approximate description of the dynamics close to the threshold. As the system moves away from the uniform state, nonlinear terms gain increasing influence and other methods are needed to study the pattern formations.

4.2   Models for spatio-temporal pattern formation

4.2.1   Reaction–diffusion systems

Reaction–diffusion systems have been used extensively to study spatio-temporal pattern formation. A general reaction–diffusion model with two components u and v has the form

$$\frac{\partial u}{\partial t} = F(u,v) + D_1 \nabla^2 u \,, \tag{4.4a}$$

$$\frac{\partial v}{\partial t} = G(u,v) + D_2 \nabla^2 v \tag{4.4b}$$

where F and G constitutes the reaction dynamics and $D_i > 0$ are diffusion coefficients. A classic example of a pattern forming mechanism is the diffusion-driven

patterns first described by Turing in 1952 [Tur52]. The mechanism leads to stable spatial patterns in a reaction–diffusion model even though the reaction dynamics have a stable equilibrium in the absence of diffusion. Under certain conditions, introducing diffusion makes the equilibrium unstable and a Turing instability occurs, [Mur03]. A central condition for these instabilities is that the components u and v of the reaction have different diffusivities. This type of instability results in stationary spatial patterns in the shape of for example stripes or spots.

Turing originally considered the mechanism for a chemical system and suggested it as an explanation for morphogenesis; i.e., the development of pattern and form in the embryo. However, the ideas are valid for any reaction–diffusion system and have become popular in theoretical ecology. In a population model, diffusion represents random movement and the reaction terms consists of the local population dynamics, which include interactions between animals in addition to individual processes, such as reproduction and mortality. When the reaction dynamics themselves are oscillatory, a reaction–diffusion model can exhibit spatio-temporal patterns. For example, predator–prey systems with oscillatory population dynamics and diffusion have been shown to exhibit traveling waves and chaotic solutions [PM99, SLF95, She01].

4.2.2 Directed movement

Most animals do not move entirely at random, but will seek what they perceive to be favorable conditions. This can often be modeled by including taxis terms in the reaction–diffusion system (4.4), resulting in the general system

$$\frac{\partial u}{\partial t} = F(u,v) - \nabla \cdot \left(u\,\theta_1 \nabla v \right) + D_1 \nabla^2 u \,, \tag{4.5a}$$

$$\frac{\partial v}{\partial t} = G(u,v) - \nabla \cdot \left(v\,\theta_2 \nabla u \right) + D_2 \nabla^2 v \tag{4.5b}$$

where θ_i are taxis coefficients. The taxis term in the first equation represent that the individuals of population u moves with velocity $\theta_1 \nabla v$. Depending on the sign of θ_1, the individuals are either attracted to or repelled by high densities of v. An example of models with taxis terms are chemotaxis models where a population is attracted to a chemical substance [HP09].

Taxis terms are sometimes describes as cross-diffusion terms. A general system with reaction terms and cross-diffusion reads

$$\frac{\partial u}{\partial t} = F(u,v) + \nabla \cdot \left(c_{11} \nabla u + c_{12} \nabla v \right), \tag{4.6a}$$

$$\frac{\partial v}{\partial t} = G(u,v) + \nabla \cdot \left(c_{21} \nabla u + c_{22} \nabla v \right) \tag{4.6b}$$

where c_{ij} are called cross-diffusion coefficients for $i \neq j$. This corresponds to rewriting equations (4.5) using

$$\begin{pmatrix} c_{11} & c_{12} \\ c_{21} & c_{22} \end{pmatrix} = \begin{pmatrix} D_1 & -u\,\theta_1 \\ -v\,\theta_2 & D_2 \end{pmatrix}$$

Hence, a taxis system can always be written in the form of cross-diffusion. To avoid unphysical systems with negative concentration, there can be no flux of a population if its concentrations is zero. This is automatically fulfilled by the taxis formulation (4.5), but not for the cross-diffusion system (4.6) where it is necessary to require $c_{12} \to 0$ for $u \to 0$ and, correspondingly, $c_{21} \to 0$ for $v \to 0$. A linear stability analysis for a general cross-diffusion system is used to investigate the effect of cross-diffusion on the Turing instability in [KH11]. The results show that in some cases cross-diffusion promotes pattern formation and in other cases it represses pattern formation.

When u and v in equation (4.5) are the densities of prey and predators, the taxis can represent the predator pursuing the prey and the prey evading the predator. Systems with both pursuit and evasion taxis has been demonstrated to exhibit a new type of waves that, unlike typical diffusive waves, can reflect at boundaries and penetrate each other [TBHB04]. In two spatial dimension, pursuit–evasion systems can also show a variety of complicated spatio-temporal patterns [BBHT04]. In such systems, it has been found that pursuit taxis without evasion taxis tends to stabilize system and act against pattern formation [LHL09]. A variation to the taxis formulation in (4.5) have been proposed for predator–prey systems where the predators pursuit the prey [ATM+01, STA03]. An inertia of the pursuit movement is included, by letting the gradient of prey density affect the acceleration of the predators instead of affecting the velocity directly. As a contrast to systems with regular taxis, they find that the pursuit with movement inertia can lead to spatio-temporal patterns in the form of traveling waves.

From an evolutionary perspective, we expect that the movements of animals should help to optimize their fitness. For a population model, a good substitute for fitness is expressed by the specific growth rate. Therefore, animals moving towards places with higher fitness value can be expressed by a taxis in the direction of the gradient of the specific growth rate; we refer to this as fitness taxis. This form of taxis has been used to investigate the distribution of a population in a spatially heterogeneous environment [CCL08]. The work was extended to two competing populations and it was found that a population performing fitness taxis has an advantage over a similar population that only moves randomly [CCLX13].

4.3   Summary of results

In Paper II, we consider spatio-temporal pattern formation in a predator–prey system with fitness taxis. Specifically we derive the conditions for pattern formation and numerically investigate the solutions.

We consider a predator–prey model with fitness taxis and diffusion. The model describes the prey density $u(x, t)$ and the predator density $v(x, t)$ for the space

coordinate $x \in \Omega \subseteq \mathbb{R}$ and time $t > 0$:

$$\frac{\partial u}{\partial t} = f(u,v)u - \nabla \cdot \big(u\,\gamma_u \nabla f(u,v)\big) + D_u \nabla^2 u\,, \tag{4.7a}$$

$$\frac{\partial v}{\partial t} = g(u,v)v - \nabla \cdot \big(v\,\gamma_v \nabla g(u,v)\big) + D_v \nabla^2 v\,. \tag{4.7b}$$

The functions f and g expresses the specific growth rate of prey and predators, respectively. They are also used as a measure for the fitness level of the individuals in the associated population. The second term of each equation represent a fitness taxis, that is, animals moving towards higher values of fitness. The fitness taxis coefficients γ_u, γ_v represent the sensitivity to spatial difference for prey and predator, respectively. The diffusion represents random movement and the diffusion coefficients for the two populations are D_u, D_v.

To derive conditions for pattern formation, we perform a linear stability analysis of the system (4.7). It is assumed the population dynamics lead to a uniform equilibrium in the absence of taxis and diffusion. The analysis leads to three different scenarios for destabilizing the uniform equilibrium. It turns out that, in all scenarios, activator–inhibitor dynamics are necessary for pattern formation. The mechanisms that generate pattern formations in the three cases are prey taxis towards other prey, predator diffusion, and a combination of these two. The pursuit and evasion taxes does not appear to be central to the pattern formation. The results are summarized in table 4.1.

Case	Taxis driven	Taxis–diffusion driven	Diffusion driven
Instability	trace	determinant	determinant
Driving mechanisms	prey taxis	prey taxis and predator diffusion	predator diffusion
Ultra-violet catastrophe	yes	yes	no

Table 4.1: Summary of cases for pattern formation.

For the taxis-driven and the taxis–diffusion-driven instabilities, the dispersion relation indicates that the growth rate of a perturbation becomes infinitely large as the wavenumber goes to infinity. This is referred to an ultra-violet catastrophe and indicates the problem is not well-posed. To prevent this, we modify the population dynamics to include nonlocal interactions. Instead of the predator only has access to prey at the exact same location, the search region of the predator is distributed in the space around it. The search region of the predator is defined with a spatial kernel and leads to a new nonlocal system containing integrals over space in the expressions for the growth rates f and g. A linear stability analysis of the nonlocal system shows the ultraviolet catastrophe has disappeared. The mechanisms for

pattern formation are the same as for the local system, though there is no longer a clear distinction between the taxis–diffusion-driven instability and the diffusion-driven instability.

We compute numerical solutions for the nonlocal system for the case of zero diffusion and different values of the taxis coefficients. We find no stationary spatial patterns, only time-varying patterns; some of the patterns are periodic and others are irregular. The solutions show standing waves, traveling waves or a combination of the two. For all solutions, the densities for prey and predators show the same pattern, only the predator solution is delayed in time compared to the prey solution.

4.4   Further results

This section presents numerical results, that were not included in Paper II, for the fitness taxis system with nonlocal population dynamics. The system equations for prey density u and predator density v are repeated here

$$\frac{\partial u}{\partial t} = \mathcal{F}(u,v)u - \nabla \cdot \gamma_u u \nabla \mathcal{F}(u,v) + D_u \nabla^2 u\,, \tag{4.8a}$$

$$\frac{\partial v}{\partial t} = \mathcal{G}(u,v)v - \nabla \cdot \gamma_v v \nabla \mathcal{G}(u,v) + D_v \nabla^2 v\,. \tag{4.8b}$$

The nonlocal population dynamics based on the Bazykin model are defined by

$$\mathcal{F}(u,v)(x) = r\left(1 - \frac{u(x)}{K}\right) - a \int_\Omega \frac{\Phi(x,y)v(y)}{1+U(y)}\,\mathrm{d}y\,, \tag{4.9a}$$

$$\mathcal{G}(u,v)(y) = \frac{aU(y)}{1+U(y)} - 1 - cv(y) \tag{4.9b}$$

where

$$U(y) = \int_\Omega u(x)\Phi(x,y)\,\mathrm{d}x\,. \tag{4.10}$$

We use a Gaussian feeding kernel

$$\Phi(x,y) = \frac{1}{\sqrt{2\pi}\sigma}e^{-\frac{(x-y)^2}{2\sigma^2}} \tag{4.11}$$

with width parameter σ. The parameter value for the population dynamics are chosen, so the system has a stable uniform equilibrium in the absence of taxis and diffusion. We consider a finite one-dimensional space $x \in \Omega = [0, L]$ discretized with $N = 800$ points. The default parameter values are listed in table 4.2. Additional information about the implementation can be found in Paper II.

4.4.1   Fitness taxis and diffusion

In Paper II, there are numerical solutions for system (4.8) with no diffusion, in which case only the trace instability can occur. In this section, we consider a system with

Figure 4.2: Solutions for prey density $u(x,t)$ for the fitness taxis coefficients (γ_u, γ_v) indicated on the figure. The remaining parameters have default values, see table 4.2.

Figure 4.3: Solutions for prey density $u(x,t)$ for the fitness taxis coefficients (γ_u, γ_v) indicated on the figure. The remaining parameters have default values, see table 4.2.

Figure 4.4: Solutions for prey density $u(x,t)$ for the fitness taxis coefficients (γ_u, γ_v) indicated on the figure. The remaining parameters have default values, see table 4.2.
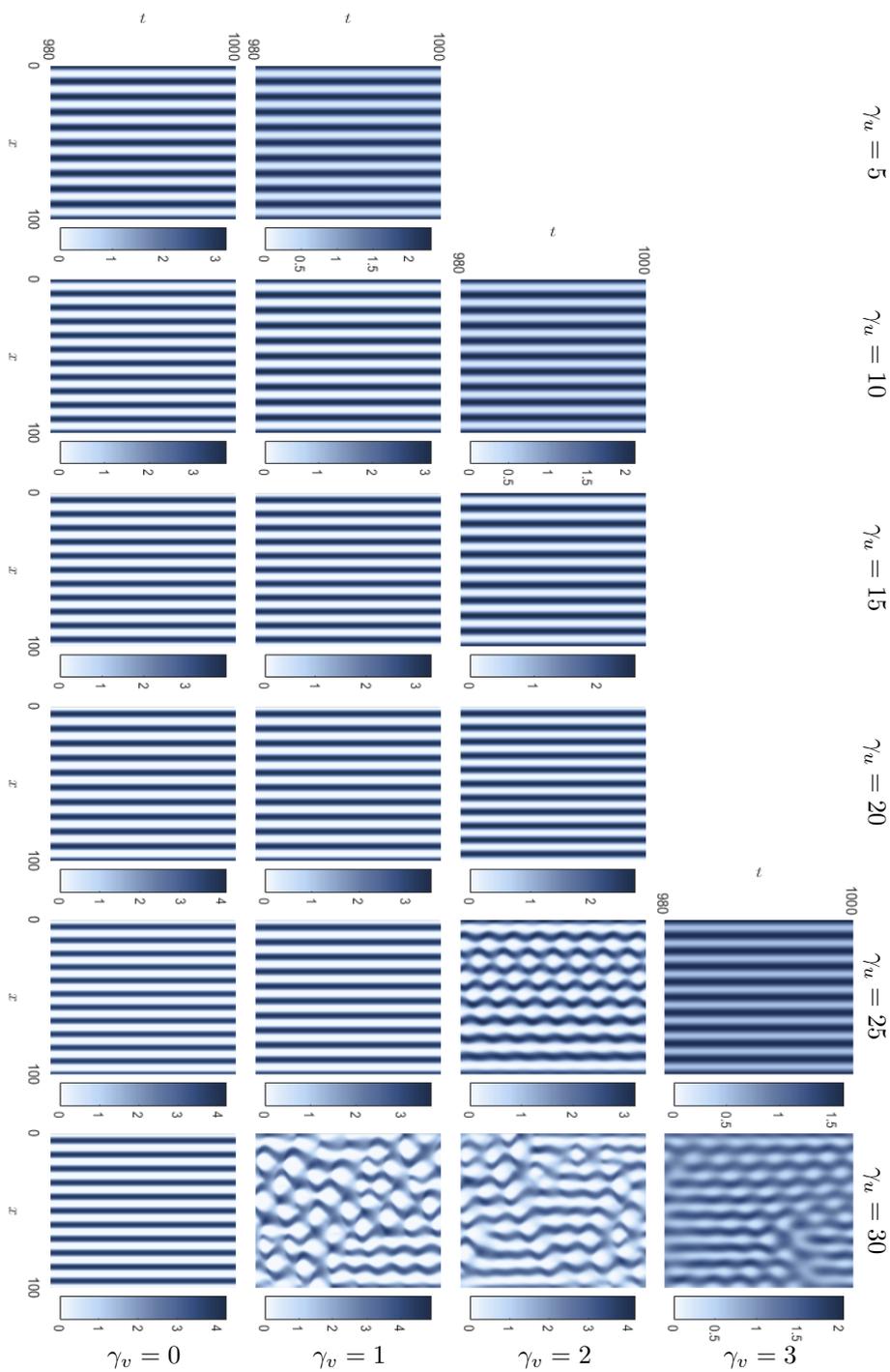
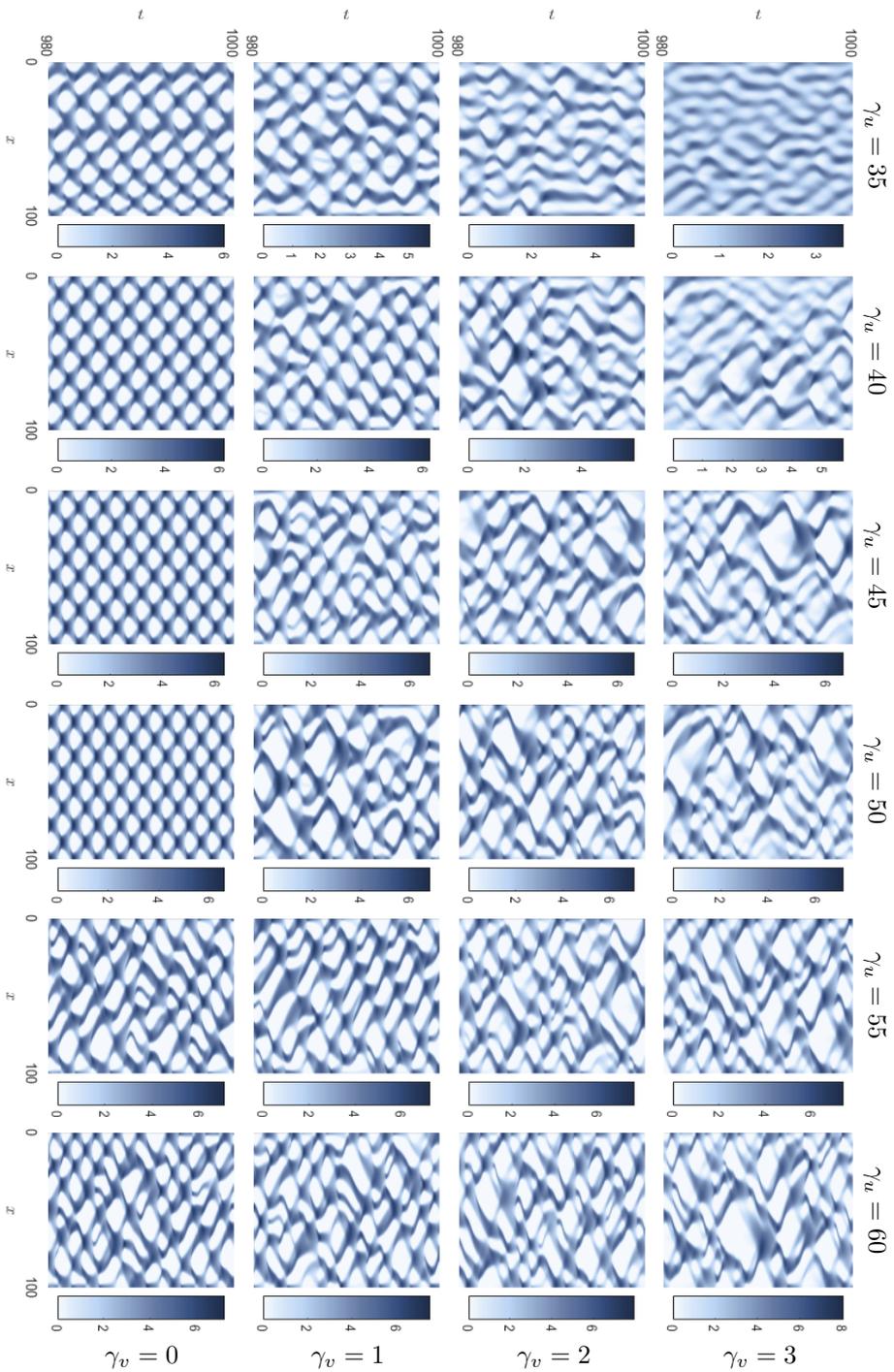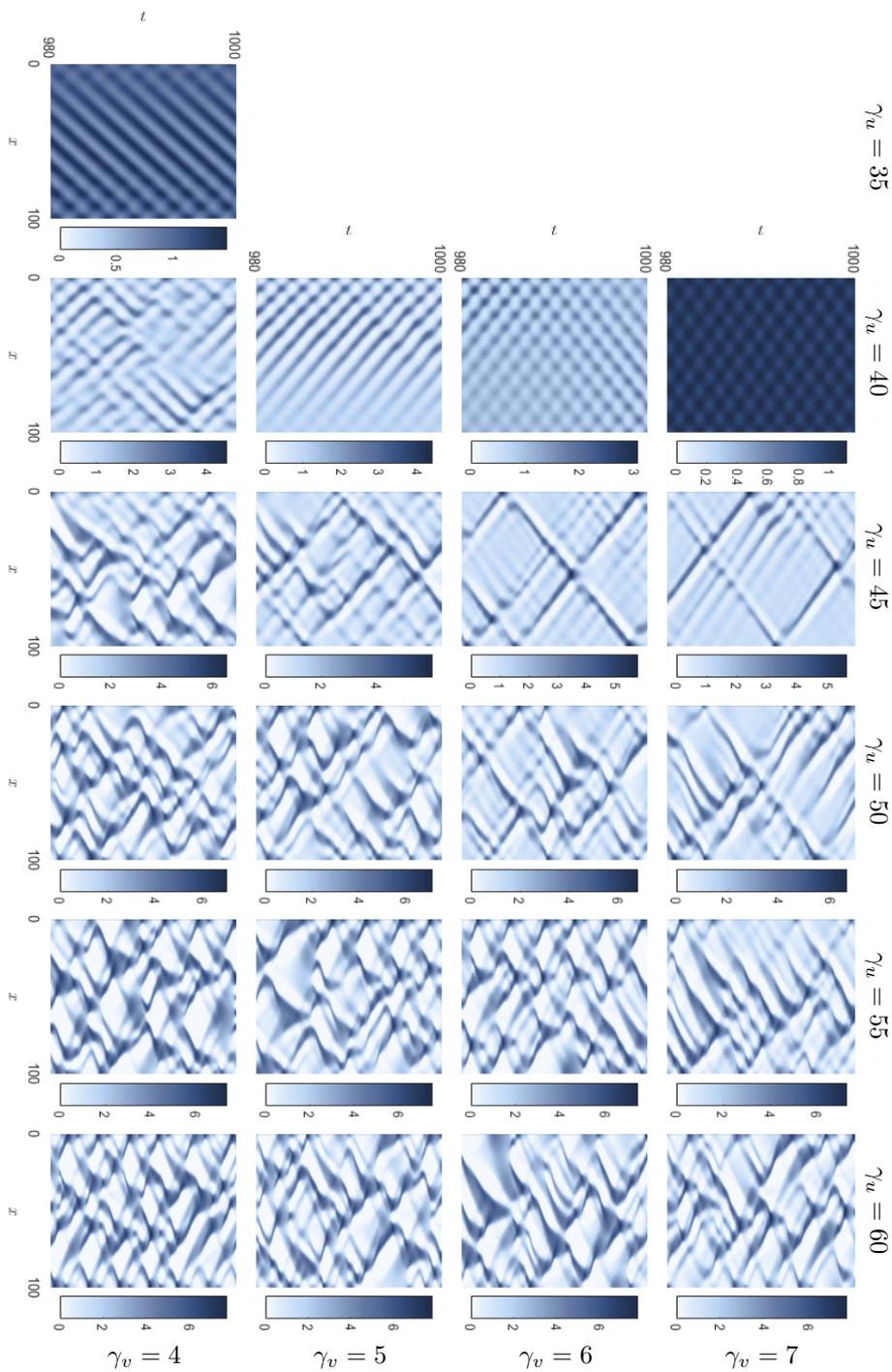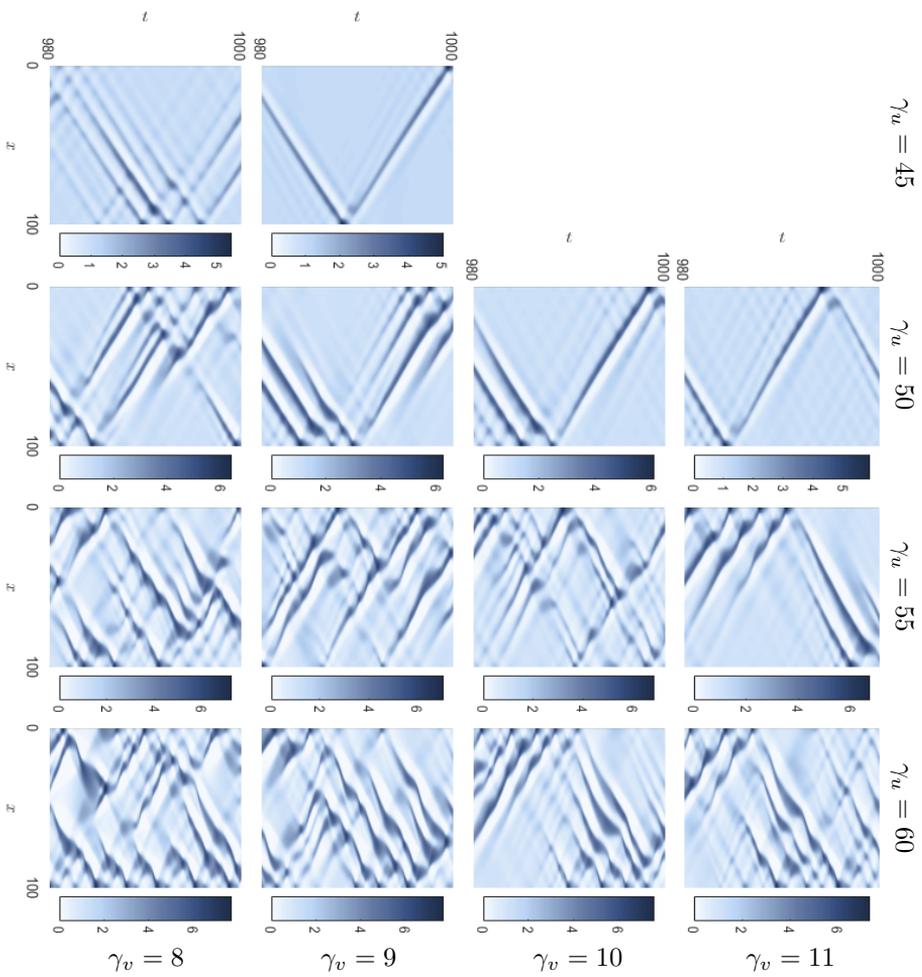Figure 4.5: Solutions for prey density $u(x,t)$ for the fitness taxis coefficients (γ_u, γ_v) indicated on the figure. The remaining parameters have default values, see table 4.2.

Parameter	r	a	c	K	D_u	D_v	L	σ
Value	2.8	5	1.5	28/3	1	15	100	1

Table 4.2: Default parameter values.

non-zero diffusion and this allows for both trace and determinant instabilities as the fitness taxis coefficients are varied. For the nonlocal system, the taxis–diffusion driven and the diffusion driven instabilities are no longer clearly separated and we only distinguish between pattern formation as a result of trace instability and determinant instability. We explore different values of the taxis coefficients γ_u and γ_v, while keeping all other parameters constant, see table 4.2. Figure 4.6 is a bifurcation diagram for the taxis coefficients indicating the regions for trace and determinant instabilities. Numerical solutions for different values of γ_u and γ_v are shown in figures 4.2-4.5; the solution are placed in a grid mimicking the bifurcation diagram in figure 4.6. For all the solutions, the predator densities is similar to the prey densities, only delayed in time and with lower amplitude. Therefore, only the solutions for the prey densities are shown.
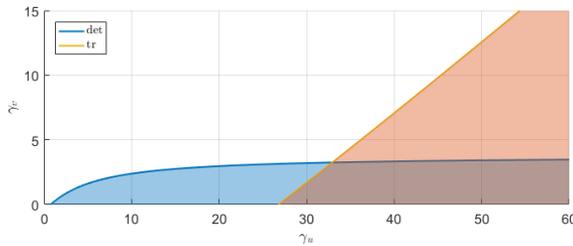

Figure 4.6: Bifurcation diagram in (γ_u, γ_v)-parameter space for system (4.8) indicating instability of the uniform equilibrium. The diffusion coefficients are $D_u = 1$, $D_v = 15$ and the population dynamics have default parameter values. The blue area indicates a determinant instability and the orange area indicates a trace instability.

First, we consider solutions in the parameter region where only the determinant instability occurs, see figure 4.2. The majority of these solutions have stationary spatial patterns with a regular spatial pattern of alternating high and low densities of animals. These pattern formations are similar to the diffusion driven patterns of a Turing instability. Near the onset of the trace instability, some of the solutions are no longer stationary and the spatial patterns show small oscillations in time.

Second, we consider solutions with parameter values belonging to the region with only the trace instability, see figures 4.4 and 4.5. All the solutions in this region show spatio-temporal patterns; some solutions are periodic and others are irregular. The periodic solution may consist of a series of standing waves resembling a checkerboard pattern, see for example the solution for $(\gamma_u, \gamma_v) = (40, 7)$ in figure 4.4. There are also periodic solutions with one or more traveling waves, see for example the solutions for $(\gamma_u, \gamma_v) = (45, 6)$ in figure 4.4 and $(\gamma_u, \gamma_v) = (45, 9)$ in figure 4.5 In

general, the solution patterns consist of a combination of traveling and standing
waves. The solution types in this region resemble the solutions for no diffusion
presented in Paper II.

Third, we consider the parameter region where both a trace and a determinant
instability occur, see figure 4.3. The solutions in this region mostly appear to be
a continuation of the spatio-temporal patterns in the region with only the trace
instability. Close to parameter region with only determinant stability, there are
stationary spatial patterns. The transition from stationary to time-varying solu-
tions occur close to the onset of the trace instability. When there is no predator
taxis $\gamma_v = 0$, some of the solutions have standings waves in all or a part of space.

Overall, the amplitude of the patterns increases with increasing prey taxis γ_u
and is mostly independent of predator taxis γ_v, except for parameter values close
to onset of pattern formation. There is only shown one solution for each set of
parameter values, though coexisting attractors were observed for several parameter
values.

4.5   Discussion

Our analysis show that in all cases pattern formation requires activator–inhibitor
dynamics. This is also required for Turing patterns where the patterns emerge
because the inhibitor (the predator) diffusive faster than the activator (the prey).
Compared to reaction–diffusion system, our system also includes fitness taxis, which
can facilitate or dampen this mechanism. The prey taxis causes the activator to
gather and move away from the inhibitor; both of which facilitate pattern forma-
tion. The predator taxis causes the inhibitor to disperse, which facilitate pattern
formation, and to pursue the activator, which act against pattern formation. The
activator–inhibitor mechanism in a system with fitness taxis can be viewed as the
prey gathering faster than the predator can follow.

We divide the pattern forming instabilities into three cases: taxis driven, taxis–
diffusion driven and diffusion driven, see table 4.1. The conditions for the diffusion
driven instability reduces to the conditions for a Turing instability when there is
no fitness taxis, and the diffusion driven patterns can be regarded as an extension
of Turing patterns. The taxis–diffusion instability comes from a combination of
prey gathering and predators diffusing. Similar to the diffusion driven instability,
this mechanism originates in a determinant stability and mostly creates stationary
patterns. As a contrast, however, this case induces an ultraviolet catastrophe. The
taxis driven instability is based solely on the gathering of prey. Mathematically
it differs from the other cases by causing a trace instability and the patterns are
spatio-temporal rather than stationary. It seems the mechanism in this case is very
different than the Turing mechanism.

It can be debated whether the mechanisms we have described are responsible
for pattern formation in real populations. The taxis driven and the taxis–diffusion
driven patterns are both facilitated by the prey having a high fitness taxis coefficient
compared to the predators. However, the restrictions on predator taxis comes

from the condition of stable reaction dynamics that leads to the requirement of activator–inhibitor dynamics. If this conditions is relaxed and oscillatory reaction dynamics are allowed, both prey and predator taxis could potentially facilitate pattern formation.

We consider a generic dimensionless model and therefore the time and length scales expressed in the patterns are also dimensionless. This makes it less clear how the patterns should be interpreted. In all numerical simulations, the solution for the predator density has closely resembled the prey density, only delayed in time and with a smaller amplitude. This is also reflected in the phase diagram, which typically shows the dynamics at a fixed point in space has the appearance of more or less regular predator–prey cycles. This suggests the patterns are a result of underlying processes in the population dynamics and that changes in density mainly reflect reproduction and mortality in the populations. On the other hand, the ultraviolet catastrophe suggest the patterns occur on a length scale that is comparable to the length scale of local interactions between individuals. Only by explicitly modeling the range of local interactions between predators and prey, was the infinitely short wavelengths avoided. This suggest it is the direct interactions between animals that shapes the patterns and such interactions could be considered for a much shorter time scale than the characteristic time scale of the population dynamics.

Conclusion

The overall topic of this thesis has been the spatial and temporal variations that occur in population densities of ecosystems. The aim was to investigate mechanisms behind such spatio-temporal variations. The thesis was divided into two specific projects. In the following, we conclude on each project and relate them to the overall theme.

The first project (chapter 3) investigated the effect of temporal variations in the environment on a size structured population. We considered a size structured population with periodic forcing of the resource. Variation of the forcing period and forcing amplitude showed similar dynamics to results for unstructured populations in the literature. Hence, our results indicate that the size structure of a population does not affects its response to imposed temporal variation. However, we did not investigate the case where the unforced size structured population displays cohort cycles. Cohort cycles are specific for structured populations and cannot occur in unstructured models and they could potentially yield interesting dynamics. This indicates a possible direction for further studies.

The second project (chapter 4) investigated the spatio-temporal pattern formations of in predator–prey system where individuals move towards higher values of fitness. We defined a generic predator–prey system with fitness taxis and diffusion, where fitness taxis refer to the populations moving in direction of higher individual fitness. The fitness values were quantified by the specific growth rates. The analysis showed that the fitness taxis was able to induce pattern formation in the system and the mechanism behind these patterns relied on the prey moving together. The numerical results showed a variety of pattern formations including stationary spatial patterns and spatio-temporal patterns. To conclude, the model with fitness taxis provides a framework for describing pattern formation and could potentially describe a mechanism for pattern formations in real ecosystems.

Bibliography

[ABG⁺16] K. H. Andersen, T. Berge, R. J. Gonçalves, M. Hartvig, J. Heuschele, S. Hylander, N. S. Jacobsen, C. Lindemann, E. A. Martens, A. B. Neuheimer, K. Olsson, A. Palacz, A. E. F. Prowe, J. Sainmont, S. J. Traving, A. W. Visser, N. Wadhwa, and T. Kiørboe. Characteristic sizes of life in the oceans, from bacteria to whales. *Annual review of marine science*, 8:217–241, 2016.

[Arn92] Vladimir I. Arnold. *Ordinary Differential Equations*. Springer, 3 edition, 1992.

[ATM⁺01] R. Arditi, Yu. Tyutyunov, A. Morgulis, V. Govorukhin, and I. Senina. Directed movement of predators and the emergence of density-dependence in predator–prey models. *Theoretical Population Biology*, 59(3):207–221, 2001.

[BBHT04] V. N. Biktashev, J. Brindley, A. V. Holden, and M. A. Tsyganov. Pursuit-evasion predator-prey waves in two spatial dimensions. *Chaos: An Interdisciplinary Journal of Nonlinear Science*, 14(4):988–994, 2004.

[CCL08] Robert Stephen Cantrell, Chris Cosner, and Yuan Lou. Approximating the ideal free distribution via reaction–diffusion–advection equations. *Journal of Differential Equations*, 245(12):3687–3703, 2008.

[CCLX13] Robert Stephen Cantrell, Chris Cosner, Yuan Lou, and Chao Xie. Random dispersal versus fitness-dependent dispersal. *Journal of Differential Equations*, 254(7):2905–2941, 2013.

[CdRP00] David Claessen, André M. de Roos, and Lennart Persson. Dwarfs and giants: Cannibalism and competition in size-structured populations. *The American Naturalist*, 155(2):219–237, 2000.

[CG09] Michael Cross and Henry Greenside. *Pattern formation and dynamics in nonequilibrium systems*. Cambridge University Press, 2009.

[CH93] M. C. Cross and P. C. Hohenberg. Pattern formation outside of equilibrium. *Reviews of Modern Physics*, 65(3):851, 1993.

[dR97] André M. de Roos. A gentle introduction to physiologically structured population models. In *Structured-population models in marine, terrestrial, and freshwater systems*, pages 119–204. Springer, 1997.

[dRMEL90] A. M. de Roos, J. A. J. Metz, E. Evers, and A. Leipoldt. A size dependent predator-prey interaction: who pursues whom? *Journal of Mathematical Biology*, 28(6):609–643, 1990.

[dRP13] André M. de Roos and Lennart Persson. *Population and community ecology of ontogenetic development.* Princeton University Press, 2013.

[Eva10] Lawrence C. Evans. *Partial Differential Equaions*, volume 19 of *Graduate Studies in Mathematics.* American Mathematical Society, 2 edition, 2010.

[FES00] Per Fauchald, Kjell Einar Erikstad, and Hege Skarsfjord. Scale-dependent predator–prey interactions: The hierarchical spatial distribution of seabirds and prey. *Ecology,*, 81(3):773–783, 2000.

[FGBS00] Jean-Marc Fromentin, Jakob Gjøsæter, Ottar N. Bjørnstad, and N. Chr. Stenseth. Biological processes and environmental factors regulating the dynamics of the norwegian skagerrak cod populations since 1919. *ICES Journal of Marine Science*, 57(2):330–338, 2000.

[FMS+06] Jan A. Freund, Sebastian Mieruch, Bettina Scholze, Karen Wiltshire, and Ulrike Feudel. Bloom dynamics in a seasonally forced phytoplankton–zooplankton model: trigger mechanisms and timing effects. *Ecological complexity*, 3(2):129–139, 2006.

[HP09] Thomas Hillen and Kevin J. Painter. A user's guide to PDE models for chemotaxis. *Journal of Mathematical Biology*, 58:183, 2009.

[HV13] Willem Hundsdorfer and Jan G. Verwer. *Numerical solution of time-dependent advection-diffusion-reaction equations*, volume 33. Springer Science & Business Media, 2013.

[KH11] Niraj Kumar and Werner Horsthemke. Effects of cross diffusion on turing bifurcations in two-species reaction-transport systems. *Physical Review E*, 83(3):036105, 2011.

[KMR92] Yu. A. Kuznetsov, S. Muratori, and S. Rinaldi. Bifurcations and chaos in a periodic predator-prey model. *International Journal of Bifurcation and Chaos*, 2(01):117–128, 1992.

[Kuz98] Yuri Kuznetsov. *Elements of applied bifurcation theory*, volume 112 of *Applied Mathematical Sciences.* Springer, 2 edition, 1998.

[LeV02] Randall J. LeVeque. *Finite volume methods for hyperbolic problems*, volume 31. Cambridge university press, 2002.

[LHL09]   J. M. Lee, T. Hillen, and M. A. Lewis. Pattern formation in prey-taxis systems. *Journal of biological dynamics*, 3(6):551–573, 2009.

[LHM+14]   Quan-Xing Liu, Peter M. J. Herman, Wolf M. Mooij, Jef Huisman, Marten Scheffer, Han Olff, and Johan van de Koppel. Pattern formation at multiple spatial scales drives the resilience of mussel bed ecosystems. *Nature communications*, 5:5234, 2014.

[MD86]   Johan A. Metz and Odo Diekmann. *The dynamics of physiologically structured populations*, volume 68. Springer, 1986.

[Mei07]   James D. Meiss. *Differential Dynamical Systems*. Mathematical Modeling and Computation. SIAM, 2007.

[MH08]   John M. McNamara and Alasdair I. Houston. Optimal annual routines: behaviour in the context of physiology and ecology. *Philosophical Transactions of the Royal Society of London B: Biological Sciences*, 363(1490):301–319, 2008.

[MM05]   Keith W. Morton and David Francis Mayers. *Numerical solution of partial differential equations: an introduction*. Cambridge university press, 2005.

[MMH+15]   Bailey C. McMeans, Kevin S. McCann, Murray Humphries, Neil Rooney, and Aaron T. Fisk. Food web structure in temporally-forced ecosystems. *Trends in ecology & evolution*, 30(11):662–672, 2015.

[Mur03]   James Dickson Murray. *Mathematical Biology II*, volume 18 of *Interdisciplinary Applied Mathematics*. Springer-Verlag New York, 3 edition, 2003.

[PLdR+98] Lennart Persson, Kjell Leonardsson, André M. de Roos, Mats Gyllenberg, and Bent Christensen. Ontogenetic scaling of foraging rates and the dynamics of a size-structured consumer-resource model. *Theoretical Population Biology*, 54(3):270–293, 1998.

[PM99]   S. V. Petrovskii and H. Malchow. A minimal model of pattern formation in a prey-predator system. *Mathematical and Computer Modelling*, 25(7):49–63, 1999.

[PRK03]   Arkady Pikovsky, Michael Rosenblum, and Jürgen Kurths. *Synchronization: a universal concept in nonlinear sciences*, volume 12 of *Cambridge Nonlinear Science Series*. Cambridge university press, 2003.

[RMK93]   Sergio Rinaldi, Simona Muratori, and Yuri Kuznetsov. Multiple attractors, catastrophes and chaos in seasonally perturbed predator-prey communities. *Bulletin of mathematical Biology*, 55(1):15–35, 1993.

[RvdK08] Max Rietkerk and Johan van de Koppel. Regular pattern formation in real ecosystems. *Trends in ecology & evolution*, 23(3):169–175, 2008.

[SdR17] Floor H. Soudijn and André M. de Roos. Approximation of a physiologically structured population model with seasonal reproduction by a stage-structured biomass model. *Theoretical Ecology*, 10(1):73–90, 2017.

[Sel06] Vidar Selås. UV-B-induced plant stress as a possible cause of ten-year hare cycles. *Population Ecology*, 48(1):71–77, 2006.

[SER⁺04] Nils Chr. Stenseth, Dorothee Ehrich, Eli Knispel Rueness, Ole Chr. Lingjærde, Kung-Sik Chan, Stan Boutin, Mark O'Donoghue, David A. Robinson, Hildegunn Viljugrein, and Kjetill S. Jakobsen. The effect of climatic forcing on population synchrony and genetic structuring of the Canadian lynx. *Proceedings of the National Academy of Sciences of the United States of America*, 101(16):6056–6061, 2004.

[She01] Jonathan A. Sherratt. Periodic travelling waves in cyclic predator–prey systems. *Ecology Letters*, 4(1):30–37, 2001.

[SKH⁺02] Nils Chr. Stenseth, Marte O. Kittilsen, Dag. Ø. Hjermann, Hildegunn Viljugrein, and Takashi Saitoh. Interaction between seasonal density-dependence structures and length of the seasons explain the geographical structure of the dynamics of voles in Hokkaido: an example of seasonal forcing. *Proceedings of the Royal Society of London B: Biological Sciences*, 269(1503):1853–1863, 2002.

[SLF95] Jonathan A. Sherratt, Mark A. Lewis, and Andrew C. Fowler. Ecological chaos in the wake of invasion. *Proceedings of the National Academy of Sciences*, 92(7):2524–2528, 1995.

[SMM97] Eckart Steffen, Horst Malchow, and Alexander B. Medvinsky. Effects of seasonal perturbations on a model plankton community. *Environmental Modeling and Assessment*, 2(1):43–48, 1997.

[SRKvN97] Marten Scheffer, Sergio Rinaldi, Yuri A. Kuznetsov, and Egbert H. van Nes. Seasonal dynamics of daphnia and algae explained as a periodically forced predator-prey system. *Oikos*, pages 519–532, 1997.

[SS93] Gary C. W. Sabin and Danny Summers. Chaos in a periodically forced predator-prey ecosystem model. *Mathematical Biosciences*, 113(1):91–113, 1993.

[SS08] Jonathan A. Sherratt and Matthew J. Smith. Periodic travelling waves in cyclic populations: field studies and reaction–diffusion models. *Journal of The Royal Society Interface*, 5(22):483–505, 2008.

[STA03]   Natalia Sapoukhina, Yuri Tyutyunov, and Roger Arditi. The role
          of prey taxis in biological control: a spatial theoretical model. *The
          American Naturalist*, 162(1):61–76, 2003.

[TBHB04] M. A. Tsyganov, J. Brindley, A. V. Holden, and V. N. Biktashev.
          Soliton-like phenomena in one-dimensional cross-diffusion systems: a
          predator–prey pursuit and evasion example. *Physica D: Nonlinear
          Phenomena*, 197(1):18–33, 2004.

[TSEP16] Uffe H. Thygesen, Lene Sommer, Karen Evans, and Toby A. Patter-
          son. Dynamic optimal foraging theory explains vertical migrations of
          bigeye tuna. *Ecology*, 97(7):1852–1861, 2016.

[TSW13]   Rachel A. Taylor, Jonathan A. Sherratt, and Andrew White. Sea-
          sonal forcing and multi-year cycles in interacting populations: lessons
          from a predator–prey model. *Journal of mathematical biology*, 67(6-
          7):1741–1764, 2013.

[Tur52]   A. M. Turing. The chemical basis of morphogenesis. *Philosophical
          Transactions of the Royal Society of London. Series B, Biological
          Sciences*, pages 37–72, 1952.

[TWS13]   Rachel A. Taylor, Andrew White, and Jonathan A. Sherratt. How
          do variations in seasonality affect population cycles? *Proceedings of
          the Royal Society B*, 280(1754):20122714, 2013.

[vdWdRP08] K. E. van de Wolfshaar, A. M. de Roos, and L. Persson. Popula-
          tion feedback after successful invasion leads to ecological suicide in
          seasonal environments. *Ecology*, 89(1):pp. 259–268, 2008.

[VSB01]   John Vandermeer, Lewi Stone, and Bernd Blasius. Categories of chaos
          and fractal basin boundaries in forced predator–prey models. *Chaos,
          Solitons & Fractals*, 12(2):265–276, 2001.

[Wig03]   Stephen Wiggins. *Introduction to Applied Nonlinear Dynamical Sys-
          tems and Chaos*, volume 2 of *Texts in Applied Mathematics*. Springer,
          2 edition, 2003.

APPENDIX A

Papers

I Dynamics of a physiologically structured population in a time-varying environment

Contents lists available at ScienceDirect

Ecological Complexity

Original Research Article

Dynamics of a physiologically structured population in a time-varying environment

Irene T. Heilmann [a,b,*], Jens Starke [a,c], Ken H. Andersen [b], Uffe Høgsbro Thygesen [b], Mads Peter Sørensen [a]

[a] Department of Applied Mathematics and Computer Science, Technical University of Denmark, Denmark
[b] Center for Ocean Life, National Institute of Aquatic Resources, Technical University of Denmark, Denmark
[c] School of Mathematical Sciences, Queen Mary University of London, United Kingdom

A B S T R A C T

Physiologically structured population models have become a valuable tool to model the dynamics of populations. In a stationary environment such models can exhibit equilibrium solutions as well as periodic solutions. However, for many organisms the environment is not stationary, but varies more or less regularly. In order to understand the interaction between an external environmental forcing and the internal dynamics in a population, we examine the response of a physiologically structured population model to a periodic variation in the food resource. We explore the addition of forcing in two cases: (A) where the population dynamics is in equilibrium in a stationary environment, and (B) where the population dynamics exhibits a periodic solution in a stationary environment. When forcing is applied in case A, the solutions are mainly periodic. In case B the forcing signal interacts with the oscillations of the unforced system, and both periodic and irregular (quasi-periodic or chaotic) solutions occur. In both cases the periodic solutions include one and multiple period cycles, and each cycle can have several reproduction pulses.

© 2016 Elsevier B.V. All rights reserved.

1. Introduction

Environmental variations are evident drivers of abundance and succession in temperate ecosystems (McMeans et al., 2015). Variations in the environment are changes in the abiotic environment, such as light and temperature, as well as in the biotic environment, such as presence of prey and predators. These conditions together affect processes such as growth and mortality for the individual. Variations may occur on very different time scales, ranging from diel patterns in light levels, over weather phenomena on weekly time scales and seasonal patterns in temperature, to decadal fluctuations such as governed by the North Atlantic Oscillation (NAO). Some of these variations are strictly periodic whereas others are less regular.

Here, we consider a model inspired by planktonic crustaceans. Planktonic crustaceans, such as daphnia in fresh water or copepods in marine environments, are subjected to environmental changes on daily to yearly time scales. They are multicellular organisms with a complex life cycle. The weight of each egg reaches approximately 1% of the individual biomass, and the eggs hatch to become nauplii which molt through successive stages to become adults. In the adult stage, all acquired food is going to survival (including building reserves) and to reproduction. The extended life implies that environmental variability can have complex effects on the organisms' life history. Planktonic crustaceans are a key link between primary producers and higher trophic levels (fish). An understanding of this link requires an understanding of how their life cycle is affected by a varying environment.

Existing literature concerning environmental variation in planktonic ecosystems has often modeled unstructured populations. Then, the ecosystem is represented as a Nutrient–Phytoplankton–Zooplankton (NPZ) model (Franks, 2002), where the zooplankton, representing planktonic crustaceans, is described by a single state variable representing their abundance or biomass. In Evans and Parslow (1985), for example, is considered a seasonal forcing that acts through influence of sunlight on photosynthesis of the phytoplankton. Studies of forcing in predator–prey models demonstrates a very rich dynamical behavior with period doublings, quasi-periodic and chaotic dynamics, as well as

* Corresponding author at: Department of Applied Mathematics and Computer Science, Technical University of Denmark, Denmark.
E-mail address: irhe@dtu.dk (I.T. Heilmann).

coexisting attractors (Rinaldi et al., 1993; Taylor et al., 2013; Vandermeer et al., 2001). These phenomena often arise in systems that oscillate even in the absence of forcing and for large forcing amplitudes. While these models illustrate the dynamics of forced systems of unicellular organisms well, they are unable to describe the life history of multi-cellular organisms such as planktonic crustaceans.

Physiologically structured population models are a well investigated class of models (de Roos and Persson, 2013; Metz and Diekmann, 1986). They are suited for modeling species when mass-specific rates of biomass productions and maintenance change significantly with the size of individuals (de Roos and Persson, 2013). In a constant environment, physiologically structured models can show equilibrium solutions as well as periodic solutions. The periodic solutions arise as a results of predator–prey dynamics or competition between adults and juveniles (de Roos and Persson, 2013). In Wolfshaar et al. (2008), a physiologically structured population model is considered with seasonal variation of environmental conditions as well as pulsed reproduction at a fixed time of year. The emphasis is on mortality and conditions for survival. Pulsed reproduction can cause similar effects to forcing, such as multiple year cycles, without explicit changes in environmental conditions. An example of this is found in Sun and de Roos (2015) for a physiologically structured population.

The aim of this paper is to analyze the response of a physiologically structured population subjected to a periodic variation of the resource production. We regard the periodic variation of the environment as a driving force of the population. If the system of the population model oscillates in a constant environment, the addition of a forcing term implies an interaction between two (or more) frequencies, and the system resembles that of a forced oscillator. Our approach is to take a well-known physiologically structured model for a daphnia population and its algae resource (de Roos, 1997). We look at two basic cases: one where the system oscillates even in the absence of forcing, and another where it reaches a stable equilibrium; and investigate the effect of adding forcing to each case. The emphasis is on the different dynamics that can occur.

2. Model

We use the Kooijman–Metz model, (de Roos et al., 1990; Kooijman and Metz, 1984), of a daphnia population feeding on an algae resource. Individual daphnia allocate energy from food intake between growth, basic metabolism and reproduction. The daphnia population is size structured, i.e., the model distinguishes between individuals of different size, whereas the algae resource is unstructured. The model was first presented in (Kooijman and Metz, 1984), where it is compared to experimental data, and in de Roos et al. (1990) the dynamic properties of the model are explored. We employ the specific formulation of the Kooijman–Metz model given in de Roos (1997):

$$\frac{\partial n(x,t)}{\partial t} + \frac{\partial g(F,x)n(x,t)}{\partial x} = -\mu n(x,t), \tag{1a}$$

$$\frac{dF(t)}{dt} = R(F) - \int_{x_0}^{x_m} I(F,x)n(x,t)dx, \tag{1b}$$

$$g(F,x_0)n(x_0,t) = \int_{x_0}^{x_m} b(F,x)n(x,t)dx. \tag{1c}$$

Eq. (1a) describes the time evolution of the daphnia population density distribution $n(x,t)$ over the length x of an individual at time t. The daphnia have a somatic growth rate $g(F,x)$ and a constant

mortality rate μ. The concentration of algae $F(t)$ evolves according to (1b); the algae grow at the rate $R(F)$ in the absence of daphnia. The integral in (1b) represents daphnia ingesting algae at the rate $I(F,x)$. The combined reproduction of the daphnia population gives rise to the boundary condition (1c) at x_0, the length of a daphnia at birth. We will present expressions for the functions in (1) shortly.

The model presented here is specifically adapted to daphnia and algae, but the assumptions and basic mechanisms behind the model could also apply to other species, such as marine copepods. As such, the Kooijman–Metz model represents a broader class of predator–prey models (de Roos et al., 1990). It resembles the Rosenzweig–MacArthur model in the sense that without size structure, i.e., if all individuals are assumed to have the same length x, the system (1) reduces to the Rosenzweig–MacArthur model, see de Roos et al. (1990) and de Roos (1997) for details.

In the following, we present the functions entering the system (1). The expressions are based on the daphnia's allocation of energy to different processes, and a detailed derivation is given in de Roos (1997). The daphnia's encounter of algae F is proportional to a Holling type II functional response,

$$h(F) = \frac{F}{F_h + F},$$

where F_h is the half-saturation constant. The ingestion rate $I(F,x)$ of daphnia is proportional to the surface area of the individual and to the functional response, giving

$$I(F,x) = \nu h(F)x^2, \tag{2}$$

where ν is a proportionality constant. The somatic growth rate of daphnia is

$$g(F,x) = \gamma(x_m h(F) - x), \tag{3}$$

where x_m is an upper bound on the length a daphnia can achieve, and γ is a proportionality constant. The maximum length of an individual thus depends on the available energy. Individuals become mature and start to reproduce when they reach a specific length x_j. Individuals above this length allocate a fixed proportion of their energy intake to reproduction. This gives a birth rate of the form

$$b(F,x) = \begin{cases} r_m h(F)x^2 & \text{for } x \geq x_j, \\ 0 & \text{for } x < x_j, \end{cases} \tag{4}$$

where r_m is a proportionality constant. Finally, the algae are assumed to have logistic growth $R(F)$ in the absence of predators:

$$R(F) = \alpha F\left(1 - \frac{F}{K}\right). \tag{5}$$

Here, α is the specific growth rate of algae and K is the carrying capacity of algae. In the basic model, $\alpha = \alpha_0$ is constant. The default parameter values are listed in Table 1 and are from de Roos (1997).

The system (1) can exhibit four types of solutions (de Roos et al., 1990; de Roos, 1997) depending on daphnia mortality μ and carrying capacity K of the algae. The daphnia population can go extinct, i.e., $n(x,t) = 0$ for all x and t, or reach a positive equilibrium, i.e., $n(x,t) = n(x)$ for all t, with a positive number of individuals in the daphnia population. Furthermore, the system can show periodic solutions, categorized as either cohort cycles or predator–prey cycles (de Roos, 1997). For cohort cycles, the population is dominated by a cohort of individuals concentrated around a single length x. When the individuals in the cohort grows larger and reaches maturity, they give birth to a new cohort that eventually takes over. The mechanism in predator–prey cycles is that first the amount of prey increases, which leads to an increase of the predator. This in turn causes the prey to diminish, which leads to a decrease of the predator, and then the cycle repeats itself. In our

Table 1
Variables and parameter values.

Symbol	Value	Unit	Description
x	–	mm	Length of individual
t	–	day	Time
$F(t)$	–	mgC/L	Density of algae food resource
$n(x, t)$	–	1/L	Number density distribution of daphnia population
x_0	0.6	mm	Length at birth
x_j	1.4	mm	Length at maturity
x_m	3.5	mm	Largest possible length for any conditions
F_h	0.164	mgC/L	Half-saturation resource level
γ	0.11	1/day	Somatic growth constant
r_m	1.0	$1/(\text{day mm}^2)$	Birth rate constant
ν	0.007	$\text{mgC}/(\text{day mm}^3)$	Ingestion constant
α_0	0.5	1/day	Specific resource growth rate
K	[0;1]	mgC/L	Carrying capacity of resource
μ	[0;0.3]	1/day	Mortality
a_f	[0;1]	–	Strength of forcing
T_f	[5;100]	day	Period of forcing

case, the daphnia population plays the role of the predator and the algae act as the prey. Predator–prey cycles are also called paradox of enrichment oscillations (Rosenzweig et al., 1971), and are similar to the oscillations in Lotka–Volterra models. The transition between cohort and predator–prey cycles in the model (1) is gradual and some solutions have characteristics of both types. The existence and stability of the different solution types depends on the parameter values.

Fig. 1 is a bifurcation diagram showing regions where different solution types exist and are stable. The parameters varied are the daphnia mortality μ and the carrying capacity K of the algae. We have used the criteria presented in de Roos et al. (1990) and de Roos (1997) to distinguish between solution types. The solutions to the equations are continued using the continuation software Coco (COCO, 2013; Dankowicz and Schilder, 2013) for Matlab (MATLAB, 2014). The solid blue line in Fig. 1 shows the existence boundary for the equilibrium solution with a non-zero number of daphnia. Below this line, the only solution is the equilibrium with zero daphnia. Based on the linear stability analysis in de Roos et al. (1990) and de Roos (1997), the dash-dot red line depicts where the positive equilibrium solution looses stability and a periodic solution emerges, corresponding to a Hopf bifurcation. An approximate separation between cohort cycles and predator–prey

Fig. 1. Bifurcation diagram for the system (1) in (μ, K)-parameter space. The solid blue line defines the boundary of existence of the positive equilibrium solution, and the dash-dot red line shows when this solution becomes unstable. Below the solid blue line only the equilibrium solution with zero daphnia exists, and above the dash-dot red line periodic solutions emerge. The dotted green line indicates an approximate boundary between the cohort and predator–prey cycles. The points marked A and B represents the two parameter cases we will use. (For interpretation of the references to color in this figure legend, the reader is referred to the web version of this article.)

cycles is indicated by the dotted green line. The transition is not characterized by a bifurcation, but by a descriptive criterion derived in de Roos et al. (1990). The criterion comes from comparing the stability conditions for the structured model to those for a corresponding unstructured model. The Hopf line has two small hairpin turns close to $\mu = 0.05$, which differs from a corresponding bifurcation diagram in de Roos (1997); presumably this is because we use a continuation approach that captures more details. We will use the parameter values indicated by the points A ($\mu = 0.25$ day^{-1}, $K = 0.5$ mgC/L) and B ($\mu = 0.25$ day^{-1}, $K = 0.7$ mgC/L) as representative cases for an equilibrium solution and a periodic solution, respectively.

The discontinuity of the birth rate function $b(F, x)$ in Eq. (4) at $x = x_j$, leads to ambiguity of certain solutions with cohort cycles, but otherwise the model is well-posed (Thieme, 1988). We will not investigate solutions with cohort cycles, so we expect the solutions are uniquely defined, even when the forcing term introduces a smooth variation of parameters.

2.1. Forcing

We proceed to introduce variation of the environment in the model (1). This can be done by letting one or more of the parameters vary with time. In Rinaldi et al. (1993), they investigate six different choices of parameters for applying periodic variation to the Rosenzweig–MacArthur model, and conclude that all six possibilities give qualitatively similar results. Here, we follow the approach by Freund et al. (2006), Taylor et al. (2013), Vandermeer et al. (2001) and introduce the forcing via the resource growth rate, α, to reflect variations in for example light and nutrient conditions. Numerical investigations reveal that this parameter has very little influence on the bifurcation diagram in Fig. 1 close to the points A and B, which is consistent with the analysis in de Roos et al. (1990). Therefore, the system does not switch between regions of the bifurcation diagram when α changes with time, and the effects of forcing will not be mixed with qualitative changes in the basic model. For a system with no daphnia, forcing of the algae growth rate, α, results in the algae stabilizing at the carrying capacity K. However, the systems we are considering are never close to extinction of daphnia, so we do not expect to see such equilibrium solutions.

The environmental variation is implemented as a sinusoidal change of the algae growth rate, α, that now becomes time-dependent:

$$\alpha(t) = \alpha_0 \left(1 + a_f \sin\left(\frac{2\pi}{T_f} t\right)\right). \tag{6}$$

We keep the mean value fixed to the default value, α_0, from the original model. The amplitude, $a_f \in [0, 1]$, is a measure of the magnitude of the variations, and T_f defines the period of the variations.

We are interested in the relation between the time scale of the forcing, T_f, and a time scale of the internal dynamics of the unforced system, T_{sys}, so we introduce the ratio: $\theta = T_f/T_{sys}$. If the unforced system (1) exhibits stable oscillations, we define the time scale T_{sys} as the period of these oscillations, and compute it directly from the solution. The parameter values in case B give an oscillatory solution with an estimated period of $T_{sys} \approx 27.6$ days. When the unforced population dynamics display damped oscillations towards a stable equilibrium, we define the time scale T_{sys} as the quasi-period of such small-amplitude transient oscillations. To estimate this value, we numerically compute the Jacobian of the discretized system at the equilibrium; the discretization of the system is described in Section 2.2. The quasi-period is determined from the imaginary part of the dominating eigenvalue of the Jacobian. An example of such dynamics arises for the parameter
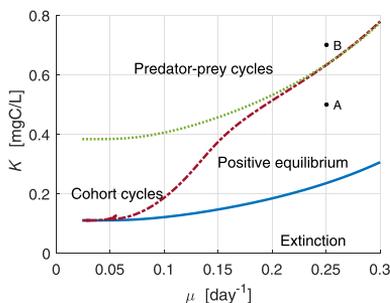
values in case A where the period is approximately $T_{sys} \approx 27.4$ days. We have varied the forcing period in the range $T_f \in [5, 100]$ days as simulations revealed the most interesting dynamics for these values.

2.2. Numerical integration

For the Kooijman–Metz model in (1), analytic solutions exist for the equilibrium solutions, but not for the periodic solutions. With the addition of forcing, the system becomes more complex and hence we concentrate on numerical solutions. We use the method of lines (Iserles, 2009; LeVeque, 2007), and discretize the partial differential equation (PDE) given by (1a) in the size variable x. This leaves a system of ordinary differential equations (ODEs) in time t, which we integrate with a fourth order Runge–Kutta method using MATLAB's ODE solver `ode45` (MATLAB, 2014). As Eq. (1a) is a type of advection or transport equation with velocity $g(F, x)$, we discretize with a first order upwind scheme (Iserles, 2009; LeVeque, 2007), where the upwind direction changes with the sign of $g(F, x)$. Simulations indicates that 300 linearly distributed discretization points is ample for resolving the solution, and we use this number in all computations. For each set of parameter values, the system is integrated in time until the solution has settled to a stable stationary or periodic state.

3. Results

3.1. Population without self-oscillations

In this section we examine the effect of the forcing (6) to the system (1) with the parameters in case A ($\mu = 0.25$ day^{-1},

$K = 0.5$ mgC/L; see Fig. 1). Without forcing, this system has a stable equilibrium solution with a non-zero daphnia population, see Fig. 2a, and transient oscillations with a period of $T_{sys} \approx 27.4$ - days, see Section 2.1. A typical solution to the forced system is stable periodic oscillations, that resembles predator–prey cycles, see Fig. 2b.

First, the forcing period is kept fixed at $T_f = 30$ days, which is close to the time scale of the unforced system T_{sys}, giving the time scale ratio $\theta \approx 1.1$. For this period, we consider a series of examples with increasing value of the forcing amplitude a_f, see Fig. 3. For each amplitude, the system is integrated until the solution has settled to a stable stationary or periodic state. To characterize the population distribution $n(x, t)$ with a single measure (for each point in time), we use the birth rate of the entire population,

$$B(t) := \int_{x_0}^{x_m} b(F, x) n(x, t) \mathrm{d}x. \tag{7}$$

This is also the right hand side of the boundary condition (1c). Initially, the solution locks in phase with the forcing, and the amplitude of the birth rate increases with the forcing amplitude a_f (Fig. 3a). Increasing the forcing amplitude further leads to a period doubling (Fig. 3b). After the period doubling, the solution changes gradually from having one dominating birth pulse for every forcing period T_f, to having one for every two forcing periods. This is a typical pattern for case A when keeping the forcing period T_f fixed and varying the forcing amplitude a_f.

For a more detailed exploration of the population's response to changes in the forcing amplitude, we do a systematic parameter sweep. This entails we repeatedly change the parameter a_f a small amount and integrate the system in time until it has settled to a stable stationary or periodic state. The final solution is used as the
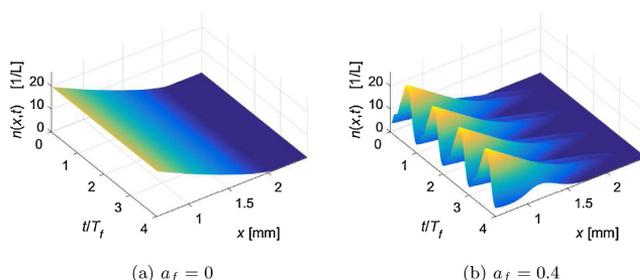

(a) $a_f = 0$ (b) $a_f = 0.4$

Fig. 2. Examples of solutions for the population density distribution $n(x, t)$ in case A ($\mu = 0.25$ day^{-1}, $K = 0.5$ mgC/L). (a) The unforced system has a stable stationary solution. (b) The forced system, with forcing amplitude $a_f = 0.4$ and forcing period $T_f = 30$ days, has a stable periodic solution with period $T_{sol} = T_f$.
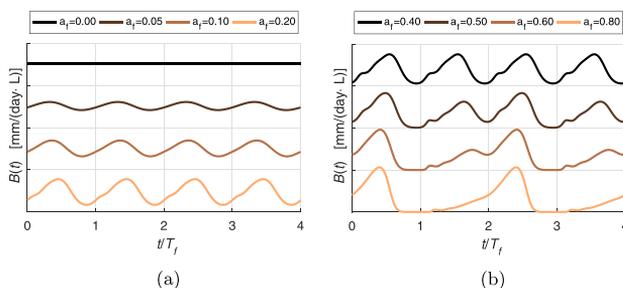

(a)   (b)

Fig. 3. Combined birth rate $B(t)$ of the population in case A ($\mu = 0.25$ day^{-1}, $K = 0.5$ mgC/L). The forcing period is kept constant for a time scale ratio of $\theta \approx 1.1$, while the forcing amplitude a_f is varied. Each section on the vertical axis represents the interval [0;6] mm/(day L). (a) The non-oscillating solution locks to the phase of the forcing and the amplitude of the birth rate increases with a_f. (b) As a_f increases further, the birth rate changes in a period doubling.

starting point in the next iteration. Experimenting showed that the transient behavior has vanished after 100 forcing periods or at least 3000 days. To have a sample of the steady state solution, the solution is integrated for 12 forcing periods or at least 360 days after the transient has vanished. For oscillatory solutions with a period up to four forcing periods, this gives a sample of at least three whole periods. First, a forward sweep runs through the values $a_f = 0, 0.1, \ldots, 1$ and then a backward sweep goes through the same values, but in opposite direction. To get an overview of the results, we characterize each solution with a few measures, which are described in the following. Fig. 4 shows the results of a parameter sweep where the forcing period is again kept constant at $T_f = 30$ days, giving the time scale ratio $\theta \approx 1.1$.

The first characteristic measure of the solutions is the local maxima B_{max} of the birth rate $B(t)$. For each iteration in the parameter sweep the values of all the local maxima, occurring after the transient behavior, are recorded and plotted against the forcing amplitude a_f, see Fig. 4a. In other words, for each peak in the birth rate $B(t)$ there is a dot indicating the height of the peak. This gives multiple points for each value of a_f, where some or all the points may coincide. The birth rate has a single repeated pulse for $a_f < 0.47$, indicating a periodic solution. However, the period of the cycle cannot be determined from this figure, as the time steps between the maxima are not shown. At $a_f \approx 0.47$, the single branch

(a)

(b)

Fig. 4. Parameter sweep in the forcing amplitude a_f for case A ($\mu = 0.25$ day^{-1}, $K = 0.5$ mgC/L) with a forcing period corresponding to the time scale ratio $\theta \approx 1.1$. The figures indicate a period doubling at $a_f \approx 0.47$ and $a_f \approx 0.97$. (a) The local maxima B_{max} of the combined birth rate for each value of a_f. (b) The period of the solution, T_{sol}, and the average time between birth pulses, δ.

divides into two, indicating a period doubling. Along with the period doubling, a third branch of maxima appears clearly below the other branches. Comparing with Fig. 3, this branch is identified as small extra peaks on the function $B(t)$.

Another characteristic measure of a solution is its period T_{sol}. The period is determined by sampling the settled solution at time intervals of length T_f, and comparing the solution at these sample points. This is used to determine whether the solution period is an integer multiple of the forcing period. The solution period T_{sol} is plotted against the forcing amplitude a_f, see Fig. 4b. The solution period jumps directly from $T_{sol} = T_f$ to $T_{sol} = 2T_f$ confirming there is a period doubling at $a_f \approx 0.47$.

We will use one more characteristic measure of a solution. The solution shifts gradually from having one birth pulse every T_f to having one pulse every $2T_f$ (Fig. 3b), and this is not reflected in the solution period that changes abruptly. Therefore, we introduce the average time distance between consecutive birth pulses, denoted δ. To compute the number of birth pulses, the notion of total variation $V_{[a,b]}(B)$, of the birth rate function B, is employed,

$$V_{[a,b]}(B) = \int_a^b |B'(t)| \, dt.$$

This reflects the sum of all the increases and decreases in the function value $B(t)$ in the interval $[a, b]$. Furthermore, the amplitude $A_{[a,b]}(B)$ of the birth rate function $B(t)$ taken for the interval $[a, b]$ is given by

$$2A_{[a,b]}(B) = \max_{t \in [a,b]} B(t) - \min_{t \in [a,b]} B(t).$$

We define the number of (full size) birth pulses $P_{[a,b]}(B)$ in a time interval $[a, b]$ as the total variation in units of the amplitude:

$$P_{[a,b]}(B) = \frac{V_{[a,b]}(B)}{4A_{[a,b]}(B)}.$$

The factor 4 comes from considering a continuous function $B(t)$ that is periodic on the interval $[a, b]$. For such a function, the total variation will measure the height of every peak twice, since each peak goes both up and down. In addition, the amplitude will measure half the height of the biggest peak. Dividing with the length of the time interval gives the average number of birth pulses per time, $\Gamma = P_{[a,b]}(B)/(b - a)$. The inverse value, $\delta = \Gamma^{-1}$, corresponds to the average time between two full birth pulses,

$$\delta = \frac{b - a}{P_{[a,b]}(B)}. \qquad (8)$$

The length of the time interval, $\Delta t = b - a$, should be an integer multiple of the forcing period T_f, and for periodic solutions it should also be an integer multiple of the solution period T_{sol}. Further, the solution is assumed to have reached a stable stationary or periodic state at time $t = a$. The value of δ is computed for each iteration in the parameter sweep, see Fig. 4b. After the period doubling at $a_f \approx 0.47$, the average time between birth pulses changes gradually from $\delta = T_f$ to $\delta = 2T_f$.

Combining the information from the different measures of the solution, we summarize the results of the parameter sweep for the time scale ratio $\theta \approx 1.1$ (Fig. 4). The solution locks in phase with the forcing for $a_f < 0.47$ with a single pulse in each forcing period, $\delta = T_f$. At $a_f \approx 0.47$, there is a period doubling followed by a gradual change in the solution to a birth pulse every $\delta = 2T_f$. At $a_f \approx 0.97$, there is another period doubling resulting in a period of $4T_f$.

Repeating the procedure of a parameter sweep for different forcing periods $T_f = 5, 6, \ldots, 100$ days and combining the results, leads to a bifurcation diagram in the parameters a_f and $\theta = T_f/T_{sys}$, see Fig. 5. For all forcing periods the solution immediately phase
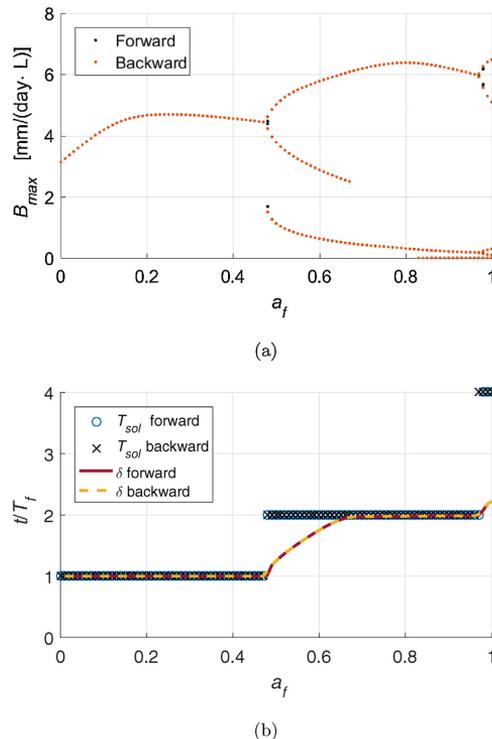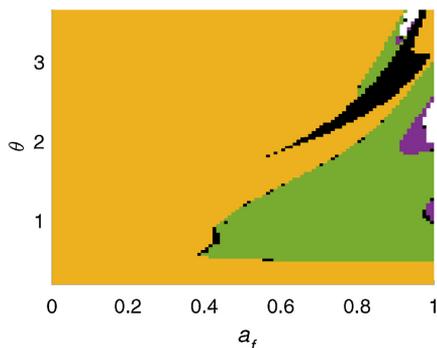
Fig. 5. Bifurcation diagram for case A (μ = 0.25 day^{-1}, K = 0.5 mgC/L) with parameters for the forcing amplitude a_f and the time ratio $\theta = T_f/T_{sys}$. The colors indicate the solution period T_{sol} in units of T_f, $T_{sol} = T_f$ is orange, $T_{sol} = 2T_f$ is green, and $T_{sol} = 4T_f$ is purple. White indicates $T_{sol} > 4T_f$ or that no period was found, while black indicates the forward solution was different from the backward solution. (For interpretation of the references to color in this figure legend, the reader is referred to the web version of this article.)

locks to the forcing when the forcing amplitude is increased above 0. There are no period doublings for amplitudes less than $a_f \approx 0.37$ or for time scale ratios less than $\theta \approx 0.37$. When θ increases, period doublings occur for larger values of forcing amplitude a_f.

Transients times become very large close to the period doublings, and hence the forward and the backward solutions

do not completely agree, since the simulations are for finite time. Therefore, we observe a hysteresis-like phenomenon, and in the theory of phase transitions this is referred to as critically slowing down (Ma, 1976). There is also an area with hysteresis (black) for large a_f and large θ, where the forward and backward solution are clearly distinct.

3.2. Self-oscillating population

In this section, we turn our attention to case B (μ = 0.25 day^{-1}, K = 0.5 mgC/L; see Fig. 1) and investigate the effect of adding forcing to the system (1), using the same approach as in case A. Without forcing, case B gives an oscillatory solution with predator–prey driven cycles, see Fig. 6a, and has a period of $T_{sys} \approx 27.6$ days (see Section 2.1). In Fig. 6b, an example is shown of the forced system where the solution locks to the forcing, that is $T_{sol} = T_f$. The solution still resembles the predator–prey cycles from the unforced system, except every other bloom of the population has a larger amplitude.

First we consider a forcing with constant period T_f = 60 days, giving the time scale ratio $\theta \approx 2.2$. The combined population birth rate $B(t)$ is plotted for different forcing amplitudes a_f, see Fig. 7. For small forcing amplitude a_f, the solution resembles the unforced solution, but the pulses are irregular. Increasing a_f results in phase locking with the forcing, where the birth rate has two pulses repeating every period. When a_f is increased further, the solution first becomes irregular and eventually periodic again, but now there is only one birth pulse in each period.

We proceed as for case A and make a parameter sweep where the forcing amplitude a_f is varied in small steps while the forcing period T_f is kept fixed. Again the local maxima B_{max} of the birth rate function $B(t)$ are recorded, as well as the solution period T_{sol} and the
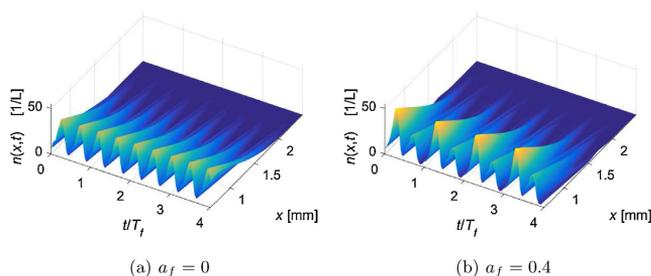
Fig. 6. Examples of solutions for the population density distribution $n(x, t)$ in case B (μ = 0.25 day^{-1}, K = 0.7 mgC/L). (a) The unforced system has a stable periodic solution with period $T_{sol} \approx T_f/2.2$. (b) The forced system, with forcing amplitude a_f = 0.4 and forcing period T_f = 60 days, has a stable periodic solution with period $T_{sol} = T_f$.

Fig. 7. Combined birth rate $B(t)$ of the population in case B (μ = 0.25 day^{-1}, K = 0.7 mgC/L). The forcing period is kept constant for a time scale ratio of $\theta \approx 2.2$, while the forcing amplitude a_f is varied. Each section on the vertical axis represents the interval [0;10] mm/(day L). The function changes between being irregular and periodic.

(a)

(b)

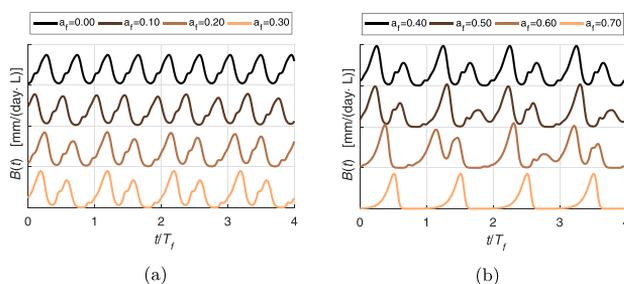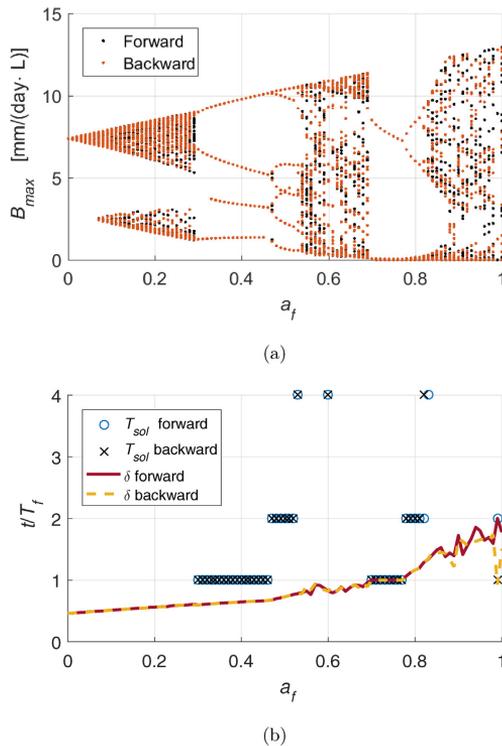**Fig. 8.** Parameter sweep in the forcing amplitude a_f for case B ($\mu = 0.25$ day^{-1}, $K = 0.7$ mgC/L) with a time scale ratio $\theta \approx 2.2$. (a) The local maxima B_{max} of the birth rate for each value of a_f. There are regions with periodic solutions and period doublings, and regions with irregular behavior. (b) The period T_{sol} of the solution and the average time δ between birth pulses. There are two intervals with period $T_{sol} = T_f$, but with different values of δ, implying a difference in the solutions.

Fig. 9. Bifurcation diagram for case B ($\mu = 0.25$ day^{-1}, $K = 0.7$ mgC/L) with parameters for the forcing amplitude a_f and the time ratio $\theta = T_f/T_{sys}$. The colors indicate the solution period T_{sol} in units of T_f, $T_{sol} = T_f$ is orange, $T_{sol} = 2T_f$ is green, $T_{sol} = 3T_f$ is blue, and $T_{sol} = 4T_f$ is purple. White indicates $T_{sol} > 4T_f$ or that no period was found, while black indicates the forward solution was different from the backward solution. (For interpretation of the references to color in this figure legend, the reader is referred to the web version of this article.)

$T_{sol} > 4$ (white area), suggesting the solutions become quasi-periodic or even chaotic. The regions with irregular solutions are interrupted by windows of periodic solutions that spreads out from points on the θ-axis and undergo period doublings when a_f increases. Similar to case A, there are hysteresis-like phenomena (black) near the period doublings, because the transient times become very large here. However, there are also larger areas of real hysteresis with existence of two distinct stable states.

Wedges with period $T_{sol} = T_f$ (yellow) are clearly visible going out from $\theta = 1, 2, 3$ and around $\theta = 1/2, 3/2, 5/2$ are some less distinct wedges with period $T_{sol} = 2T_f$ (green). This structure resembles the Arnold tongues found in the Mathieu's differential equation, see e.g., Arnold (1992). The average time between pulses is not shown, but generally δ/T_f increases when moving down and to the right in Fig. 9. Close to the θ-axis, the tongue from $\theta = 1$ have exactly $\delta = T_f$, whereas the tongues from $\theta = 2, 3$ have varying values around $\delta \approx 0.7T_f$, $0.45T_f$, respectively.

4. Discussion

We have studied the effect of environmental variations on a physiologically structured population. This was done by taking a size structured model by Kooijman and Metz (de Roos et al., 1990; Kooijman and Metz, 1984) and introducing forcing, both when the unforced system exhibit an equilibrium solution (case A) and when it exhibits an oscillatory solution (case B). In each case, the amplitude and period of the forcing were varied systematically.

Environmental variations can be more or less regular, in both frequency, amplitude and shape. If the cycles of the variations are close to being periodic, we expect the results presented here will still be applicable. In reality, some variations might be far from periodic and could even resemble random noise, and then a different approach would be needed. Here, we have chosen to focus on periodic variations.

In case A, the unforced system has a stable equilibrium solution with oscillatory transient behavior, and the results of adding forcing are summarized in Fig. 5. When forcing with low amplitudes (a_f close to 0) is introduced, the population oscillates in phase with the forcing. When the forcing amplitude is increased, the system undergoes (one or more) period doublings, and thus show solutions with longer periods than that of the forcing. The

average time δ between consecutive pulses (Fig. 8). As the forcing amplitude is increased from zero, B_{max} shows increasing irregular behavior and δ shows increasing distance between the birth pulses. The solution locks to the forcing frequency at $a_f \approx 0.30$, and is followed by at least one period doubling. When the amplitude a_f is increased further, the periodic solutions break down and the solutions become irregular again. At $a_f \approx 0.70$, the irregular solutions are succeeded by another window of periodic solutions containing at least one period doubling. Both intervals of phase locking start with a period of $T_{sol} = T_f$, but the time between birth pulses is less than the forcing period, i.e., $\delta < T_f$ in the first interval, whereas it is exactly $\delta = T_f$ in the second interval. In the second interval, the forcing frequency completely dominates the solution and the influence of the oscillations in the unforced system are no longer visible. This example displays some features that are also characteristic for other values of θ. These general features include that as the forcing amplitude a_f increases, the solution gradually changes from being dominated by the period T_{sys} of the unforced system to being dominated by the forcing period T_f.

To construct a bifurcation diagram in the parameters a_f and θ, we repeated the simulations for a range of forcing periods $T_f = 5, 6, \ldots, 100$ days, and combined the results, see Fig. 9. In large regions of the parameter space, the solutions are irregular or have a period
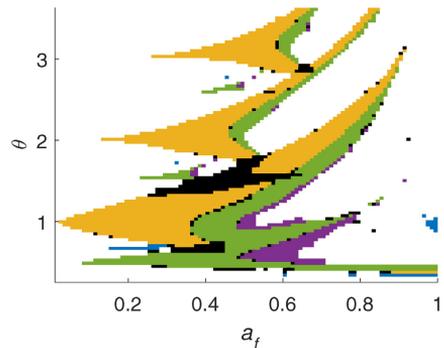
period doublings occur for lower forcing amplitude when θ is close to 1, i.e., when the forcing frequency is close to the systems internal frequency. These results suggest that the population oscillates in phase with the environmental variations, though period doublings may occur, particularly near resonance frequencies.

The system in case B exhibits a stable periodic solution in the absence of forcing. The effects of forcing are summarized in Fig. 9 and resembles the classic pattern of Arnold tongues (Arnold, 1992). The tongues start at rational values of θ and represents windows of phase-locking. Period doublings occur as the forcing amplitude a_f is increased. The broadest tongues are the ones starting at integer values of θ, corresponding to forcing periods of $T_f \approx 27.6$, 55.2, 82.7 days. These tongues represent solutions that have the same period as the forcing (before period doublings), but with different number of birth pulses per cycle. Outside the tongues are regions with irregular (chaotic or quasi-periodic) solutions. These regions generally become more dominant when moving away from $\theta = 1$.

Our findings agree with similar studies of forcing in predator–prey models without size structure. Forcing of the unstructured Rosenzweig-MacArthur model reveals bifurcations diagrams with Arnold tongues similar to Fig. 9, for parameters giving oscillatory solutions in the absence of forcing, as in case B (Taylor et al., 2013; Vandermeer et al., 2001). For parameters corresponding to case A, i.e., parameters where the unforced system displays oscillatory decay towards a stable equilibrium, forcing of the Rosenzweig-MacArthur model gives results resembling those in Fig. 5 (Taylor et al., 2013).

The tongues of phase-locking in case B start at rational values of the ratio $\theta = T_f / T_{sys}$. We believe this pattern is general for environmental variations with period T_f and populations with self-oscillations with period T_{sys}. Therefore, our results could also apply to populations of other species. For example, for a population with internal oscillation period of $T_{sys} = 6$ months subjected to an annual variation, we have $\theta = 2$ and thus expect the population to have two birth pulses repeating each year for a wide range of forcing amplitudes.

References

Arnold, V.I., 1992. Ordinary Differential Equations. Springer.
COCO, 2013. Continuation Core and Toolboxes, https://sourceforge.net/projects/cocotools.
Dankowicz, H., Schilder, F., 2013. Recipes for Continuation, vol. 11. SIAM.
de Roos, A.M., Persson, L., 2013. Population and Community Ecology of Ontogenetic Development. Princeton University Press.
de Roos, A., Metz, J., Evers, E., Leipoldt, A., 1990. A size dependent predator–prey interaction: who pursues whom? J. Math. Biol. 28 (6), 609–643, http://dx.doi.org/10.1007/BF00160229.
de Roos, A.M., 1997. A gentle introduction to physiologically structured population models. In: Structured-Population Models in Marine, Terrestrial, and Freshwater Systems. Springer, pp. 119–204.
Evans, G.T., Parslow, J.S., 1985. A model of annual plankton cycles. Biol. Oceanogr. 3 (3), 327–347, http://dx.doi.org/10.1080/01965581.1985.10749478.
Franks, P.J., 2002. NPZ models of plankton dynamics: their construction, coupling to physics, and application. J. Oceanogr. 58 (2), 379–387, http://dx.doi.org/10.1023/A:1015874028196.
Freund, J.A., Mieruch, S., Scholze, B., Wiltshire, K., Feudel, U., 2006. Bloom dynamics in a seasonally forced phytoplankton–zooplankton model: trigger mechanisms and timing effects. Ecol. Complex. 3 (2), 129–139, http://dx.doi.org/10.1016/j.ecocom.2005.11.001.
Iserles, A., 2009. A First Course in the Numerical Analysis of Differential Equations. Cambridge University Press.
Kooijman, S., Metz, J., 1984. On the dynamics of chemically stressed populations: the deduction of population consequences from effects on individuals. Ecotoxicol. Environ. Saf. 8 (3), 254–274, http://dx.doi.org/10.1016/0147-6513(84)90029-0.
LeVeque, R.J., 2007. Finite Difference Methods for Ordinary and Partial Differential Equations: Steady-State and Time-Dependent Problems, vol. 98. SIAM.
Ma, S.-k., 1976. Modern Theory of Critical Phenomena. Benjamin-Cummings.
MATLAB, 2014. Version 8.4.0.150421 (R2014b) The MathWorks Inc., Natick, MA.
McMeans, B.C., McCann, K.S., Humphries, M., Rooney, N., Fisk, A.T., 2015. Food web structure in temporally-forced ecosystems. Trends Ecol. Evol. 30 (11), 662–672, http://dx.doi.org/10.1016/j.tree.2015.09.001.
Metz, J.A., Diekmann, O., 1986. The Dynamics of Physiologically Structured Populations, vol. 68. Springer.
Rinaldi, S., Muratori, S., Kuznetsov, Y., 1993. Multiple attractors, catastrophes and chaos in seasonally perturbed predator–prey communities. Bull. Math. Biol. 55 (1), 15–35, http://dx.doi.org/10.1007/BF02460293.
Rosenzweig, M.L., et al., 1971. Paradox of enrichment: destabilization of exploitation ecosystems in ecological time. Science 171 (3969), 385–387.
Sun, Z., de Roos, A.M., 2015. Alternative stable states in a stage-structured consumer-resource biomass model with niche shift and seasonal reproduction. Theor. Popul. Biol., http://dx.doi.org/10.1016/j.tpb.2015.04.004.
Taylor, R.A., Sherratt, J.A., White, A., 2013. Seasonal forcing and multi-year cycles in interacting populations: lessons from a predator–prey model. J. Math. Biol. 67 (6–7), 1741–1764, http://dx.doi.org/10.1007/s00285-012-0612-z.
Thieme, H., 1988. Well-posedness of physiologically structured population models for *Daphnia magna*. J. Math. Biol. 26 (3), 299–317, http://dx.doi.org/10.1007/BF00277393.
Vandermeer, J., Stone, L., Blasius, B., 2001. Categories of chaos and fractal basin boundaries in forced predator–prey models. Chaos Solitons Fractals 12 (2), 265–276, http://dx.doi.org/10.1016/S0960-0779(00)00111-9.
van de Wolfshaar, K.E., de Roos, A.M., Persson, L., 2008. Population feedback after successful invasion leads to ecological suicide in seasonal environments. Ecology 89 (1), 259–268, http://dx.doi.org/10.1890/06-2058.1.

II   Spatio-temporal pattern formation in predator– prey systems with fitness taxis

This manuscript has been submitted to Ecological Complexity.

Spatio-temporal Pattern Formation in Predator-Prey Systems with Fitness Taxis

Irene T. Heilmann[*,1,2], Mads Peter Sørensen[1], and Uffe Høgsbro Thygesen[1,2]

[1]Department of Applied Mathematics and Computer Science, Technical University of Denmark
[2]Center for Ocean Life, National Institute of Aquatic Resources, Technical University of Denmark

Abstract

We pose a spatial predator–prey model in which the movement of animals is not purely diffusive, but also contains a drift term in the direction of higher specific growth rates. We refer to this as fitness taxis. We conduct a linear stability analysis of the resulting coupled reaction–advection–diffusion equations and derive conditions under which spatial patterns form. We find that for some parameters, short waves grow with unbounded speeds, which we refer to as an ultraviolet catastrophe. To eliminate this, we introduce spatial kernels in the model, yielding coupled integro-differential equations, and conduct a similar stability analysis for this system. Through numerical simulation, we find that a variety of patterns can emerge, including stationary spatial patterns, standing and travelling waves, and seemingly chaotic spatio-temporal patterns. We argue that fitness taxis represents a simple and generic extension of diffusive motion, is ecologically plausible, and provides an alternative mechanism for formation of patterns in spatially explicit ecosystem models, with emphasis on non-stationary spatio-temporal dynamics.

Key words   Pattern formation • Predator–prey systems • Fitness taxis • Cross-diffusion

1   Introduction

Most populations in nature are not homogeneously distributed in space, but cluster together in patterns of different shapes and geometry. These patterns can arise as a response to heterogeneous environments [Cobbold et al., 2015], but they can also emerge in homogeneous environments through self–organization. For example, young mussel beds in a tidal area [van de Koppel et al., 2005] display stripe–like patterns. The mechanism for this pattern formation is mutual

[*]Corresponding author. DTU Compute, Asmussens Allé, Building 303B, 2800 Kgs. Lyngby, Denmark; `irhe@dtu.dk`

protection against wave disturbance, giving positive feedback on short spatial scales, combined with competition between mussels for algal resources, giving negative feedback on longer scales. The mechanism is therefore an example of scale-dependent feedback, a general principle behind pattern formation [Rietkerk and van de Koppel, 2008].

When patterns emerge in homogeneous environments, they can be seen as an inherent property of the system, as the example of mussel beds demonstrate. An archetypal mechanism for such self-organized patterns is the Turing diffusion-driven instability in partial differential equations of reaction–diffusion type. Turing [1952] originally conceived this as a mechanism for pattern formation in chemical systems, specifically explaining morphogenesis. The classical Turing patterns assume stable reaction dynamics in the absence of spatial effects, while the feedback between the reaction dynamics and transport gives rise to an instability which ultimately leads to stationary spatial patterns. The Turing mechanism has also been considered in trophic systems, first as a hypothesized mechanism for patchiness in plankton communities [Levin and Segel, 1976, Malchow, 1993]. In such models, the Turing diffusion-driven instability may appear in conjunction with a Hopf bifurcation in the reaction dynamics [e.g., Banerjee and Petrovskii, 2011], and the combination of these two instabilities may give rise to large variety of spatio-temporal patterns, including irregular chaotic type patterns [Huang et al., 2017]. Spatio-temporal patterns in such systems may also emerge without the Turing mechanism, for example when the local population dynamics are unstable [Petrovskii and Malchow, 1999].

However, the relevance of the Turing mechanism in predator–prey systems can be questioned from an evolutionary perspective. In Turing models, the diffusion term, which corresponds to random unbiased movements of individuals, always leads to a net migration of individuals from regions with higher densities to regions with lower densities, and this transport is crucial for maintaining the stationary spatial patterns. When stationary Turing patterns have formed, the regions with high densities also have positive surplus production. This surplus production is then transported by diffusion to regions with low densities, where the surplus production is negative. Since even organisms as primitive as bacteria and algae are capable of directing their motion towards more attractive regions [Brown and Berg, 1974, Eggersdorfer and Häder, 1991, Kay et al., 2008], this leads to the question why animals would move from regions with positive production to regions with negative production, and next, if patterns can emerge in models where animals do not just move randomly. This suggests the inclusion of cross-diffusion terms, modeling pursuit–evasion movements in predator-prey models [Tsyganov et al., 2004, Biktashev et al., 2004], which may lead to a quasi-soliton type of wave that are not seen in reaction–diffusion systems. Regarding the possibility of pattern formation in such predator–prey models, a taxis of predators towards higher prey concentrations has been shown not to destabilize the uniform steady state [Lee et al., 2009, Wang and Zhang, 2015]

The assumption behind the present paper is that the movements of predators and prey are neither completely random nor a response to just the other species, as in pursuit and evasion, but also a response to the densities of conspecifics. We propose the notion of *fitness taxis* as a simple and generic movement model: Animals have a preference for moving towards more favourable regions. Specifically, we include an advective component to the flux of animals, which is in the direction of the spatial gradient of the specific growth rate of those animals. Our

model thus continues in the direction set out by Cantrell et al. [2008], who used such an advective term in a model of a single species and investigated the effect of heterogeneous environment, and by [Cantrell et al., 2013] who extended to two competing populations. The overarching question initiating our work is if and how spatial and spatiotemporal patterns may form in predator-prey models, when each species performs fitness taxis.

Our predator–prey model consists of two coupled reaction–advection–diffusion equations and the initial model is local, corresponding to predators only consuming prey which are at the same location as the predator. It turns out that for some parameter combinations, this system is not well posed; the growth rate of spatial disturbances diverges as the wave number diverges. With an analogy to physics, we refer to this as an ultraviolet catastrophe. We circumvent this problem by allowing the predator to consume prey within a specified spatial range, introducing a spatial kernel which describes the rate with which predators at one location encounter prey at a different location. Thus, the growth rate of predators depend on an integral over space of the prey densities, and the mortality of prey depend on a similar integral of predator densities. Similar non-local models have been studied previously [Grindrod, 1988, Malchow et al., 2008, Banerjee and Volpert, 2016a,b]. This kernel effectively smoothes out small-scale fluctuations in densities, eliminating the ultraviolet catastrophe.

The outline of the manuscript is as follows: First, we pose a local predator–prey model with fitness taxis, and conduct a stability analysis of the spatially uniform equilibrium solution. Next, we pose the non-local model based on a spatial kernel and conduct a similar stability analysis. Further, we perform numerical simulations of patterns in one spatial dimension. Finally, we offer some conclusions.

2 Fitness taxis in a generic predator-prey model

We study a predator–prey system where animals move both randomly and towards higher values of their individual fitness, quantified through their specific growth rate. The model is

$$\frac{\partial u}{\partial t} = f(u,v)u - \nabla \cdot (u\,\gamma_u \nabla f(u,v)) + D_u \nabla^2 u, \tag{1a}$$

$$\frac{\partial v}{\partial t} = g(u,v)v - \nabla \cdot (v\,\gamma_v \nabla g(u,v)) + D_v \nabla^2 v \tag{1b}$$

for the prey density $u(x,t)$ and the predator density $v(x,t)$ in space $x \in \Omega$ for time $t > 0$. The first term in each equation is the population dynamics. The functions f and g give the specific growth rate of prey and predators, respectively, combining reproduction and mortality. The last term in each equation represents random movement (diffusion) where $D_u, D_v \geq 0$ are the diffusion coefficients for prey and predators, respectively. The second term in each equation is a fitness taxis where the animals move towards better conditions. Here, the specific growth rates are used to measure fitness and accordingly the animals move up the gradients of f and g. The fitness taxis coefficients $\gamma_u, \gamma_v \geq 0$ express the sensitivity to spatial differences in fitness of prey and predators,

respectively. The fitness gradients can be written as

$$\nabla f(u,v) = \frac{\partial f(u,v)}{\partial u}\nabla u + \frac{\partial f(u,v)}{\partial v}\nabla v\,,$$

$$\nabla g(u,v) = \frac{\partial g(u,v)}{\partial u}\nabla u + \frac{\partial g(u,v)}{\partial v}\nabla v\,,$$

showing the fitness taxis of both populations can be divided into movement along the gradient of prey density and along the gradient of predator density. The sign of the partial derivatives of f and g determines whether the direction is toward higher or lower densities. For the analysis of the model, we consider the one-dimensional space domain $x \in \mathbb{R}$.

3 Linear stability analysis

To determine the conditions for pattern formation in the system (1), we perform a linear stability analysis [Cross and Hohenberg, 1993]. We consider an equilibrium solution (u^*, v^*) for the population dynamics with positive density of prey and predators, that is $u^*, v^* > 0$, $f(u^*, v^*) = g(u^*, v^*) = 0$. This will be a homogeneous equilibrium solution of the full system (1), and we consider the stability of this equilibrium towards spatial perturbations.

The linearization of the system (1) gives

$$\frac{\partial \tilde{u}}{\partial t} = u^* \left(f_u^* \tilde{u} + f_v^* \tilde{v} \right) - \gamma_u u^* \left(f_u^* \nabla^2 \tilde{u} + f_v^* \nabla^2 \tilde{v} \right) + D_u \nabla^2 \tilde{u}\,, \tag{2a}$$

$$\frac{\partial \tilde{v}}{\partial t} = v^* \left(g_u^* \tilde{u} + g_v^* \tilde{v} \right) - \gamma_v v^* \left(g_u^* \nabla^2 \tilde{u} + g_v^* \nabla^2 \tilde{v} \right) + D_v \nabla^2 \tilde{v}\,. \tag{2b}$$

where $\tilde{u}$, $\tilde{v}$ are small perturbations of the equilibrium (u^*, v^*). Partial derivatives evaluated at the equilibrium are denoted as $f_u^* := \frac{\partial f}{\partial u}(u^*, v^*)$, etc. For a harmonic perturbation with wave number k and growth rate λ, we obtain an eigenvalue problem for a stability matrix $M(k)$ with eigenvalue λ. The stability matrix is

$$\boldsymbol{M}(k) = \boldsymbol{A} + k^2 \boldsymbol{T} - k^2 \boldsymbol{D} \tag{3}$$

where matrices $\boldsymbol{A}$, $\boldsymbol{T}$ and $\boldsymbol{D}$ describe population dynamics, fitness taxis and diffusion, respectively, and are given by

$$\boldsymbol{A} = \begin{pmatrix} u^* f_u^* & u^* f_v^* \\ v^* g_u^* & v^* g_v^* \end{pmatrix}\,, \tag{4a}$$

$$\boldsymbol{T} = \begin{pmatrix} \gamma_u u^* f_u^* & \gamma_u u^* f_v^* \\ \gamma_v v^* g_u^* & \gamma_v v^* g_v^* \end{pmatrix}\,, \tag{4b}$$

$$\boldsymbol{D} = \begin{pmatrix} D_u & 0 \\ 0 & D_v \end{pmatrix}\,. \tag{4c}$$

Notice that $\boldsymbol{T} = \mathrm{diag}(\gamma_u, \gamma_v)\boldsymbol{A}$. The equilibrium solution is unstable if and only if there exists a wave number $k \geq 0$ such that an eigenvalue λ of the stability matrix $\boldsymbol{M}(k)$ has positive real part. This occurs if and only if the stability matrix $\boldsymbol{M}(k)$ has positive trace or negative determinant. We are interested in the pattern formations induced by movement and therefore require that the

equilibrium (u^*, v^*) is stable for the population dynamics, i.e. that $\boldsymbol{M}(0) = \boldsymbol{A}$ is stable, i.e.

$$\text{tr}[\boldsymbol{A}] = a_{11} + a_{22} < 0 \,, \tag{5}$$

and

$$|\boldsymbol{A}| = a_{11}a_{22} - a_{12}a_{21} > 0 \,. \tag{6}$$

where a_{ij} is the element (i, j) in $\boldsymbol{A}$. In the following, we will assume these two conditions are met.

The trace condition and a taxis–driven instability

The equilibrium is unstable in the full system whenever the trace of the stability matrix is positive. The trace of the stability matrix is given by

$$\text{tr}\,[\boldsymbol{M}(k)] = \text{tr}[\boldsymbol{A}] + k^2 \,\text{tr}[\boldsymbol{T} - \boldsymbol{D}] \,. \tag{7}$$

Since the population dynamics are stable, i.e. condition (5), we see that $\text{tr}\,\boldsymbol{M}(k) > 0$ for some $k > 0$ if and only if $\text{tr}[\boldsymbol{T} - \boldsymbol{D}] > 0$. This leads to the following sufficient condition for instability,

$$a_{11}\gamma_u + a_{22}\gamma_v > D_u + D_v \,. \tag{8}$$

Fulfilling this condition together with condition (5), entails the parameters a_{11} and a_{22} have opposite sign; a structure that is known as activator–inhibitor dynamics [Murray, 2003]. For brevity, we focus on the case where the prey is the activator and the predator is the inhibitor, i.e.

$$a_{11} > 0 \,, \quad a_{22} < 0 \,. \tag{9}$$

The trace condition (8) for instability is sketched in (γ_u, γ_v)-parameter space in Fig. 1a. It is assumed the population dynamics fulfill conditions (5), (6), (9). The region for instability has the boundary $\text{tr}\,[\boldsymbol{T} - \boldsymbol{D}] = 0$ (orange line), which is a straight line that intersects the horizontal axis at $\gamma_1 := (D_u + D_v)/a_{11} \geq 0$ and has the slope $-a_{11}/a_{22} \in (0, 1)$.

Since we have assumed prey activation, $a_{11} > 0$, the term $a_{11}\gamma_u$ is positive and represents prey moving towards higher prey densities when spatial fluctuations are small. The condition (8) will be met if the is taxis coefficient of the prey is sufficiently high, and hence we refer to this instability as taxis-driven. Similarly, our assumption $a_{22} < 0$ implies that predator taxis tends to stabilize the equilibrium, as does diffusion.

When the trace condition for instability is met, the trace of the stability matrix grows to infinity, $\text{tr}\,[\boldsymbol{M}(k)] \to \infty$, as the wavenumber grows to infinity, $k \to \infty$. Since the trace of a matrix is equal to the sum of its eigenvalues, it follows that $\Re(\lambda_i(k)) \to \infty$ when $k \to \infty$ for at least one eigenvalue $\lambda_i(k)$. This entails that, close to the equilibrium, perturbations with an infinitely short wavelength grow infinitely fast. This phenomenon is colloquially known as an ultraviolet catastrophe, by analogy to a short-wave divergence in classical physics, and implies that the model is not well posed. We address this issue in section 4.
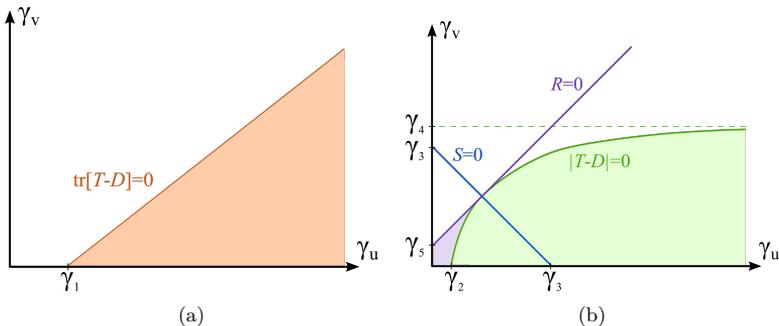
5

Figure 1: Sketch of bifurcation diagram for system (1) showing the stability of the homogeneous equilibrium. (a) The trace condition for taxis-driven instability holds in the orange area. (b) The determinant condition for instability holds in the colored areas. The green area is taxis–diffusion driven instability and the violet area is diffusion driven instability. This figure assumes conditions (5), (6) and (9), and in addition $D_u, D_v > 0$, $\gamma_3 > 0$ and $\gamma_5 > 0$.

The determinant condition for instability

The equilibrium also becomes unstable if the determinant of the stability matrix is negative. The determinant of the stability matrix is given by

$$|\boldsymbol{M}(k)| = k^4|\boldsymbol{T} - \boldsymbol{D}| + k^2 S + |\boldsymbol{A}|\,, \tag{10}$$

$$S := \gamma_u|\boldsymbol{A}| + \gamma_v|\boldsymbol{A}| - a_{11}D_v - a_{22}D_u\,, \tag{11}$$

which we view as as a quadratic in k^2 with the discriminant

$$R := S^2 - 4\,|\boldsymbol{A}|\,|\boldsymbol{T} - \boldsymbol{D}|\,, \tag{12}$$

and two roots k_1^2, k_2^2. Since we have assumed $|\boldsymbol{A}| > 0$ for stable population dynamics, the determinant condition for instability entails a negative value of $|\boldsymbol{T} - \boldsymbol{D}|$ or S. Correspondingly, the determinant instability is split into two cases.

Taxis–diffusion driven instability

First, we consider the case $|\boldsymbol{T} - \boldsymbol{D}| < 0$. The quadratic is concave, has two real roots with opposite signs, and is negative for sufficiently large wave numbers k. The inequality $|\boldsymbol{T} - \boldsymbol{D}| < 0$ can be written as

$$a_{11}\gamma_u D_v + a_{22}\gamma_v D_u > \gamma_u\gamma_v|\boldsymbol{A}| + D_u D_v\,. \tag{13}$$

This condition, together with conditions (5)-(6) for stable population dynamics, necessitates opposite signs of a_{11} and a_{22}. As with the trace instability, we will assume prey activation, i.e. $a_{11} > 0$ and $a_{22} < 0$, i.e., condition (9).

The region for instability condition (13) is sketched in (γ_u, γ_v)-coordinate space in Fig. 1b (green area). The population dynamics are assumed to fulfill conditions (5), (6) and (9). The region for instability has the boundary $|\boldsymbol{T} -$

6

$\boldsymbol{D}| = 0$ (solid green line). For $D_u, D_v > 0$, this is a hyperbola that crosses the horizontal axis at $\gamma_2 := D_u/a_{11} > 0$ and has the horizontal asymptote $\gamma_4 := a_{11}D_v/|\boldsymbol{A}| > 0$ (dashed green line). For $D_v = 0$, the condition cannot be met and for $D_u = 0$, the region is bounded by the horizontal line $\gamma_v = \gamma_4$.

The taxis and diffusion coefficients enter in several terms of instability condition (13), making the mechanisms behind these pattern formations less obvious than the previous case. The only term in condition (13), where increasing values of the coefficients makes the inequality less restrictive, is the term $a_{11}\gamma_u D_v$. Therefore, the only movements that can facilitate pattern formation are prey taxis (toward higher prey density) and predator diffusion. Predator taxis and prey diffusion, on the other hand, will only tend to stabilize the equilibrium. Since the instability in this case requires both taxis and diffusion, we refer to it as a taxis–diffusion driven instability.

The taxis–diffusion driven instability also results in solutions with an ultraviolet catastrophe (appendix A).

Diffusion–driven instability

Finally, we consider the case $|\boldsymbol{T} - \boldsymbol{D}| > 0$, where the quadratic is convex, i.e.

$$a_{11}\gamma_u D_v + a_{22}\gamma_v D_u < \gamma_u \gamma_v |\boldsymbol{A}| + D_u D_v \,. \tag{14}$$

The determinant condition for instability entails two positive real roots of the determinant. This results in the two additional conditions $S < 0$ and $R > 0$. By using expression (11) for S, the condition $S < 0$ becomes

$$a_{11}D_v + a_{22}D_u > (\gamma_u + \gamma_v)|\boldsymbol{A}| \,. \tag{15}$$

This inequality can only be fulfilled at the same time as conditions (5), (6) for stable population dynamics if a_{11} and a_{22} have opposite signs. As before, we will presume $a_{11} > 0$ and $a_{22} < 0$, i.e., condition (9). Using expression (12) for R and some algebra, the condition $R > 0$ results in

$$|\boldsymbol{A}|^2(\gamma_u - \gamma_v)^2 + (a_{11}D_v + a_{22}D_u)^2 + 2|\boldsymbol{A}|(a_{11}D_v - a_{22}D_u)(\gamma_u - \gamma_v) \\ > 4|\boldsymbol{A}|D_u D_v \,. \tag{16}$$

If conditions (14), (15), (16) are all met, the equilibrium is unstable for wavenumbers in the range $k_1 < k < k_2$. The determinant of the stability matrix is positive for $k > k_2$ and, therefore, this case does not lead to an ultra-violet catastrophe. If there is no taxis movement, $\gamma_u = \gamma_v = 0$, the conditions for this case amounts to the conditions for Turing patterns [Murray, 2003]. We will refer to the instabilities in this case as diffusion–driven instabilities.

The values of (γ_u, γ_v) that fulfill the three conditions (14), (15), (16) for diffusion–driven instabilities are illustrated in Fig. 1b (purple area). It is presumed the population dynamics fulfills conditions (5), (6) and (9) and that $D_u, D_v > 0$. The boundary $|\boldsymbol{T} - \boldsymbol{D}| = 0$ (green line) of condition (14) has already been described in connection with the taxis–diffusion driven case. Condition (15) has the boundary $S = 0$ (blue line), which is a straight line with slope -1 that intersects both axes at $\gamma_3 := (a_{11}D_v + a_{22}D_u)/|\boldsymbol{A}|$. The value of γ_3 can be negative, in which case the condition cannot be met. In condition (16), the taxis coefficients only enter as their difference $(\gamma_v - \gamma_u)$. Solving

the inequality (16) for the difference $(\gamma_v - \gamma_u)$ gives the two possible regions

$$\gamma_v - \gamma_u < \xi_0 - \Delta\xi\,, \tag{17a}$$

$$\gamma_v - \gamma_u > \xi_0 + \Delta\xi\,. \tag{17b}$$

where

$$\xi_0 = \frac{a_{11}D_v - a_{22}D_u}{|\boldsymbol{A}|}, \quad \Delta\xi = \frac{2\sqrt{-a_{12}a_{21}D_uD_v}}{|\boldsymbol{A}|}\,.$$

Conditions (6), (9) imply that $a_{12}a_{21} < 0$ and it follows that ξ_0 and $\Delta\xi$ are both non-negative. Inequality (17b) cannot be fulfilled along with $S < 0$, since $\gamma_3 \leq \xi_0$. Hence, it is only necessary to consider the region defined by (17a). The boundary (purple line) of this region is a straight line with slope 1 that intersects the vertical axis at $\gamma_5 := \xi_0 - \Delta\xi$. The intersection γ_5 is drawn as positive though it can have either sign. Thus, the plot shows the situation where diffusion-driven Turing patterns arise in the absence of fitness taxis $(\gamma_u = \gamma_v = 0)$.

The three conditions (14), (15), (16) for diffusion–driven instability are related. From the definition (12) of R, it follows that $S = 0$ and $|\boldsymbol{T} - \boldsymbol{D}| = 0$ implies $R = 0$. Hence, the three lines intersect eachother at the same point. Additionally, if $|\boldsymbol{T} - \boldsymbol{D}| < 0$ (green area) then $R > 0$ and therefore the line $R = 0$ must lie entirely in the region of $|\boldsymbol{T} - \boldsymbol{D}| > 0$. To discuss the mechanism of the instability we mainly consider the line $S = 0$ and the points γ_3 and γ_5, see fig. 1b. The value of the taxis coefficients γ_u, γ_v are bounded from above by the condition $S < 0$ and are further restricted by the other two conditions. Increasing the value of prey diffusion D_u, increases the value of γ_3 and can also increase the value of γ_5 (if D_u is sufficiently large); both of which helps to increase the region for instability. However, for sufficiently large values of D_u the condition $S < 0$ cannot be met. Increasing the value of predator diffusion D_v, does not affect the value of γ_3 and can increase the value γ_5 (if D_v is sufficiently large); it also moves the line $S = 0$ up and to the right. The main driving mechanism for the diffusion–driven instability is, therefore, predator diffusion.

Summary of the stability analysis

The three different cases that lead to pattern formation are summarized in Table 1. For all cases, it is required that the population dynamics has $a_{11} > 0$ and $a_{22} < 0$. This expresses that, at the equilibrium, the prey will benefit from a higher prey density, while the predators will suffer from a higher predator density. The prey taxis towards other prey are vital to both the taxis driven and the taxis–diffusion driven instability. The pursuit and evasion movements, that can be expected in a predator–prey system, do not cause the instabilities that lead to pattern formation, though they may play a role in shaping them. The taxis driven and the taxis–diffusion driven case both result in an ultraviolet catastrophe with pattern formations on an infinitesimal length scale. The prey taxis towards other prey acts like a negative diffusivity, and this creates the ultraviolet catastrophe.

When the ultra-violet catastrophe is present, for the linearized model, short-wave perturbations will grow with diverging speeds. Although we may - formally - compute the dynamics of perturbations in spectral domain, these perturbations may grow unbounded, if they contain short waves, and it will not be possible

Table 1: Summary of cases. The row containing "driving terms" indicate the terms that must be sufficiently large for patterns to emerge.

Case	Taxis driven	Taxis–diffusion driven	Diffusion driven
Instability	trace	determinant	determinant
Conditions	$\mathrm{tr}[\boldsymbol{T} - \boldsymbol{D}] > 0$	$|\boldsymbol{T} - \boldsymbol{D}| < 0$	$|\boldsymbol{T} - \boldsymbol{D}| > 0,\ R > 0,\ S < 0$
Necessary condition	$\frac{\gamma_u}{\gamma_v} > \frac{-a_{22}}{a_{11}}$	$\frac{\gamma_u D_v}{\gamma_v D_u} > \frac{-a_{22}}{a_{11}}$	$\frac{D_v}{D_u} > \frac{-a_{22}}{a_{11}}$
Driving terms	$a_{11}\gamma_u$	$a_{11}\gamma_u D_v$	$a_{11} D_v$
Ultra-violet catastrophe	yes	yes	no

to compute the solutions in natural domain with the inverse Fourier transform. Thus, the system is not well posed. The ultraviolet catastrophe also conflicts with the underlying assumptions for a density model. The use of abundance densities to describe the populations implies that the model is only valid on lengths scale significantly larger than the length of an individual; fluctuations in densities at length scales that are smaller than the scale of the individual are meaningless. In short, an ultraviolet catastrophe indicates a model fallacy at short scales.

In summary, the model may possess a variety of pattern forming mechanisms, but when patterns are predicted at the infinitesimal length scale, some modification of the model is required to guarantee well-posedness so that the patterns can be studied.

4   A non-local Bazykin model

In this section we present a modification of the model (1) which eliminates the ultraviolet catastrophe. The idea in the modification is to let trophic interactions occur not just between animals which are at the exact same point in space, but also between animals which are within a short range of eachother. This is achieved with an integration kernel, which then also smoothes out short-wave fluctuations. Similar approaches have been pursued previously; e.g. [Grindrod, 1988, Malchow et al., 2008, Banerjee and Volpert, 2016a].

To make the discussion specific, we start with the Bazykin predator-prey model [Bazykin, 1998, p. 67], see also [McGehee et al., 2008]. In non-dimensional form it reads

$$\frac{\mathrm{d}u}{\mathrm{d}t} = f(u,v)u = ru\left(1 - \frac{u}{K}\right) - \frac{auv}{1+u}\,, \tag{18a}$$

$$\frac{\mathrm{d}v}{\mathrm{d}t} = g(u,v)v = \frac{auv}{1+u} - v - cv^2\,, \tag{18b}$$

and has four parameters $a, c, r, K > 0$. Relative to the classical Lotka-Volterra model, the model has logistic growth of prey, density-dependent predator mor-

tality, and a Holling type II functional response. The system may have from zero to three equilibrium solutions (u^*, v^*) with positive values of both prey and predator [McGehee et al., 2008]. Linearization around such an equilibrium gives

$$\boldsymbol{A} = \begin{pmatrix} -\frac{ru^*}{K} + \frac{au^*v^*}{(1+u^*)^2} & -\frac{au^*}{1+u^*} \\ \frac{av^*}{(1+u^*)^2} & -cv^* \end{pmatrix}. \tag{19}$$

Inspecting the diagonal, we see that the Bazykin model has $a_{22} < 0$ whereas the sign of a_{11} depends on the balance between the stabilizing effect of the carrying capacity K, and the destabilizing effect of the type II functional response.

We now aim to modify the feeding term

$$\eta(u,v) = \frac{a}{1+u} uv, \tag{20}$$

which enters in both the equation for prey and for predators in (18). It is convenient to interpret the expression as composed of (nondimensionalized) encounter rate uv and a predator saturation effect $\frac{1}{1+u}$, which is reduced at high prey densities, while the parameter a arises during non-dimensionalization and combines predator background mortality, handling time, and assimilation efficiency. We now change this expression to allow a predator to feed in a region around it, introducing the encouter kernel $\Phi(x,y)$, such that the encounter rate between prey at position x and predators at position y is $u(x)\Phi(x,y)v(y)$ (omitting the time argument). The total rate with which a predator at position y encounters prey is then

$$U(y) = \int_\Omega u(x)\Phi(x,y)\,\mathrm{d}x. \tag{21}$$

and the saturation of a predator at position y is $\frac{1}{1+U(y)}$. We thus define the feeding rate of the predators at position y on the prey at position x to be

$$\frac{a}{1+U(y)} u(x)\Phi(x,y)v(y). \tag{22}$$

This leads to the following specific growth rates for prey and predators, respectively

$$\mathcal{F}(u,v)(x) = r\left(1 - \frac{u(x)}{K}\right) - a\int_\Omega \frac{\Phi(x,y)v(y)}{1+U(y)}\,\mathrm{d}y, \tag{23a}$$

$$\mathcal{G}(u,v)(y) = \frac{aU(y)}{1+U(y)} - 1 - cv(y). \tag{23b}$$

The operators $\mathcal{F}$ and $\mathcal{G}$ replace the specific growth rates f and g in (18). Even though the two equations have different expression for the feeding term, they are both consistent with the total amount of prey eaten by all predators: $\int_\Omega \int_\Omega h(x,y)\,\mathrm{d}x\,\mathrm{d}y$.

In the following, we consider specifically a Gaussian encounter kernel that depends on the distance between prey and predator,

$$\Phi(x,y) = \frac{1}{\sqrt{2\pi}\sigma} e^{-\frac{|x-y|^2}{2\sigma^2}}. \tag{24}$$

The parameter σ determines the range of the predator. In the limit $\sigma \to 0$, the encounter kernel collapses into a Dirac delta function and the modified population dynamics (23) becomes equivalent to the original system (18).

When the population dynamics takes the form (23), the full system reads

$$\frac{\partial u}{\partial t} = \mathcal{F}(u,v)u - \nabla \cdot [\gamma_u u \nabla(\mathcal{F}(u,v))] + D_u \nabla^2 u \,, \tag{25a}$$

$$\frac{\partial v}{\partial t} = \mathcal{G}(u,v)v - \nabla \cdot [\gamma_v v \nabla(\mathcal{G}(u,v))] + D_v \nabla^2 v \,. \tag{25b}$$

4.1 Linear stability analysis of the non-local model

To investigate the effect the encounter kernel has on pattern formation, the linear stability analysis is repeated for the system (25) with the population dynamics (23). This system has the same homogeneous equilibrium solution (u^*, v^*) as the system without kernel, and the corresponding stability matrix $\hat{\boldsymbol{A}}(k)$ is derived in Appendix B:

$$\hat{\boldsymbol{M}}(k) = \hat{\boldsymbol{A}}(k) + k^2 \hat{\boldsymbol{T}}(k) - k^2 \boldsymbol{D} \,. \tag{26}$$

where, as for the system without kernel, $\hat{\boldsymbol{A}}(k)$ derives from the population dynamics, $\hat{\boldsymbol{T}}(k) = \operatorname{diag}(\gamma_u, \gamma_v)\hat{\boldsymbol{A}}(k)$ from the taxis, while the diffusive dispersal gives rise to the same matrix $\boldsymbol{D}$ as in (4c). The stability matrix for the population dynamics is

$$\hat{\boldsymbol{A}}(k) = \begin{pmatrix} -\frac{ru^*}{K} + \frac{au^*v^*}{(1+u^*)^2}e^{-\sigma^2 k^2} & -\frac{au^*}{1+u^*}e^{-\frac{\sigma^2 k^2}{2}} \\ \frac{av^*}{(1+u^*)^2}e^{-\frac{\sigma^2 k^2}{2}} & -cv^* \end{pmatrix} \,. \tag{27}$$

Comparing with the system without kernel, i.e. (19), it is observed that $\hat{\boldsymbol{A}}(0) = \boldsymbol{A}$ and the difference between the two matrices grows with increasing wavenumber k. The two matrices only differ for terms related to the feeding rate; as k grows, these terms gradually vanish in $\hat{\boldsymbol{A}}(k)$. Correspondingly, the stability matrices $\hat{\boldsymbol{M}}(k)$ and $\boldsymbol{M}(k)$ are identical for $k = 0$ and differs increasingly with growing wavenumber k. In the limit $k \to \infty$,

$$\hat{\boldsymbol{M}}(k) \to \begin{pmatrix} -\infty & 0 \\ 0 & -\infty \end{pmatrix}$$

This shows the dynamics are stable for sufficiently large wavenumbers k and, hence, there is no ultra-violet catastrophe. The comparison suggests that close to the equilibrium the two systems behave similarly, except the kernel prohibits an ultra-violet catastrophe.

It is no longer possible to derive general closed form expressions for the boundary of the trace and determinant instabilities in (γ_u, γ_v)-parameter space, but it is possible to set up conditions that define those lines. In the subsequent section, we illustrate this numerically.

4.2 Numerical examples

For numerical analysis, the system (25) with the population dynamics (23) is solved with method of lines, i.e. discretized with N points in space which leads to $2N$ coupled ordinary differential equations (ODEs). These ODEs are propagated in time using a standard Runge-Kutta method, viz. `ode45` in Matlab [MATLAB, 2016]. The spatial discretization uses the finite volume approach with a second order central approximation of the diffusion term and a first order upwind approximation of the taxis term.

While the previous analysis assumed an infinite spatial domain, numerical analysis necessitates a finite domain, $x \in \Omega = [0, L]$. At the boundary, no-flux boundary conditions are enforced,

$$\gamma_u u \nabla \mathcal{F}(u, v) - D_u \nabla u = 0, \quad x = 0, L,$$
$$\gamma_v v \nabla \mathcal{G}(u, v) - D_v \nabla v = 0, \quad x = 0, L.$$

The finite spatial domain has implications for the encounter kernel. To ensure that the kernel integrates to 1 over the spatial domain, the Gaussian kernel $\Phi(x, y)$ in (24) is reflected at the boundaries $x = 0, L$ and the mirror images are added:

$$K(x, y) = \Phi(-x, y) + \Phi(x, y) + \Phi(2L - x, y), \quad x, y \in [0, L].$$

This mirror kernel $K(x, y)$ is used instead of $\Phi(x, y)$. Since the Gaussian $\Phi(x, y)$ is practically zero outside $x \in [-L, 2L]$, the mirror kernel fulfills $\int_0^L K(x, y) \, dx \cong 1$, implying it is normalized for all predator positions $y \in [0, L]$. Since $\Phi(x, y)$ only depends on the distance between x and y, it follows that $K(x, y) = K(y, x)$ and, hence, the kernel is also normalized for all prey positions $x \in [0, L]$. We note that an alternative approach is used by [Grindrod, 1988], where the spatial smoothing at each time step is done by solving an elliptic equation, so that the kernel is the Green's function for this equation.

4.2.1 Parametrization

For the population dynamics (23), we use the parameter values $r = 2.8$, $a = 5$, $c = 1.5$, $K = 28/3$, for which the Bazykin model has a single equilibrium with positive density of both prey and predator, namely $(u^*, v^*) = (1, 1)$. The linearization (19) at this equilibrium reveals that the the equilibrium is stable and that $a_{11} > 0$ and $a_{22} < 0$. We let the kernel width define the spatial scale, i.e. we set $\sigma = 1$, and fix the domain width at $L = 30$. To focus on the implications of the fitness taxis, we study a system without diffusion, $D_u = D_v = 0$. The taxis coefficients γ_u and γ_v are varied.

The system is discretized with $N = 800$ points in space and integrated in time $t \in [0, 500]$. To avoid the transient behavior of the system, the solutions are only shown for times $t \geq 400$. The initial condition for both prey $u(x, 0)$ and predators $v(x, 0)$ are small random perturbations to the equilibrium solution.

4.2.2 Results

Without diffusion, any pattern formation will emerge as a result of a taxis-driven instability, as shown in the previous. Figure 2 shows the values of the
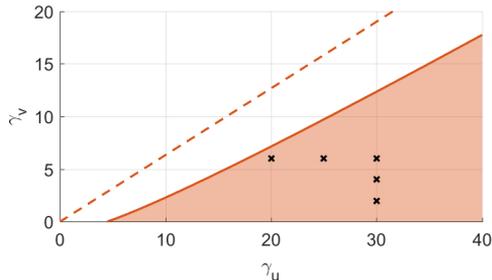
Figure 2: Pattern formation in the non-local Bazykin model (25,23). The orange area indicates the values of (γ_u, γ_v) that can result in pattern formation. These pattern formations are all from a taxis-driven instability and the dashed line indicates where the boundary of this region lies for the corresponding system without encounter kernel, i.e. with $\sigma = 0$.

taxis coefficients γ_u, γ_v that can lead to pattern formation. Note that the kernel reduces the region for pattern formation.

Fig. 3 presents solutions for different values of the taxis coefficients γ_u, γ_v, marked in figure 2. For each solution, it shows the prey density $u(x,t)$ and the predator density $v(x,t)$ as well as a (u,v)-phase portrait for the point $x = 7.5$.

The solutions show different types of dynamics. The solution for $\gamma_u = 20$, $\gamma_v = 6$ consists of standing waves, see Fig. 3a-3c. At each point in space, the densities of prey and predators form regular oscillations around the equilibrium density $(u^*, v^*) = (1, 1)$. At all points, a burst in prey is followed by a burst in predators and the phase portrait shows a typical predator–prey cycle. With increased taxis of the prey ($\gamma_u = 30$, $\gamma_v = 6$), a traveling wave of prey emerges on top of the standing waves, followed by a wave of predators (Fig. 3g-3i). At the boundaries, the wave stops and another wave continue in the opposite direction; the result is close to a reflection of the wave. The phase portrait shows two main cycles; one for the wave moving to the right and the other for the wave moving left. In this solution, the variations in density are so large that the prey intermittently all but go extinct locally.

The character of the solutions changes gradually from standing waves to traveling waves as the prey taxis coefficient γ_u is increased and the predator taxis coefficient γ_v is decreased (compare Figs. 3a-3c with Figs. 3g-3i). In general, the solutions consist of a mix between the two types of waves. Near the bifurcation line in Fig. 2, the solutions are standing waves with small amplitude, while further away from this line, the amplitude increases, traveling waves emerge and eventually irregular solutions appear. Based on numerous numerical experiments not shown here, these observations seem to be general for the taxis-driven instability.

In all the solutions, the predator density resembles a delayed version of the prey density with smaller amplitude variations. This is reflected in the phase portraits as predator–prey cycles. In no simulations did the system reach an equilibrium.
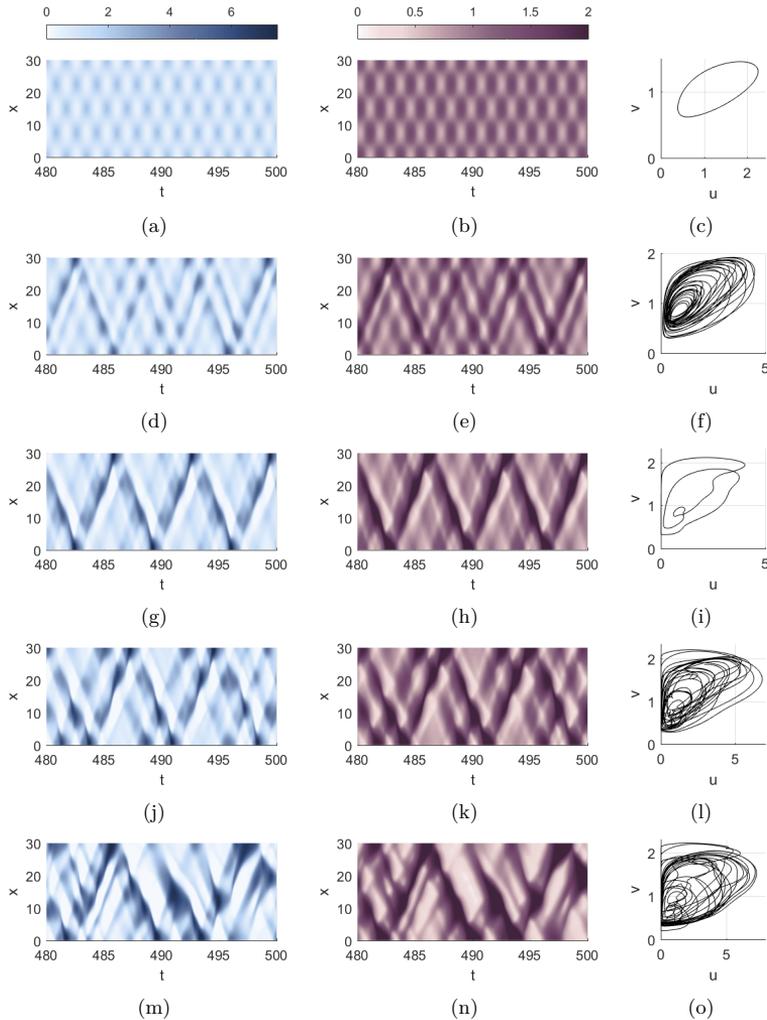
Figure 3: Numerical solutions to system (23), (25). First row: $\gamma_u = 20$, $\gamma_v = 6$. Second row: $\gamma_u = 25$, $\gamma_v = 6$. Third row: $\gamma_u = 30$, $\gamma_v = 6$. Fourth row: $\gamma_u = 30$, $\gamma_v = 4$. Fifth row $\gamma_u = 30$, $\gamma_v = 2$. Left column: Prey densities $u(x,t)$. Center column: Predator densities $v(x,t)$. Right column: Phase plots $\{(u(x,t), v(x,t)) : t \geq 0\}$ for the point $x = 7.5$.

5 Discussion

We have presented a spatial predator-prey model, where the animals move towards higher fitness, measured by the specific growth rate. The model has been

14

investigated with a linear stability analysis and with numerical solutions. The basic model (1) displays an ultra-violet catastrophe, when the pattern formations is driven by fitness taxis, or a combination of fitness taxis and diffusion. This situation can emerge because the population dynamics are completely localized in space. As a consequence, we modified the Bazykin population dynamics to have predators feed in a neighborhood around them, using an encounter kernel. This removed the ultra-short wavelengths in the patterns without changing the basic mechanisms in the model, and we found that the resulting model can display a variety of patterns, of which many are spatiotemporal.

The background for our work was the well-known Turing diffusion-driven instability, which has also been suggested as a mechanism for pattern formation in trophic systems. However, animals rarely move completely randomly, as a diffusion model suggests, and this raises the question how oriented movement of animals impact pattern formation. Realizing that movement ecology is a field in itself [Nathan et al., 2008], it is hardly useful to include the entire complexity of animal motion in a study of pattern formation. Starting from simplicity, it is plausible that predators would move in the direction of higher prey abundance, and conversely that prey would flee from predators, which would lead to cross-diffusion models. However, we would also expect animals to respond to conspecifics. We argue that a simple and generic model of directed motion is that of fitness taxis, i.e. animals have a preference for moving towards regions where their fitness is higher. This raises the question which measure of fitness to use; a familiar question [Mylius and Diekmann, 1995] where the ultimate answer would be to identify evolutionarily stable movement strategies. A pragmatic and useful simplification appears to be to assume that animals are attracted to high specific growth rates, i.e. the model considered here. Similar reasoning has appeared before (e.g. [Grindrod, 1988], Cantrell et al. [2013] and the references therein) but to our belief, the present study is the first time such fitness taxis has been considered in a predator-prey context with a view towards pattern formation.

While our numerical simulations clearly show waves of prey followed by waves of predators, the linear stability analysis reveals that the pattern formations are not caused by pursuit and evasion. Rather, the key pattern initiating mechanism is that prey are attracted to other prey, since the mortality due to predation decreases with the prey density. Thus, pattern formation occurs when the prey taxis is large; the predator taxis, in turn, is stabilizing. Although this may conflict with our general perception that predators are faster and have better cognitive abilities than prey, it should be kept in mind that the taxis coefficients are coarse descriptions of complex stimulus-response processes, and a between-species comparison of these parameters at the present generic level is difficult.

Referring to table 1, the possible instabilities can be divided into three categories: Taxis-driven, taxis-diffusion driven, and diffusion driven. The latter reduces to the Turing mechanism in absence of taxis, and is essentially the same mechanism. Thus, it requires feedback between population dynamics and the movement of animals, and therefore only exists in a bounded interval of wave numbers: Longer waves are attenuated by population dynamics, while shorter waves are attenuated by diffusion.

The two other categories of instabilities rely on strong prey taxis. These instabilities also exist in very short waves, i.e. they feature an ultraviolet catastrophe, and thus they are purely behavioral: Even if the cues that drive these

patterns come from growth rates, the actual population dynamics are not needed for patterns to form. To achieve a well-posed model, we introduced the encounter kernel, which essentially defines the scale of the individual, beneath which a continuous model ceases to be meaningful. Thus, the patterns that are formed by this mechanism are limited by the scale of the individual. Note that in figure 3a, the patch size is 7.5 times the radius of the encounter kernel, which is 1 in this simulation; thus, the resulting patterns are comparable in size to the range of the individual. The driver behind these instabilities is the tendency of prey to group in order to reduce predation mortality. Algebraically, they come in two flavors: The taxis-driven instability, and the taxis-diffusion driven instability. The first is easiest to understand: All the models considered here display prey activation, and the effect of taxis is to strengthen this activation. As the taxis coefficient of the prey increases, eventually the activation will be stronger than the inhibition of the predator, and the result is a Hopf bifurcation. The taxis-diffusion driven instability is more subtle, since it relies on an intricate interplay between taxis and diffusion. Algebraically, the mechanism is identical to the classical Turing mechanism, and the explanation is similar, although it relies strictly on movements and not on population dynamics: Now, the taxis matrix T has positive determinant, but $T - D$ has negative determinant, so that a saddle emerges. A small-scale aggregation of prey attracts more prey due to reduced predation mortality. This, in turn, attracts predators. In absence of diffusion, the aggregation of predators would cause the prey to flee, and the system would spiral back to a homogeneous state. However, if the predators diffuse rapidly, they will not aggregate strongly enough to overcome the activation. Thus, the prey aggregate faster than the predators, and the pattern emerges.

While the model is capable of displaying a variety of patterns, a critical question is to which degree these patterns resemble patterns observed in real ecosystems, and more broadly how the model elucidates spatiotemporal dynamics and patterns in trophic systems. The conclusion from our study is that, if the directed motion of animals is responsible for patterns to emerge and under the hypothesis of the model, these patterns rely on prey grouping to reduce mortality, they will be spatiotemporal and contain standing or traveling waves, the fluctuations in prey abundances will be larger than those of the predator abundances, and the patterns will exist on scales which characterize the foraging behavior of the individual predator. While a comparison with patterns in real ecosystems is outside the scope of our work, our study adds to our understanding of the mechanisms that can explain spatiotemporal patterns in generic mathematical models of predator-prey interactions.

Acknowledgements

References

M. Banerjee and V. Volpert. Prey-predator model with a nonlocal consumption of prey. *CHAOS*, 26(083120):1–12, 2016a. doi: 10.1063/1.4961248.

M. Banerjee and V. Volpert. Spatio-temporal pattern formation in rosenzweig–macarthur model: Effect of nonlocal interactions. *Ecological Complexity*, 30:2–10, 2016b. doi: 10.1016/j.ecocom.2016.12.002.

Malay Banerjee and Sergei Petrovskii. Self-organised spatial patterns and chaos in a ratio-dependent predator–prey system. *Theoretical Ecology*, 4(1):37–53, 2011.

Alexander D Bazykin. *Nonlinear dynamics of interacting populations*, volume 11. World Scientific, 1998.

V. N. Biktashev, J. Brindley, A. V. Holden, and M. A. Tsyganov. Pursuit-evasion predator-prey waves in two spatial dimensions. *Chaos: An Interdisciplinary Journal of Nonlinear Science*, 14(4):988–994, 2004. doi: 10.1063/1.1793751.

D. A. Brown and H. C. Berg. Temporal stimulation of chemotaxis in *Escherichia coli*. *Proc. Nat. Acad. Sci.*, 71(4):1388–1392, 1974. doi: 10.1073/pnas.71.4.1388.

Robert Stephen Cantrell, Chris Cosner, and Yuan Lou. Approximating the ideal free distribution via reaction–diffusion–advection equations. *Journal of Differential Equations*, 245(12):3687–3703, 2008. doi: 10.1016/j.jde.2008.07.024.

Robert Stephen Cantrell, Chris Cosner, Yuan Lou, and Chao Xie. Random dispersal versus fitness-dependent dispersal. *Journal of Differential Equations*, 254(7):2905–2941, 2013. doi: 10.1016/j.jde.2013.01.012.

C. A. Cobbold, F. Lutscher, and J. A. Sherratt. Diffusion-driven instabilities and emerging spatial patterns in patchy landscapes. *Ecological Complexity*, 24:69–81, 2015. doi: 10.1016/j.ecocom.2015.10.001.

Mark C Cross and Pierre C Hohenberg. Pattern formation outside of equilibrium. *Reviews of modern physics*, 65(3):851, 1993.

Birgit Eggersdorfer and Donat-P Häder. Phototaxis, gravitaxis and vertical migrations in the marine dinoflagellate prorocentrum micans. *FEMS Microbiology Letters*, 85(4):319–326, 1991. doi: 10.1111/j.1574-6968.1991.tb04758.x.

Peter Grindrod. Models of individual aggregation or clustering in single and multi-species communities. *Journal of Mathematical Biology*, 26(6):651–660, 1988. doi: 10.1007/BF00276146.

T. Huang, H. Zhang, H. Yang, N. Wang, and F. Zhang. Complex patterns in a space- and time-discrete predator-prey model with beddington-deangelis functional response. *Communication on Nonlinear Science and Numerical Simulations*, 43:182–199, 2017. doi: 10.1016/j.cnsns.2016.07.004.

R.R. Kay, P. Langridge, D. Traynor, and O. Hoeller. Changing directions in the study of chemotaxis. *Nature Reviews Molecular Cell Biology*, 9(6):455–463, 2008. doi: 10.1038/nrm2419.

J. M. Lee, T. Hillen, and M. A. Lewis. Pattern formation in prey-taxis systems. *Journal of biological dynamics*, 3(6):551–573, 2009. doi: 10.1080/17513750802716112.

S.A. Levin and L.A. Segel. Hypothesis for origin of planktonic patchiness. *Nature*, 259:659, 1976.

Horst Malchow. Spatio-temporal pattern formation in nonlinear non-equilibrium plankton dynamics. *Proceedings of the Royal Society of London B: Biological Sciences*, 251(1331):103–109, 1993.

Horst Malchow, Sergei V Petrovskii, and Ezio Venturino. *Spatiotemporal patterns in ecology and epidemiology: theory, models, and simulation.* Chapman & Hall/CRC London, 2008.

MATLAB. *Version 9.1.0.441655 (R2016b).* The MathWorks Inc., Natick, Massachusetts, 2016.

Edward A McGehee, Noel Schutt, Desiderio A Vasquez, and Enrique Peacock-Lopez. Bifurcations, and temporal and spatial patterns of a modified lotka–volterra model. *International Journal of Bifurcation and Chaos*, 18(08):2223–2248, 2008. doi: 10.1142/S0218127408021671.

James Dickson Murray. *Mathematical Biology II*, volume 18 of *Interdisciplinary Applied Mathematics.* Springer-Verlag New York, 3 edition, 2003. doi: 10.1007/b98869.

S.D. Mylius and O. Diekmann. On evolutionarily stable life histories, optimization and the need to be specific about density dependence. *Oikos*, 74:218–224, 1995. D034.

Ran Nathan, Wayne M Getz, Eloy Revilla, Marcel Holyoak, Ronen Kadmon, David Saltz, and Peter E Smouse. A movement ecology paradigm for unifying organismal movement research. *Proceedings of the National Academy of Sciences*, 105(49):19052–19059, 2008. doi: 10.1073/pnas.0800375105.

S. V. Petrovskii and H. Malchow. A minimal model of pattern formation in a prey-predator system. *Mathematical and Computer Modelling*, 25(7):49–63, 1999. doi: 10.1016/S0895-7177(99)00070-9.

Max Rietkerk and Johan van de Koppel. Regular pattern formation in real ecosystems. *Trends in ecology & evolution*, 23(3):169–175, 2008.

M. A. Tsyganov, J. Brindley, A. V. Holden, and V. N. Biktashev. Soliton-like phenomena in one-dimensional cross-diffusion systems: a predator–prey pursuit and evasion example. *Physica D: Nonlinear Phenomena*, 197(1):18–33, 2004. doi: 10.1016/j.physd.2004.06.004.

A. M. Turing. The chemical basis of morphogenesis. *Philosophical Transactions of the Royal Society of London. Series B, Biological Sciences*, pages 37–72, 1952.

Johan van de Koppel, Max Rietkerk, Norbert Dankers, and Peter M. J. Herman. Scale-dependent feedback and regular spatial patterns in young mussel beds. *The American Naturalist*, 165(3):E66–E77, 2005.

W. Wang, X. Wang and G. Zhang. Global bifurcation of solutions for a predator–prey model with prey-taxis. *Mathematical Methods in the Applied Sciences*, 38:431–443, 2015. doi: 10.1002/mma.3079.

A   The ultraviolet catastrophe in the taxis-diffusion driven instability

We show that when the system displays the taxis-diffusion driven instability, it also displays an ultraviolet catastrophe. Note that $|\boldsymbol{M}(k)| \to -\infty$ does not necessarily in itself imply that an eigenvalue of of $\boldsymbol{M}(k)$ tends to $+\infty$. However, the eigenvalues are given by

$$\lambda_{1,2}(k) = \tfrac{1}{2}\operatorname{tr}[\boldsymbol{M}(k)] \pm \tfrac{1}{2}\sqrt{\operatorname{tr}[\boldsymbol{M}(k)]^2 - 4|\boldsymbol{M}(k)|}$$

For sufficiently large wave numbers k, the determinant of $\boldsymbol{M}(k)$ is negative and both eigenvalues are real. The largest eigenvalue can be written as

$$\lambda_1(k) = \tfrac{1}{2}\operatorname{abs}(\operatorname{tr}[\boldsymbol{M}(k)])\left(\operatorname{sgn}(\operatorname{tr}[\boldsymbol{M}(k)]) + \sqrt{1 - \frac{4|\boldsymbol{M}(k)|}{\operatorname{tr}[\boldsymbol{M}(k)]^2}}\right).$$

By using expressions (7), (10) for the trace and determinant of $\boldsymbol{M}(k)$, it is seen the fraction under the square-root has the limit

$$-\frac{4|\boldsymbol{M}(k)|}{\operatorname{tr}[\boldsymbol{M}(k)]^2} \to -\frac{4|\boldsymbol{T}-\boldsymbol{D}|}{\operatorname{tr}[\boldsymbol{T}-\boldsymbol{D}]^2} > 0 \quad\text{for}\quad k \to \infty.$$

Expression (7) also shows that $\operatorname{tr}[\boldsymbol{M}(k)]) \to \pm\infty$ for $k \to \infty$. Returning to the expression for the largest eigenvalue, we can now conclude that

$$\lambda_1(k) \to \infty \quad\text{for}\quad k \to \infty.$$

This shows that the system has an ultra-violet catastrophe.

B   Linear stability analysis for the non-local system

In this section we perform a linear stability analysis of the non-local system (25) assuming a one-dimensional infinite space domain, $x \in \Omega = \mathbb{R}$. We require that the encounter kernel $\Phi(x,y)$ is normalized, that is

$$\int_{-\infty}^{\infty} \Phi(x,y)\,\mathrm{d}y = 1 \quad \forall x \in \Omega,$$

$$\int_{-\infty}^{\infty} \Phi(x,y)\,\mathrm{d}x = 1 \quad \forall y \in \Omega.$$

Additionally, we assume that the kernel only depends on the distance between prey and predator, in which case it can be written as $\Phi(x,y) = \phi(x-y)$. It is convenient to introduce the integral operator

$$\begin{aligned}
\mathcal{K}(w)(x) &= \int_{-\infty}^{\infty} w(y)\Phi(x,y)\,\mathrm{d}y \\
&= \int_{-\infty}^{\infty} w(y)\phi(x-y)\,\mathrm{d}y \qquad (29)
\end{aligned}$$

This integral has the form of a convolution, $\mathcal{K}(w) = w * \phi$. We also assume $\Phi(x,y) = \Phi(y,x)$, implying

$$\mathcal{K}(w)(y) = \int_{-\infty}^{\infty} w(x)\Phi(x,y)\,\mathrm{d}x\,.$$

With this notation for the integrals, the operators $\mathcal{F}$ and $\mathcal{G}$ in Eq. (23) for the non-local population dynamics can be written as

$$\mathcal{F}(u,v) = r\left(1 - \frac{u}{K}\right) - a\mathcal{K}\left(\frac{v}{1 + \mathcal{K}(u)}\right), \tag{30a}$$

$$\mathcal{G}(u,v) = \frac{a\mathcal{K}(u)}{1 + \mathcal{K}(u)} - 1 - cv\,. \tag{30b}$$

The normalization of the kernel implies that any constant function $w(x) = w^*$ is unchanged by the integral operator, $\mathcal{K}(w^*) = w^*$. The positive equilibrium (u^*, v^*) for the Bazykin model (18) therefore fulfills

$$\mathcal{F}(u^*, v^*) = f(u^*, v^*) = 0\,, \quad \mathcal{G}(u^*, v^*) = g(u^*, v^*) = 0\,.$$

Hence, (u^*, v^*) is a homogeneous equilibrium for the non-local population dynamics (23) and also the full non-local system (25).

Linearization around equilibrium

The equations are linearized around (u^*, v^*) by considering a small perturbation to the homogeneous equilibrium

$$u(x,t) = u^* + \epsilon\tilde{u}(x,t)\,, \tag{31a}$$
$$v(x,t) = v^* + \epsilon\tilde{v}(x,t)\,, \tag{31b}$$

for some $\epsilon > 0$. Since $\mathcal{K}$ is a linear operator and the kernel is normalized, it follows that $\mathcal{K}(u) = u^* + \epsilon\mathcal{K}(\tilde{u})$. This property, together with an expansion around $\epsilon = 0$, leads to

$$\frac{1}{1 + \mathcal{K}(u)} = \frac{1}{1 + u^* + \epsilon\mathcal{K}(\tilde{u})} = \frac{1}{1 + u^*} - \epsilon\frac{\mathcal{K}(\tilde{u})}{(1 + u^*)^2} + \mathcal{O}(\epsilon^2)\,.$$

Here, we implicitly assume all functions are evaluated at a point, such that $\mathcal{K}(u)$ refers to $\mathcal{K}(u(\cdot,t))(x)$ and the equation is for all values of x, t. Inserting the solution (31) in the population dynamics (30) and using these properties, gives

$$\mathcal{F}(u,v) = r\left(1 - \frac{u^* + \epsilon\tilde{u}}{K}\right) - a\mathcal{K}\left(\frac{v^* + \epsilon\tilde{v}}{1 + u^* + \epsilon\mathcal{K}(\tilde{u})}\right)$$

$$= r - \frac{ru^*}{K} - \epsilon\frac{r\tilde{u}}{K} - a\mathcal{K}\left(\frac{v^*}{1 + u^*} + \epsilon\frac{\tilde{v}}{1 + u^*} - \epsilon\frac{v^*\mathcal{K}(\tilde{u})}{(1 + u^*)^2} + \mathcal{O}(\epsilon^2)\right)$$

$$= r - \frac{ru^*}{K} - \frac{av^*}{1 + u^*} + \epsilon\left(-\frac{r\tilde{u}}{K} - \frac{a\mathcal{K}(\tilde{v})}{1 + u^*} + \frac{av^*\mathcal{K}(\mathcal{K}(\tilde{u}))}{(1 + u^*)^2}\right) + \mathcal{O}(\epsilon^2)$$

and

$$\mathcal{G}(u,v) = a\frac{u^* + \epsilon\mathcal{K}(\tilde{u})}{1 + u^* + \epsilon\mathcal{K}(\tilde{u})} - 1 - cv^* - \epsilon c\tilde{v}$$

$$= \frac{au^*}{1 + u^*} - 1 - cv^* + \epsilon\frac{a\mathcal{K}(\tilde{u})}{1 + u^*} - \epsilon\frac{au^*\mathcal{K}(\tilde{u})}{(1 + u^*)^2} + \epsilon c\tilde{v} + \mathcal{O}(\epsilon^2)$$

Recognizing the expressions for $f(u^*, v^*) = 0$ and $g(u^*, v^*) = 0$ in these equations, we get

$$\mathcal{F}(u,v) = \epsilon\,\mathcal{F}_u^*(\tilde{u}) + \epsilon\,\mathcal{F}_v^*(\tilde{v}) + \mathcal{O}(\epsilon^2)\,,$$
$$\mathcal{G}(u,v) = \epsilon\,\mathcal{G}_u^*(\tilde{u}) + \epsilon\,\mathcal{G}_v^*(\tilde{v}) + \mathcal{O}(\epsilon^2)$$

with the four linear operators $\mathcal{F}_u^*$, $\mathcal{F}_v^*$, $\mathcal{G}_u^*$ and $\mathcal{G}_v^*$:

$$\mathcal{F}_u^*(\tilde{u}) = -\frac{r}{K}\tilde{u} + \frac{av^*}{(1 + u^*)^2}\mathcal{K}(\mathcal{K}(\tilde{u}))\,, \tag{32a}$$

$$\mathcal{F}_v^*(\tilde{v}) = -\frac{a}{1 + u^*}\mathcal{K}(\tilde{v})\,, \tag{32b}$$

$$\mathcal{G}_u^*(\tilde{u}) = \frac{a}{(1 + u^*)^2}\mathcal{K}(\tilde{u})\,, \tag{32c}$$

$$\mathcal{G}_v^*(\tilde{v}) = -c\tilde{v}\,. \tag{32d}$$

The solution (31) is inserted into the full system (25) using (32). By discarding $\mathcal{O}(\epsilon^2)$ terms, a set of equations for the perturbations are obtained

$$\frac{\partial\tilde{u}}{\partial t} = u^*\left(\mathcal{F}_u^*(\tilde{u}) + \mathcal{F}_v^*(\tilde{v})\right) - \gamma_u u^*\nabla^2\left(\mathcal{F}_u^*(\tilde{u}) + \mathcal{F}_v^*(\tilde{v})\right) + D_u\nabla^2\tilde{u}\,, \tag{33a}$$

$$\frac{\partial\tilde{v}}{\partial t} = v^*\left(\mathcal{G}_u^*(\tilde{u}) + \mathcal{G}_v^*(\tilde{v})\right) - \gamma_v v^*\nabla^2\left(\mathcal{G}_u^*(\tilde{u}) + \mathcal{G}_v^*(\tilde{v})\right) + D_v\nabla^2\tilde{v}\,. \tag{33b}$$

This is the linearization of Eqs. (25).

Eigenvalue problem

The next step is to employ a solution ansatz for the perturbation. Here, we use

$$\begin{pmatrix}\tilde{u}(x,t)\\\tilde{v}(x,t)\end{pmatrix} = e^{\lambda t + ikx}\begin{pmatrix}\tilde{u}_0\\\tilde{v}_0\end{pmatrix}\,.$$

where λ is the growth rate of the perturbations and k is the wave number. Applying the integration operator in Eq. (29) to the perturbation ansatz gives

$$\mathcal{K}(\tilde{u})(x,t) = \int_{-\infty}^{\infty} u_0 e^{\lambda t} e^{iky}\phi(x - y)\,\mathrm{d}y$$

$$= u_0 e^{\lambda t} e^{ikx}\int_{-\infty}^{\infty} e^{-ik(x-y)}\phi(x - y)\,\mathrm{d}y$$

$$= \tilde{u}(x,t)\int_{-\infty}^{\infty} e^{-ikz}\phi(z)\,\mathrm{d}z$$

$$= \tilde{u}(x,t)\mathfrak{F}(\phi)(k)\,.$$

In the last line, the integral is written as the Fourier transform $\mathfrak{F}$ of ϕ. (This may differ by a constant factor, depending on the specific definition of the Fourier transform that is used.) The same calculations can be applied to $\tilde{v}$ and Eq. (32) now gives

$$\mathcal{F}_u^*(\tilde{u}) = \left(-\frac{r}{K} + \frac{av^*}{(1+u^*)^2}(\mathfrak{F}(\phi)(k))^2\right)\tilde{u}\,,$$

$$\mathcal{F}_v^*(\tilde{v}) = -\frac{a}{1+u^*}\mathfrak{F}(\phi)(k)\tilde{v}\,,$$

$$\mathcal{G}_u^*(\tilde{u}) = \frac{a}{(1+u^*)^2}\mathfrak{F}(\phi)(k)\tilde{u}\,,$$

$$\mathcal{G}_v^*(\tilde{v}) = -c\tilde{v}\,.$$

These expressions are inserted into the linearized system (33) resulting in the eigenvalue problem

$$\lambda\begin{pmatrix}\tilde{u}_0 \\ \tilde{v}_0\end{pmatrix} = \hat{\boldsymbol{M}}(k)\begin{pmatrix}\tilde{u}_0 \\ \tilde{v}_0\end{pmatrix}$$

for the stability matrix

$$\hat{\boldsymbol{M}}(k) = \hat{\boldsymbol{A}}(k) + k^2\hat{\boldsymbol{T}}(k) - k^2\boldsymbol{D}\,, \tag{35}$$

where

$$\hat{\boldsymbol{A}}(k) = \begin{pmatrix} -\frac{ru^*}{K} + \frac{au^*v^*}{(1+u^*)^2}(\mathfrak{F}(\phi)(k))^2 & -\frac{au^*}{1+u^*}\mathfrak{F}(\phi)(k) \\ \frac{av^*}{(1+u^*)^2}\mathfrak{F}(\phi)(k) & -cv^* \end{pmatrix}\,, \tag{36a}$$

$$\hat{\boldsymbol{T}}(k) = \begin{pmatrix} \gamma_u & 0 \\ 0 & \gamma_v \end{pmatrix}\hat{\boldsymbol{A}}(k)\,, \tag{36b}$$

$$\boldsymbol{D} = \begin{pmatrix} D_u & 0 \\ 0 & D_v \end{pmatrix}\,. \tag{36c}$$

The stability matrix $\hat{\boldsymbol{M}}(k)$ has the same structure as for the local system (compare with Eqs. (3), (4)), but the matrix $\hat{\boldsymbol{A}}(k)$ for population dynamics now depends on the wave number k. The homogeneous equilibrium (u^*, v^*) is unstable in the full non-local system (25) if, and and only if, the stability matrix has a positive trace or a negative determinant.

Specifically, for the Gaussian kernel in Eq. (24), the Fourier transform is

$$\mathfrak{F}(\phi)(k) = e^{-\frac{\sigma^2 k^2}{2}}\,. \tag{37}$$

By defining the positive constants

$$c_1 = \frac{ru^*}{K}\,, \tag{38a}$$

$$c_2 = \frac{au^*v^*}{(1+u^*)^2}\,, \tag{38b}$$

$$c_3 = cv^*\,, \tag{38c}$$

$$c_4 = \frac{av^*}{(1+u^*)^2}\,, \tag{38d}$$

$$c_5 = \frac{au^*}{1+u^*} \tag{38e}$$

23

the matrix $\hat{\boldsymbol{A}}(k)$ becomes

$$\hat{\boldsymbol{A}}(k) = \begin{pmatrix} -c_1 + c_2 e^{-\sigma^2 k^2} & -c_5 e^{-\frac{\sigma^2 k^2}{2}} \\ c_4 e^{-\frac{\sigma^2 k^2}{2}} & -c_3 \end{pmatrix} . \tag{39}$$

Stability of population dynamics

To concentrate on pattern formations induced by movement, we again require the population dynamics are stable for the homogeneous equilibrium (u^*, v^*). When the population dynamics are non-local, the related stability matrix $\hat{\boldsymbol{A}}(k)$ becomes a function of the wave number k and the conditions for stability are generalized to

$$\mathrm{tr}\left[\hat{\boldsymbol{A}}(k)\right] = \hat{a}_{11}(k) + \hat{a}_{22}(k) < 0 \qquad \forall k , \tag{40}$$

$$\left|\hat{\boldsymbol{A}}(k)\right| = \hat{a}_{11}(k)\hat{a}_{22}(k) - \hat{a}_{12}(k)\hat{a}_{21}(k) > 0 \quad \forall k \tag{41}$$

where $\hat{a}_{ij}(k)$ is element (i, j) in matrix $\hat{\boldsymbol{A}}(k)$. Using Eq. (39) gives

$$\mathrm{tr}\left[\hat{\boldsymbol{A}}(k)\right] = -c_1 - c_3 + c_2 e^{-\sigma^2 k^2} ,$$

$$\left|\hat{\boldsymbol{A}}(k)\right| = c_1 c_3 + c_6 e^{-\frac{\sigma^2 k^2}{2}} , \qquad c_6 := c_4 c_5 - c_2 c_3 .$$

The trace expression attains its maximum value for $k = 0$ and, thus, condition (40) can be reduced to $\mathrm{tr}[\hat{\boldsymbol{A}}(0)] < 0$. Depending on the sign of c_6, the determinant expression has either a minimum or a maximum at $k = 0$ and this is the only extremum. For $k \to \pm\infty$ the expression approaches the positive limit $c_1 c_3$. Therefore, condition (41) reduces to $|\hat{\boldsymbol{A}}(0)| > 0$. Since $\hat{\boldsymbol{A}}(0) = \boldsymbol{A}$, the equilibrium (u^*, v^*) is stable in the non-local population dynamics if, and only if, it is stable in the local population dynamics.

Trace instability

If the trace of the stability matrix is positive, $\mathrm{tr}[\hat{\boldsymbol{M}}(k)] > 0$, the equilibrium is unstable. For a general stability matrix (35),

$$\mathrm{tr}\left[\hat{\boldsymbol{M}}(k)\right] = (1 + \gamma_u k^2)\hat{a}_{11}(k) + (1 + \gamma_v k^2)\hat{a}_{22}(k) - (D_u + D_v)k^2 . \tag{42}$$

A positive trace together with condition (40) for stable population dynamics implies that $\hat{a}_{11}(k)$ and $\hat{a}_{22}(k)$ must have opposite sign for some wave number k. As for the local system, we assume the prey population is the activator and the predator population is the inhibitor, that is, $\hat{a}_{11}(k) > 0$ and $\hat{a}_{22}(k) < 0$ for some k. Hence, the trace instability is also driven by prey taxis toward higher prey density for the non-local system.

Using Eq. (39) for $\hat{\boldsymbol{A}}(k)$, reveals the wave number only enters expression (42) for the trace of the stability matrix in the form k^2. For $k^2 \geq 0$, we therefore define the trace function

$$\hat{p}(k^2) := c_2(\gamma_u k^2 + 1)e^{-\sigma^2 k^2} - (c_1 \gamma_u + c_3 \gamma_v + D_u + D_v)k^2 - c_1 - c_3 \tag{43}$$

$$= \mathrm{tr}\left[\hat{\boldsymbol{M}}(k)\right] .$$

The function is illustrated in Fig. 4. The function starts at $\hat{p}(0) = \text{tr}[\boldsymbol{A}] < 0$ and initially it may be increasing, but eventually it will start to decrease as it approaches the line

$$\hat{p}(k^2) \rightarrow -\left(c_1\gamma_u + c_3\gamma_v + D_u + D_v\right)k^2 - c_1 - c_3$$

for $k^2 \rightarrow \infty$. To determine if there is a trace instability, it suffices to check if the trace function $\hat{p}(k^2)$ has a maximum and if the function value is positive at this point.
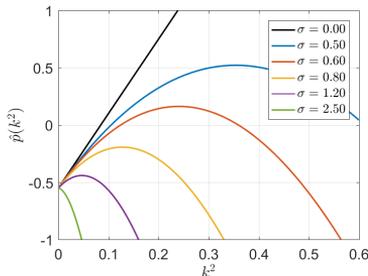

Figure 4: The trace function $\hat{p}(k^2)$ for different values of kernel width σ. Parameter values are $D_u = 1$, $D_v = 15$, $\gamma_u = 30$, $\gamma_v = 4$ and the default for population dynamics, see section 4.2.

To see the effect of the kernel, the width σ is varied, while keeping all other parameters fixed, see Fig. 4. For fixed k^2, increasing the width σ results in a lower value of the trace $\hat{p}(k^2)$. Hence, increasing the value of σ, restricts the trace instability to a smaller interval of k^2 and, for sufficiently large values of σ, the instability disappears. This shows, that if the local system does not have a trace instability, the addition of the encounter kernel cannot introduce one.

The next step is to find the bifurcation line for trace instability in (γ_u, γ_v) parameter space, corresponding to Fig. 1a for the local system. The onset of trace instability occurs when the function $\hat{p}(k^2)$ has a maximum with function value 0. The bifurcation line is found by solving $\hat{p}(k^2) = 0$ and $\hat{p}'(k^2) = 0$ simultaneously for γ_u and γ_v. It is not possible to find a direct relation between γ_u and γ_v, but it is possible to derive a parametrized curve with k^2 as parameter. The result is

$$\gamma_u(k^2) = \frac{c_1 + c_3}{c_2\sigma^2}k^{-4}e^{\sigma^2 k^2} - k^{-2} - \frac{1}{\sigma^2}k^{-4}, \tag{44a}$$

$$\gamma_v(k^2) = -\frac{c_1(c_1 + c_3)}{c_2 c_3 \sigma^2}k^{-4}e^{\sigma^2 k^2} - \frac{D_u + D_v}{c_3}k^{-2} + \frac{2c_1 + c_3}{c_3\sigma^2}k^{-4}$$
$$- \frac{c_2}{c_3\sigma^2}k^{-4}e^{-\sigma^2 k^2}. \tag{44b}$$

This line is illustrated for different values of σ in Fig. 5. Increasing the kernel width σ, decreases the region for trace instability.
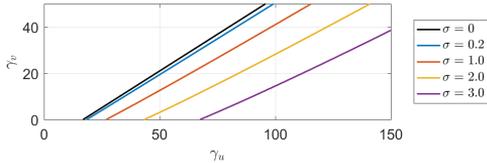
Figure 5: Bifurcation line for trace instability for different values of σ. For each value of σ, a trace instability occurs below the corresponding line. Parameter values are $D_u = 1$, $D_v = 15$ and the default for population dynamics, see section 4.2.

Determinant instability

The equilibrium also becomes unstable if the determinant of the stability matrix is negative, $|\hat{\boldsymbol{M}}(k)| < 0$. The stability matrix in Eq. (35) gives

$$
\begin{aligned}
\left|\hat{\boldsymbol{M}}(k)\right| = \left|\hat{\boldsymbol{A}}(k)\right|(1 + k^2\gamma_u)(1 + k^2\gamma_v) &- \hat{a}_{11}(k)(1 + k^2\gamma_u)k^2 D_v \\
&- \hat{a}_{22}(k)(1 + k^2\gamma_v)k^2 D_u + k^4 D_u D_v \,.
\end{aligned}
\tag{45}
$$

In general, a negative value of the determinant along with conditions (40)-(41) for stable population dynamics, requires that $\hat{a}_{11}(k)$ and $\hat{a}_{22}(k)$ have opposite signs for some wave number k. As before, it is assumed that $\hat{a}_{11}(k) > 0$ and $\hat{a}_{22}(k) < 0$ for some k. The only terms that can be negative, and thereby act as driver of the determinant instability, are $k^4 \hat{a}_{11}(k)\gamma_u D_v$ and $k^2 \hat{a}_{11}(k)D_v$. This corresponds to the taxis–diffusion driven case ($|\boldsymbol{T} - \boldsymbol{D}| < 0$) and the diffusion driven case ($S < 0$), respectively, for the local system. For the non-local system, the distinction between the two cases is less clear and we will not attempt to separate them. The determinant instability can occur without fitness taxis ($\gamma_u = \gamma_v = 0$), but not without diffusion ($D_u = D_v = 0$).

Using expression (39) for $\hat{\boldsymbol{A}}(k)$ with expression (45) for the determinant gives

$$
\left|\hat{\boldsymbol{M}}(k)\right| = q_1(k^2) + q_2(k^2)e^{-\sigma^2 k^2} =: \hat{q}(k^2)
\tag{46}
$$

where q_1 and q_2 are the two parabolas

$$
\begin{aligned}
q_1(k^2) &= (c_1\gamma_u + D_u)(c_3\gamma_v + D_v)k^4 + \big(c_3(c_1\gamma_u + D_u) + c_1(c_3\gamma_v + D_v)\big)k^2 \\
&\quad + c_1 c_3 \,, \\
q_2(k^2) &= (c_6\gamma_v - c_2 D_v)\gamma_u k^4 + (c_6\gamma_u + c_6\gamma_v - c_2 D_v)k^2 + c_6 \,.
\end{aligned}
$$

The determinant function $\hat{q}(k^2)$ is defined by Eq. (46) for $k^2 \geq 0$ and plotted for various cases in Fig. 6. The function has the initial value $\hat{q}(0) = |\boldsymbol{A}| > 0$ and for $k^2 \to \infty$, it approaches the parabola $q_1(k^2)$. The values of $q_1(k^2)$ are positive and increases with k^2. This leaves three scenarios for the determinant function; either it is monotonically increasing, it has a minimum, or it has a maximum followed by a minimum. The condition for determinant instability amounts to that the function $\hat{q}(k^2)$ must have a minimum with negative function value.
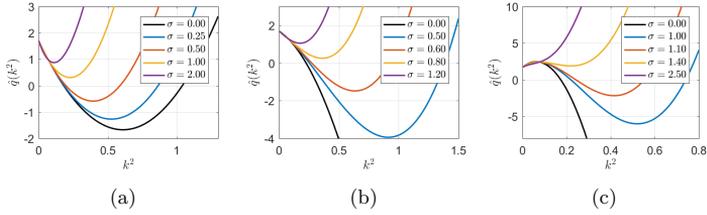
26

Figure 6: The determinant function $\hat{q}(k^2)$ for several values of σ in three different cases. Parameter values are $D_u = 1$, $D_v = 15$ and the default for population dynamics, see section 4.2. (a) $\gamma_u = 0.5$, $\gamma_v = 0.5$. (b) $\gamma_u = 3$, $\gamma_v = 2$. (c) $\gamma_u = 20$, $\gamma_v = 2$.

Next, we consider the effect of the kernel width σ on the determinant instability, when all other parameters are fixed. Since $q_1(k^2)$ is positive, a determinant instability can only occur when $q_2(k^2)$ is negative. For any fixed value of k^2 where $q_2(k^2) < 0$, an increase in kernel width σ increases the value of the function $\hat{q}(k^2)$. Hence, increasing the value of σ, confines the determinant instability to a smaller interval of k^2 and, for sufficiently large values of σ, the determinant instability vanishes. This means, the non-local system cannot have a determinant instability if the corresponding local system for $\sigma = 0$ does not.

The onset of determinant instability occurs when the function $\hat{q}(k^2)$ has a minimum value of zero and can be found solving $\hat{q}(k^2) = 0$ and $\hat{q}'(k^2) = 0$ simultaneously. The equations are solved for the taxis coefficients γ_u and γ_v and, similar to the trace instability, the result is a parametrized curve in k^2,

$$
\gamma_u(k^2) = \Big[(D_u k^2 + 2c_1) c_4 c_5 D_v \sigma^2 k^4 e^{-\sigma^2 k^2} - 2\big(c_1 c_3 + c_6 e^{-\sigma^2 k^2}\big)^2
$$
$$
- 2c_3 D_u k^2 \big(c_1 c_3 + c_6 e^{-\sigma^2 k^2}\big) \pm SQ(k^2) \Big] \Big/
$$
$$
\Big[2k^2 \big(c_1 c_3 + c_6 e^{-\sigma^2 k^2}\big)^2 - 2c_1 c_4 c_5 D_v \sigma^2 k^6 e^{-\sigma^2 k^2} \Big] \tag{47a}
$$
$$
\gamma_v(k^2) = \Big[c_4 c_5 D_u D_v k^4 e^{-\sigma^2 k^2} \Big(D_v \sigma^2 k^4 \big(c_1 + c_2 e^{-\sigma^2 k^2}\big)
$$
$$
+ \sigma^2 k^2 \big(c_1 c_3 - c_6 e^{-\sigma^2 k^2}\big) - 2\big(c_1 c_3 + c_6 e^{-\sigma^2 k^2}\big) \Big)
$$
$$
\mp \Big(c_1 c_3 + c_6 e^{-\sigma^2 k^2} + D_v k^2 \big(c_1 - c_2 e^{-\sigma^2 k^2}\big) \Big) SQ(k^2) \Big] \Big/
$$
$$
\Big[c_4 c_5 D_u D_v \sigma^2 k^8 e^{-\sigma^2 k^2} \big(- c_1 c_3 + c_6 e^{-\sigma^2 k^2}\big)
$$
$$
\pm k^2 \big(c_1 c_3 + c_6 e^{-\sigma^2 k^2}\big) SQ(k^2) \Big] \tag{47b}
$$

where

$$
SQ(k^2) = \Big[\big(c_4 c_5 D_u D_v \sigma^2 k^6 e^{-\sigma^2 k^2}\big)^2 - 4(c_1 c_4 c_5 D_v + c_3 c_6 D_u) \sigma^2 k^4 e^{-\sigma^2 k^2}
$$
$$
+ 4\big(c_1 c_3 + c_6 e^{-\sigma^2 k^2}\big)^2 \Big]^{1/2}
$$

The solution gives two curves since the determinant function $\hat{q}(k^2)$ can have both a maximum and a minimum. The branch belonging to the minimum

corresponds to the bifurcation point and is illustrated for several values of σ in figure 7. When there is no encounter kernel $\sigma = 0$, the bifurcation line corresponds to a combination of the lines $R = 0$ and $|\boldsymbol{T} - \boldsymbol{D}| = 0$ in Fig. 1b. The encounter kernel decreases the region for determinant instability and lowers the maximum value of the predator taxis coefficient γ_v that allows a determinant instability.
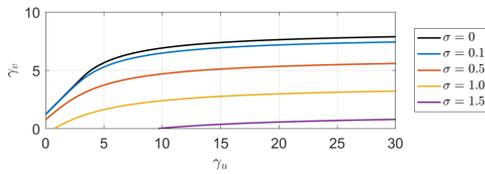

Figure 7: Bifurcation lines for determinant instability for different values of σ. For each value of σ, the system has a determinant instability below the corresponding line. Parameter values are $D_u = 1$, $D_v = 15$ and the default for population dynamics, see section 4.2.